THREE-DIMENSIONAL CELL-BASED PLATFORM (MICROWELL-NEURAL STEM CELL) FOR SCREENING COMPOUNDS AGAINST CONNECTIVITY-RELATED TARGETS

by

LINA WANG

(Under the Direction of William S. Kisaalita)

ABSTRACT

A three-dimensional (3D) cell-based platform for high-throughput screening (HTS) was developed. This platform was comprised of neural stem cell (NSC)-derived neural networks in interconnected microwell structures.

To apply SU-8 microwell structures for human neural stem cell (hNSC) culture, SU-8 microstructures were modified to be biocompatible for hNSC culture. Then hNSCs locomotion within SU-8 microwells was studied by time-lapse recording. Combining fluorescent dyes and confocal microscopy, cell morphology, cytoskeleton organization and resting membrane potential (V_m) were measured for cells on 2D flat surface and within SU-8 microstructures. Microwell architecture affected hNSC morphology, cytoskeleton organization as well as V_m establishment in a quasi-3D manner, which is consistent with other 2D/3D comparison studies. This study moves one step forward in combining hNSCs and microwell structures to form a quasi-3D neural network for drug screening.

To apply microwell-hNSC platform for HTS, micropatterns were fabricated in nano-fibrous poly-L-lactic acid (PLLA) films by laser micromachining and the resulting scaffolds were characterized with respect to architecture, thermal, mechanical and mass transport

properties. Also, hNSCs were successfully cultured in these micropatterned nano-fibrous scaffolds (MNFSs). The scaffolds were incorporated in high-density well plates (e.g., 96-well plates), creating a platform for HTS of drugs with physiologically more relevant neural networks.

To establish a protocol for hNSCs synaptic development in early differentiation, ginsenosides Rg1 and Rb1, major pharmacologically active ingredients from Ginseng, were applied in the differentiation media for hNSCs, together with brain-derived neurotrophic factor (BDNF). Cell locomotion and neurite extension were observed by time-lapse microscopy and analyzed by ImageJ software. The expression of synaptic formation was confirmed by immunostaining of synaptophysin (SYN) or/and the co-localization of synapsin I and microtubule associated protein-2 (MAP-2). Results have shown that administration of BDNF/ginsenosides (Rg1 and Rb1) combination in differentiation medium promoted cell survival, enhanced neurite outgrowth and synaptic marker expression during differentiation. High cell density promotes synaptic marker expression in BDNF/ginsenosides combination medium.

INDEX WORDS: microwell structure, human neural stem cell, three-dimensional, neural network, high-throughput screening, SU-8 microfabrication, poly-L-lactic acid, laser micromachining, brain-derived neurotrophic factor, ginsenosides

THREE-DIMENSIONAL CELL-BASED PLATFORM (MICROWELL-NEURAL STEM CELL) FOR SCREENING COMPOUNDS AGAINST CONNECTIVITY-RELATED TARGETS

by

LINA WANG

B.E., Zhejiang University, China, 2004

A Dissertation Submitted to the Graduate Faculty of The University of Georgia in Partial Fulfillment of the Requirements for the Degree

DOCTOR OF PHILOSOPHY

ATHENS, GEORGIA

2010

THREE-DIMENSIONAL CELL-BASED PLATFORM (MICROWELL-NEURAL STEM CELL) FOR SCREENING COMPOUNDS AGAINST CONNECTIVITY-RELATED TARGETS

by

LINA WANG

Major Professor:	William S. Kisaalita
Committee:	Steven Stice Yiping Zhao Bingqian Xu

Electronic Version Approved:

Maureen Grasso
Dean of the Graduate School
The University of Georgia
August 2010

ACKNOWLEDGEMENTS

This is a great opportunity to express my deep and sincere gratitude to my supervisor, Dr. William S. Kisaalita, for his generous support, encouragement and supervision throughout my Ph.D. study. His invaluable suggestions and guidance enabled me to accomplish these research projects. His wide knowledge, creative and logical thinking and passionate attitude towards research inspired me a lot.

I am also highly thankful to Dr. Steven Stice, Dr. Yiping Zhao, Dr. Bingqian Xu for their valuable suggestions throughout this study. And I really appreciate the kindness of Dr. Zhengwei Pan, Dr. John Shields and Dr. Jianguo Fan for allowing me to use their equipment and for their technical help in my experiments.

I am pleased to thank all my colleagues, Dr. Ze-Zhi Wu, Dr. Ke Cheng, Ms. Yinzhi Lai, Ms. Jenny Mumaw, Mr. Jianfeng Zhou, Mr. Guojun Chen, for their support and help in the work. I always enjoyed working with them.

I owe my loving thanks to my family for their love and support. They are always there for me. I also warmly thank my old friends, Ms. Limin Li, Ms. Jin Yan, Ms. Li Li, for their support all these years. I wish to extend my warmest thanks to my roommates, Ms. Xiaoling Yang and Ms. Yang Hu, to whom I can talk about anything in life and work.

The financial support of the University of Georgia is gratefully acknowledged.

TABLE OF CONTENTS

Page

LIST OF TABLES

Page

LIST OF FIGURES

Page

CHAPTER 1

INTRODUCTION

1.1 Motivation

We are interested in developing a three-dimensional (3D) neural network-based assay for high-throughput screening (HTS) of compounds against mental and neurodegenerative disorders. Mental and/or neurodegenerative disorders are among the most devastating illnesses; however, there are few effective drugs for such diseases (Seow et al., 2007). For example, currently used drugs for schizophrenia still have shortcomings (Javitt et al., 2008); Ziprasidone, a FDA approved drug for treating schizophrenia since 2001, may cause severe side effects such as seizures, irregular heartbeat and so on. Effective drug discovery against these disorders is in great demand, which calls for novel HTS assays for screening available molecular libraries to identify more effective small molecules as drug leads.

Synaptic function and neurotransmission system, which underlie neural network connectivity, are involved in biological mechanisms for mental and neurodegenerative disorders (Cutler et al., 2001; Law et al., 2004; Meador-Woodruff et al., 2003; Hashimoto et al., 2007). Susceptible genes for schizophrenia, such as *Dysbindin* (Dickman and Davis, 2009), *Neuregulin-1* (Wen et al., 2010) and *DISC1* (Kim et al., 2009; Enomoto et al., 2009)

have been associated with network connectivity. Thus, neural networks may act as an effective platform for screening available molecular libraries. Upon drug exposure, the changes in network connectivity are usually compound and concentration specific (Gross et al, 1995; Gross et al, 1997) and depend on the number of synapses per cell, as well as the state of cell maturation (Maeda et al., 1995; O'Donovan, 1999). The ability to genetically engineer synaptical model cells (Dreosti et al., 2009; Migita et al., 2009) and the use of optical detection methods in most HTS formats makes neural networks formed *in vitro* attractive in drug discovery (Chiappalone et al., 2003). However, *in-vitro* screening of drugs that affect neural network function *in vivo* is still primitive as current assays rely on single cellular responses from two-dimensional (2D) cell cultures (Jordan et al., 2007). Three-dimensional (3D) cell-based assays may yield physiologically more relevant results (Cukierman et al., 2001; Kunz-Schughart et al., 2004; Mueller-Klieser, 2004; Liu et al., 2007), and thus have the potential to bridge the gap between 2D assays and preclinical animal testing, saving time and cost by reducing compound attribution. Thus, we aim to engineer a 3D neural network-based assay for HTS in drug discovery.

1.2 Specific Objectives

As a first step in providing a 3D cell-based platform for HTS, comprised of neural stem cell-derived neural networks housed in interconnected microwell structures, we have worked on the following specific objectives:

Objective 1: Optimizing the architecture of interconnected microwells microstructures for 3D microenvironments. We started with SU-8 (epoxy-based negative photoresist)

microstructures. Neural stem cells (NSCs) were integrated with SU-8 microstructures with different structural parameters (i.e. well size, channel width and length). The cell-microstructure interaction was studied with respect to morphology, cytoskeleton organization and cell locomotion during the first 24 hours of plating. This study provides a better understanding of the relationship between microstructure architecture and the resultant quasi-3D neural network formation.

Objective 2: Integrating 3D interconnected microwell microstructures with currently used HTS systems (e.g. 96-well plates) for neural network activity readout. We fabricated poly-L-lactic acid (PLLA) micropatterned nano-fibrous scaffolds (MNFSs) for neural network formation *in vitro*. And we integrated the MNFSs with 96-well plates and established the feasibility of stimulating neural networks by chemical means in this platform for neural network activity readout.

Objective 3: Establishing a NSC differentiation condition for neural network connectivity development, reflected by synaptic formation. We explored the effects of BDNF/ginsenosides (Rg1 and Rb1) combination on hNSC differentiation. We also studied the effects of cell density on hNSC differentiation with respect to synaptic formation.

1.3 Significance

The novelty of the project lies in combining the fields of material science/engineering and biotechnology to create a neural network *in vitro* that will more closely emulate the *in-vivo* counterparts and be more amenable to integration in existing HTS instrumentation formats (e.g., 96-well plates). The successful implementation of the project provides a better understanding of the role the architecture of high-aspect-ratio structures in NSC growth and differentiation. It also provides a way to utilize NSCs as an unlimited cell source in assay/biosensor technology, and establishes procedures for creating controllable neural networks *in vitro*.

1.4 References

Chiappalone M, Vato A, Tedesco MB, Marcoli M, Davide F, Martinoia S. Networks of neurons coupled to microelectrode arrays: a neuronal sensory system for pharmacological applications. Biosensors and Bioelectronics 2003;18: 627-34

Cukierman E, Pankov R, Stevens DR, Yamada KM. Taking cell-matrix adhesions to the third dimension. Science 2001;294:1708-12

Cutler NR, Sramek JJ. Review of the next generation of Alzheimer's disease therapeutics: challenges for drug development. Prog Neuropsychopharmacol Biol Psychiatry 2001; 25(1): 27-57

Dickman DK and Davis GW. The schizophrenia susceptibility gene dysbindin controls synaptic homeostasis. Science 2009;326:1127-30

Dreosti E, Odermatt B, Dorostkar MM, Lagnado L. A genetically encoded reporter of synaptic activity in vivo. Nature methods 2009;6(12):883-9

Enomoto A, Asai N, Namba T, Wang Y, Kato T, Tanaka M, Tatsumi H, Taya S, Tsuboi D, Kuroda K, Kaneko N, Sawamoto K, Miyamoto R, Jijiwa M, Murakumo Y, Sokabe M, Seki Y, Kaibuchi K, Takahashi M. Roles of Disrupted-In-Schizophrenia 1-intefracting protein girdin in postnatal development of the dentate gyrus. Neuron 2009;63(6):774-87

Gross GW, Rhoades BK, Azzazy HME, Wu M. The use of neuronal networks on multielectrode arrays as biosensors. Biosensors & Bioelectronics 1995;10:553-67

Gross GW, Harsch A, Rhoades BK, Gopel W. Odor, drug and toxin analysis with neuronal networks in vitro: extracellular array recording of network responses. Biosensors & Bioelectronics 1997;12(5):373-93

Hashimoto R, Tankou S, Takeda M, Sawa A. Postsynaptic density: a key convergent site for schizophrenia susceptibility factors and possible target for drug development. Drugs Today (Barc) 2007;43(9):645-54

Javitt DC, Spencer KM, Thaker GK, Winterer G, Hajós M. Neurophysiological biomarkers for drug development in schizophrenia. Nature reviews: drug discovery 2008; 7: 68-83

Jordan S, Johnson JL, Regardie K, Chen R, Koprivica V, Tadori Y, Kambayashi J, Kitagawa H, Kikuchi T. Dopamine D2 receptor partial agonists display differential or contrasting characteristics in membrane and cell-based assays of dopamine D2 receptor signaling. Progress in Neuro-Psychopharmacology & Biological Psychiatry 2007;31:348-56

Kim JY, duan X, Liu CY, Jang MY, Guo JU, Pow-anpongkul N, Kang E, Song H, Ming GL. DISC1 regulates new neuron development in the adult brain via modulation of AKt-mTOR signaling through KIAA1212. Neuron 2009;63:761-73

Kunz-Schughart LA, Freyer JP, Hofstaedter F, Ebner R. The use of 3-D cultures for high-throughput screening: the multicellular spheroid model. J. Biomol. Screen. 2004;9:273-85

Law AJ, Weickert CS, Hyde TM, Kleinman JE, Harrison PJ. Reduced spinophilin but not microtubule-associated protein 2 expression in the hippocampal formation in schizophrenia and mood disorders: molecular evidence for a pathology of dendritic spines. Am J Psychiatry. 2004;161(10):1848-55

Liu XS, Zhang ZG, Zhang RL, Gregg SR, Meng H, Chopp M. Comparison of in vivo and in vitro gene expression profiles in subventricular zone neural progenitor cells from the adult mouse after middle cerebral artery occlusion. Neuroscience 2007;146:1053-61

Maeda E, Robinson HPC, Kawana A. The mechanisms of generation and propagation of synchronized bursting in developing networks of cultured neurons. J. Neurosci. 1995;15(10): 6834-45

Meador-Woodruff JH, Clinton SM, Beneyto M, McCullumsmith RE. Molecular abnormalities of the glutamate synapse in the thalamus in schizophrenia. Ann N Y Acad Sci. 2003;1003:75-93

Migita S, Tateeishi A, Keinanen K Haruyama T. Engineered synapse model cell: genetic construction and chemical evaluation for reproducible high-throughput analysis Anal Bioanal chem. 2009;396(3):1153-7

Mueller-Klieser W. The use of 3-D cultures for high-throughput screening: The multicellular spheroid model. Journal of Biomolecular Screening 2004;9(4):273-85

O’Donovan MJ. The origin of spontaneous activity in developing networks of the vertebrate nervous system. Curr. Opin. Neurobiol. 1999;9:94-104

Seow D, Gauthier S. Pharmacotherapy of Alzheimer’s disease. Can. J. Psychiatry 2007;52(10): 620-29

Wen L, Lu Y-S, Zhu X-H, Li X-M, Woo R-S, Chen Y-J, Yin, D-M, Lai C, Terry AV, Vazdarjanova Jr.A, Xiong W-C, Mei L. Neuregulin 1 regulates pyramidal neuron activity via ErbB4 in parvalbumin-positive interneurons. PNAS 2010;107(3): 1211-1216

CHAPTER 2

LITERATURE REVIEW

2.1. 3D Cultures are Physiologically More Relevant

Direct and indirect evidence, in support of the notion that biological activity of 3D cultures may more closely mirror what happens *in vivo*, has appeared in the literature for the past three decades (Cukierman et al., 2001; Liu et al., 2007). This is probably best exemplified in the field of experimental oncology that adopted 3D multicellular tumor spheroids (MCTS) to mimic *in vivo* situation (Mueller-Klieser, 2004; Kunz-Schughart et al, 2004). Multicellular spheroids have been able to fully recapitulate the multicellular mediated drug resistance of EMT6 tumors (Graham et al., 1994), which was inherently induced *in vivo* but completely lost when cancer cells were dissociated and cultured in monolayers. Weaver et al. (1997) have been able to show the phenotypic transformation of malignant cells in a 3D collagen gel configuration upon treatment with integrin antibodies, while this has never been possible in monolayer cultures. In another study, two tumorigenic cell lines (HT-1080 fibrosarcoma and MDA-MB-231 carcinoma) showed protease-independent amoeboid movement within 3D collagen matrix (Wolf et al., 2003). This challenges the traditional screening for anti-metastatic agents against proteolytic activity with 2D monolayer cultures, and 3D spheroids should become mandatory test systems in cancer therapeutic screening programs.

For voltage-gated calcium channels (VGCCs), Martinez-Pinna et al. (2002) used microelectrodes to examine which types of high threshold Ca^{2+} channels are activated by depolarization of intact (3D) and dissociated (2D) sympathetic neurons from adult mouse superior cervical ganglia. Marked differences were observed in specific channel (N-type, P/Q-type, and L-type) currents between 2D and 3D, leading to the conclusion that traditional 2D culture of sympathetic neurons results in biological activity that only partially reflects the situation *in vivo*. Also, modified expression and regulatory properties of VGCCs were observed in neonatal rat myocytes cultured on aligned and flat thin collagen gels and the changes were attributed to differences in cell shape (Walsh and Parks, 2002).

2.2. Microfabricated 3D Cell Culture Systems Offer Many Advantages

To date, approaches to culturing cells in 3D microenvironment include: multicellular aggregates (Albrecht et al., 2006; De Bank et al., 2007), nanofibers (Matthews et al., 2002), polymer scaffolds (Drury and Mooney, 2003; Levenberg et al., 2003; Cheng et al., 2008) and microstructured substrates (Wu et al., 2006; Wang et al., 2009). Multicellular aggregates have become a predominant approach for creating 3D microenvironment for cancer cells, which offers significant advantages in the research of tumor biology and therapeutics over 2D culture systems (Kunz-Schughart et al., 2004; Birgersdotter et al., 2005). Electrospinning is an efficient fabrication process that uses an electric field to control the deposition of polymer fibers onto a target substrate, which leads to complex, seamless, 3D structures. The fiber diameters can be well controlled from several microns down to 100 nm or less. Consequently these fibers have a large surface area per unit mass. Depending on the specific polymer being used, a range of fabric properties can be achieved, such as strength, weight, and porosity. The

structural, material, and biological properties of electrospun scaffolds suggest that they may represent a nearly ideal engineered scaffold for cell-based biosensor.

With the development in tissue engineering, polymer scaffolds have become appealing 3D cell culture systems *in vitro* (Cushing and Anseth, 2007) and promising platform for 3D cell-based biosensor (O'Connor et al., 2000a; Mao and Kisaalita, 2004). However, these polymers have several limitations. First, it is difficult to guarantee precise control of the aspect ratio (height over width) with these structures. Second, limited mass transportation in scaffolds affects nutrient supply, waste drainage and drug exposure. Third, the properties of polymer scaffolds may limit the extent to which optical or electrical detection may be applicable.

With the advancement in the field of semiconductor devices, the techniques for fabricating micro-structured substrata are now highly developed (Weibel et al., 2007). Microfabrication, which can produce a miniaturized, inexpensive platform for "cell-culture-on-a-chip", offers unique opportunities for engineering a 3D environment for cell culture and other cell-based microdevices (Park and Shuler, 2003; Li et al, 2003; Tourovskaia et al., 2005; Koh and Pishko, 2006). High-aspect-ratio micropatterns have also been proposed and applied to study cell growth, differentiation and function in a 3D microenvironment *in vitro* (Chin et al., 2004; Hung et al., 2005; Wu et al., 2006).

In comparison with other 3D cell culture systems formed from polymers, microfabricated patterns have many advantages. First, the technique has been well developed. The aspect ratio can be well controlled in the fabrication process and the fabrication of microstructures can be

scaled up to meet the need of HTS. Second, microstructures can be compatible with optical as well as bioelectrical analytical methods. Third, unlike cells embedded in polymer scaffolds, cells cultured in microstructures are better exposed to growth media and drug supply; thus the mass transportation limitation problem can be minimized in the microfabricated patterns, which is an essential aspect in HTS. Fourth, microfluidic devices can be built on microstructures, which can provide a dynamic microenvironment for cell culture (Hung et al., 2005). In addition, the microwell and channels connecting microwells, as proposed in this study, can provide guidance for neural cell growth and neural network formation. It is possible to guide neural cell growth through the structures and obtain controllable neural networks *in vitro*. Thus these microstructures possess a unique advantage over all other 3D cell culture systems with regard to neural network formation.

2.3. Susceptible Schizophrenia Genes Promote Drug Discovery for Schizophrenia

Schizophrenia is one of the devastating mental disorders, and affects 1% of the world population. It is difficult for people with schizophrenia to tell the difference between real and unreal experiences, to think logically, to have normal emotional responses, and to behave normally in social situations. It is a complex disease, and multiple factors, such as biological factors and environmental factors, can trigger this illness. Even though the causes of schizophrenia are still unknown, treatments are available which focus on elimination the symptoms of the disease. Among these treatments, antipsychotic medication is one effective way. Antipsychotic medications have been available since the middle of 1950's and these commonly used drugs include clozapine, ziprasidone, olanzapine and so on. However, these drugs still have shortcomings; for example, Ziprasidone (Geodon), a FDA approved drug for

treating schizophrenia since 2001, may cause severe side effects such as seizures, irregular heartbeat and so on. Clozapine (Clozari) is an effective medication that treats psychotic symptoms, hallucinations, and breaks with reality, but it can sometimes cause a loss of white blood cells. Thus, effective drug discovery against this disorder is in great demand. With the development of schizophrenia genetics research (Figure 2.1), susceptible schizophrenia genes have been discovered, which provides potential drug targets for drug discovery. These susceptible genes include *Dysbindin, Neuregulin-1 (NRG-1), Disrupted-in-Schizophrenia 1 (DISC1), Regulator of G protein signaling 4 (RGS4), Catechol-o-methyltransferase (COMT), proline dehydrogenase (PRODH)* and so on (Gogos and Gerber, 2006; O'Tuathaigh et al., 2007). In the target-driven drug discovery paradigm, novel assays compatible with high throughput screening (HTS) are the state-of-art for screening available molecular libraries to identify more effective small molecules as drug leads.

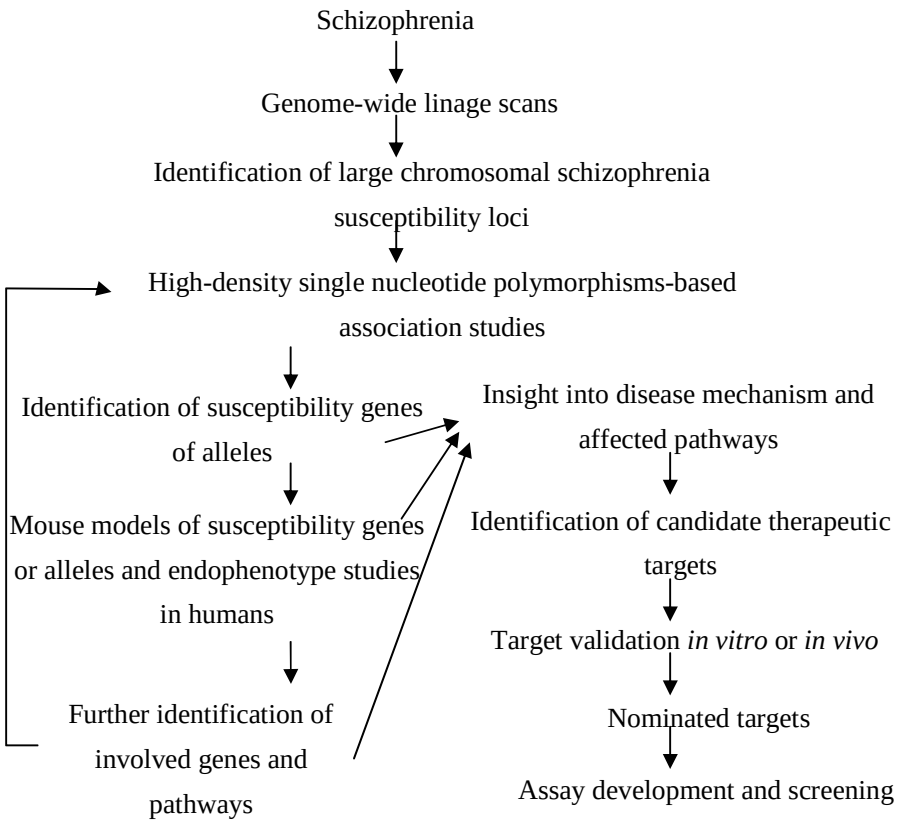

Figure 2.1. Flow diagram of the schizophrenia genetics research process and its potential application to drug discovery. It shows a comprehensive system with which to identify the genes and molecular pathways involved in schizophrenia pathogenesis. This knowledge base provides a framework for target-driven drug-discovery efforts (Gogos and Gerber, 2006).

2.4. Neural Networks Provide an Effective Platform for Screening Available Molecular Libraries in Schizophrenia Drug discovery

Synaptic functions (e.g. presynaptic proteins such as synaptophysin, postsynaptic proteins such as MAP-2) and neurotransmission systems (e.g. metabotropic glutamate receptor 5 (mGluR5), N-methyl-D-aspartic acid receptors (NMDARs), gamma-aminobutyric acid receptors (GABARs)), which underlie neural network connectivity, are involved in biological mechanisms for mental and neurodegenerative disorders (Cutler et al., 2001; Law et al., 2004; Meador-Woodruff et al., 2003; Gogos and Gerber, 2006; Hashimoto et al., 2007;

Wang H et al., 2009). Susceptible genes for schizophrenia, such as *Dysbindin, NRG-1, DISC1, RGS4, COMT* and so on, have been associated with synaptic function and neurotransmission systems (Table 2.1). Studies have shown that distance between the neuronal assemblies communicating with each other affect network oscillation frequency (Ford et al., 2007), which is an important biomarker for schizophrenia. Taken together, network activity could be applied to develop assays for screening compounds against mental and neurodegenerative disorders. Upon drug exposure, the changes in network connectivity are usually compound and concentration specific (Gross et al, 1995; Gross et al, 1997) and depend on the number of synapses per cell, as well as the state of cell maturation (Maeda et al., 1995; O'Donovan, 1999). The ability to genetically engineering synaptical model cells (Dreosti et al., 2009; Migita et al., 2009) and the use of optical detection methods in most HTS formats makes controllable neural networks formed *in vitro* attractive in drug discovery (Chiappalone et al., 2003).

Table 2.1. Summary of schizophrenia susceptibility genes and their function related to neural network connectivity (O'Tuathaigh et al., 2007).

Gene	Location	Function
NRG-1	8p21-p22	Synapse formation, neuronal migration, synaptic plasticity; Regulation of (1) NMDA & AMPA receptor function (2) NMDA & GABA receptor subunit expression
RGS 4	1q21-q22	Regulation of G protein-coupled receptors
Dysbindin	6p22.3	Regulation of synaptic structure and signalling
DISC1	1q42	Neuronal migration, neuronal differentiation
COMT	22q11	Involved in DA metabolism, particularly in frontal cortex
PRODH	22q11	Regulation of cortical Ach function, metabolic precursor of glutamate in subpopulation of glutamate neurons

2.5. *In-Vitro* Neural Network Formation

Commonly used methods to form neural networks *in vitro* can be categorized into the following three forms: random forming, chemical patterning, and structural guiding (Kane et al., 1999; Craighead et al., 2001). Though randomly formed neural networks provide a useful method for studying the physiology of neurons in a simplified environment, they are not easy to manipulate. Chemical patterning can control neural cell growth. Microlithographic materials and techniques (Nicolau et al. 1999), microcontact printing (Vogt et al., 2005; Zhang et al., 1999) and self-assembled monolayers (Yousaf et al., 2001) are mainly used to tailor the properties of the substrates for patterning neural network. Topographical structures can provide physical guidance for neural network formation *in vitro*. Micropatterned substrates have long been considered a promising approach for the creation of defined neuronal networks *in vitro*. Unlike chemical patterning, high-aspect-ratio microstructures are thought to provide quasi-3D microenvironments for neural cell growth and neural network formation (Wu et al., 2006b; Wang et al., 2009). Microstructures made of agarose (Suzuki et al., 2004.), PMDS (Griscom et al, 2001) and SU-8 (Merz and Fromherz, 2005) have been reported to control neuron outgrowth and synapse formation *in vitro*.

In this project, substrates were fabricated from SU-8 to guide neural network formation. SU-8, which is an epoxy-based negative photoresist, can form a film with a thickness from 1µm to 200µm with the spin coating processes. Films can be processed with photolithography to pattern high-aspect-ratio (>20) structures with high optical transparency, straight sidewalls, and excellent thermal stability. SU-8 is commonly used in fabrication of microfluidics and microelectromechanical system (MEMS) parts (Chung et al., 2005; Gross

et al., 2007). Also, SU-8 microstructures are considered a novel platform for integrating with cell culture and studying cell fate *in vitro* (Chin et al., 2004; Wu et al., 2006; Wang et al., 2009). SU-8 fabricated high-aspect-ratio microstructures have been characterized and applied to integrate with human neuroblastoma cells (SH-SY5Y) (Wu et al., 2006; Wang et al., 2009). These studies showed that high-aspect ratio SU-8 microstructures are not merely "folded 2D" structures; instead, these structures provide cells a different microenvironment as compared with 2D substrates which affect cell growth and differentiation in a 3D manner.

2.6. Evaluation of Neural Network Connectivity

Development of *in vitro* systems in which neural network formation can be controlled and neural network functionality can be semiquantified is applicable in cell-based biosensors which target neural network function. In functional neural networks, neurons communicate and influence other neurons through synapses. Communication across synapses is mediated by the release of neurotransmitters from the presynaptic terminals that influence the excitability of postsynaptic neurons by activating specific receptor ion channel molecules. Synapse formation is a critical event in the establishment of functional network. Proteins on the surface of the synaptic vesicle in the presynaptic terminal evidently mediate this process and these proteins have been considered as markers for synapse formation (Südhof and Jahn, 1991; Serpinskaya et al., 1999). In these studies on synapse formation *in vitro*, double-immunostaining for synapsin I and microtubule associated protein-2 (MAP-2) can identify both pre- and postsynaptic specializations (Ma et al., 1998; Liu et al., 2000). Synaptophysin is another marker protein of the synaptic vesicles, the expression of which marks the synaptic differentiation of neural progenitor cells with the capability of forming

synaptic connection (Kim et al., 2005). Also, it plays essential roles in synaptic plasticity (Fletcher et al., 1991; Janz et al., 1999). Fluorescence imaging of presynaptic uptake and release of styryl dyes such as FM1-43 has provided valuable insights into synaptic function (Pyle et al., 1999; Kay et al., 1999).

For neural network functionality evaluation, immunostaining for synapse formation is not sufficient and network connectivity establishment can provide further evidence. Neural network connectivity can be characterized by signal propagation through networks, and it is suggested that successful signal propagation over the network depends on the number of synapses per cell, the synaptic density and state of maturation, the degree of process extension and cell excitability (Maeda et al., 1995; O'Donovan, 1999). Electrophysiological measurements made with micropipette electrodes and microfabricated electrode play an important role (James et al., 2004; Giugliano et al., 2004; Merz and Fromherz, 2005) in understanding signal propagation and network connectivity has been monitored by electrical recording to evaluate the network functionality (Morimoto et al., 1998; O'Shaughnessy et al., 2003; Moe et al., 2005). However, this method is difficult to integrate with current HTS platforms. With the help of the calcium fluorescent indicators, optical monitoring of calcium transients has become another powerful approach for signal observation and detection (Jimbo et al, 1993; Meyer and Teruel, 2003). The rapid development of calcium imaging techniques, which enable optical monitoring of neuronal electrical activities, enables the application of neuronal networks as a cell-based biosensor HTS platform. One of the advantages of optical monitoring is that it enables simultaneous recording of large number of cells within neural networks with no need for specific instrumentation.

2.7. Stem Cells Present Powerful Tools in Drug Discovery

Currently used cell sources for neural cell-based assays in drug discovery include primary neural cells, neuroblastoma cells, and stem cells (SCs). The use of these primary cultures is accompanied by excessive animal sacrifice and frequent cell isolation, which can be cost prohibitive. The use of neuroblastoma cell lines offers advantages over primary neural cultures due to the unlimited expansion of the tumorigenic cell populations. However, the formation of the physiologically relevant neural networks with these cells is less desirable due to cellular abnormality (Banker and Goslin, 1998). Alternatviely, SCs proved powerful tools in drug discovery as well as in cell therapy because of their ability to self-renew and their potential to form all cell lineages in the body (Conley et al., 2004; Crook JM, Kobayashi, 2008; Shi, 2009; Marchetto et al., 2010). Specifically, they maintain developmental potential to form neural cells (Bain et al., 1995; Shin et al., 2005).

Human embryos are the main sources for producing human pluripotent stem cells (hPSCs) that are genetically unmodified so far. Alternative methods for producing hPSCs include somatic cell nuclear transfer or therapeutic cloning (Figure 2.2). However the therapeutic application of either approach has been experiencing both ethical and technical difficulties (Koch et al., 2009). Reprogramming human somatic cells into induced pluripotent stem cells (iPSCs) without the need of embryos or eggs will solve the technical and ethical problems. Furthermore, iPSCs from patients can be patient-specific and disease-specific. And Figure 2.3 presents application of iPSC-based disease modeling in drug discovery as well as in cell therapy.

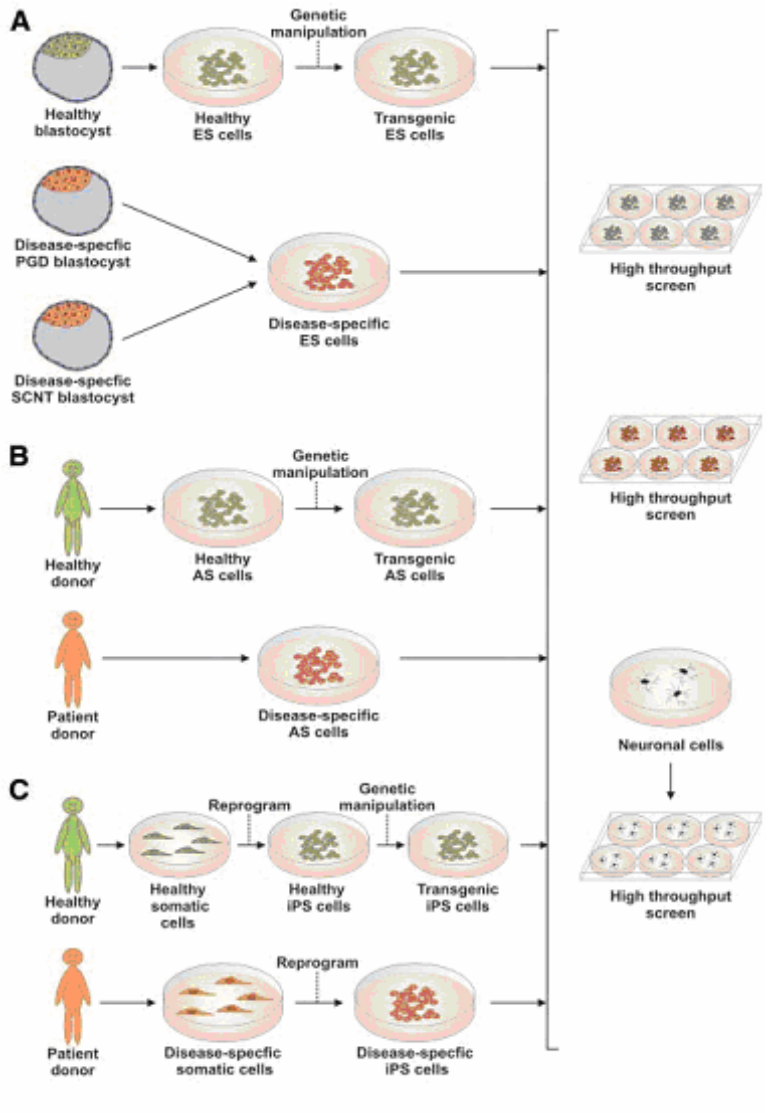

Figure 2.2 Schematic illustration of stem cell-based disease modeling and drug discovery. A: Human embryonic stem cell disease-models can potentially be produced by: (i) targeted gene disruption of cells derived from healthy blastocysts, (ii) cell line isolation from congenitally defective preimplantation embryos identified by preimplantation genetic diagnosis, or (iii) cell line isolation from blastocysts produced by somatic cell nuclear transfer. B: Human adult stem cell disease-models can be derived by: (i) targeted gene manipulation of cells from a healthy donor, or (ii) cell line isolation from a patient. C: Human induced pluripotent stem cell disease-models can be produced by reprogramming somatic cells from either a healthy or patient donor, with the former requiring targeted gene disruption to mimic mutations relevant to a disease state. High throughput screening of compound libraries with undifferentiated stem cells and their neural derivatives is subsequently performed to assess the efficacy (including toxicity and other undesirable effects) of potential drug candidates. (Crook and Kobayashi, 2008)

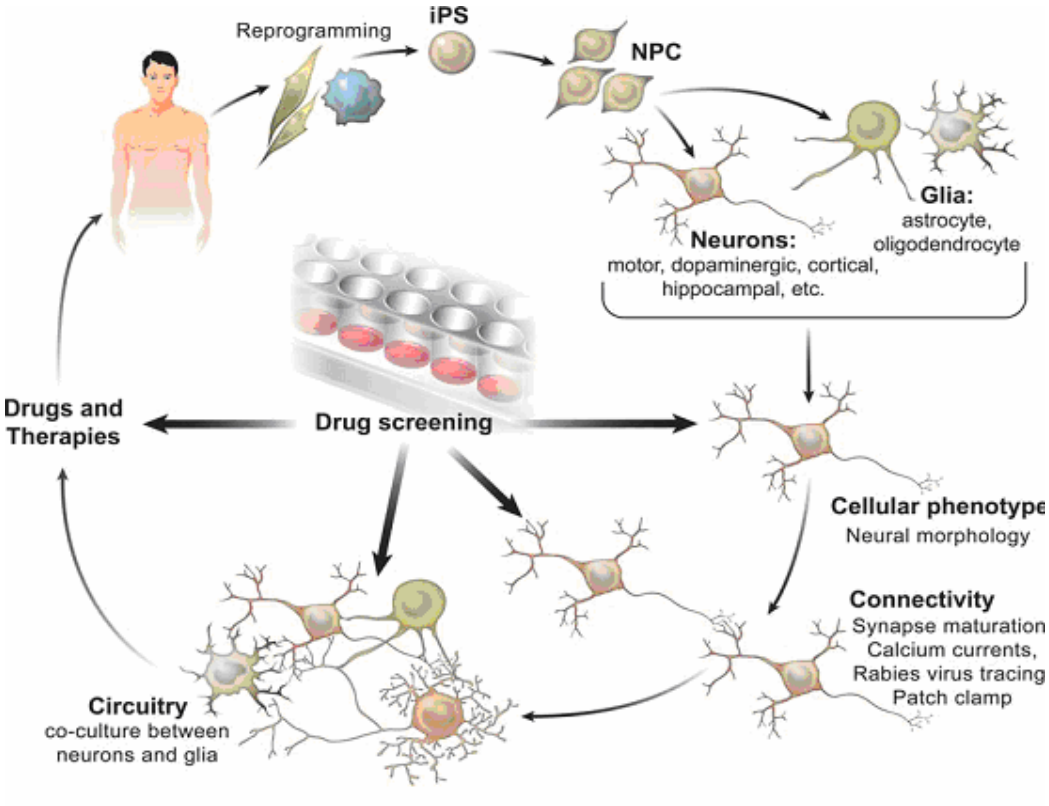

Figure 2.3 iPSC model for neurodegenerative and neurodevelopmental diseases. Human iPSC from neurologic patients and controls are generated after somatic tissue reprogramming (ex. skin or blood cells). Neural progenitor cells are generated and are further differentiated into neurons and/or glial cells. Neurons are then differentiated into subtypes of neurons such as dopaminergic, cholinergic, etc. Cellular phenotype is assessed by measuring neuronal morphology (i.e., process branching, spine density/size/maturation). Next, connectivity and circuitry integration can be analyzed by calcium influx transients, electrophysiology and transneuronal tracing with Rabies virus. In addition, the cross talk between neurons and glia can be studied to tease out autonomous and non-autonomous aspects of the disease. Once a distinct disease-related phenotype is identified, drug-screening platforms can be developed to test compounds that improve cellular phenotype. Therapeutic compounds could emerge from the screenings, potentially benefiting neurologic patients. (Marchetto et al., 2010)

Neural stem cells (NSCs), derived from SCs, appeared normal morphologically and displayed normal features of immunoreactivity when tested for neuron-specific elements (Tzeng, 2002; O'Connor et al., 2000b). They are as vulnerable as normal neurons to excitotoxic death (Qu et al., 2003). Electrophysiological analysis showed that cell membrane of ES derived neuron contained voltage-dependent channels. Action potentials were readily triggered by current injection (Fraichard et al., 1995). There is a large body of literature demonstrating the early expression of voltage-gated calcium channels (VGCCs) in NSCs as well as NSC-derived neurons (Gottmann et al., 1988; Sah et al., 1997; Arnhold et al., 2000; Deisseroth et al., 2004; Moe et al., 2005). Recently, astrocytes have been shown to potentiate transmitter release at single hippocampal synapses (Perea and Araque, 2007); suggesting that co-culturing neurons and glial cells has potential to provide constructs that will more closely mimic the *in vivo* situation. Using specific media, several investigators have differentiated NSCs and shown that in addition to staining positive for nerve cells, also stain positive for glial cell markers (Lin et al., 2004; Mahoney and Anseth, 2006). These results show that NSCs offer unique opportunity for studying the developmental profile of VGCC functions as well as neural network activities in terms of calcium transients.

2.8 Brain-Derived Neurotrophic Factor (BDNF) Supports and Promotes Neural Cell Development

Neurotrophins include nerve growth factor (NGF), brain-derived neurotrophic factor (BDNF), neurotrophin-3 (NT-3), neurotrophin-4/5 (NT-4/5) and neurotrophin-6 (NT-6), which are chemicals that help to stimulate and control neurogenesis and play an important role in normal neural development. These proteins initiate their biological functions by

interacting with their cognate receptors. Neurotrophins activate two different receptor classes: the tropomyosin-related kinase (Trk) family of receptor tyrosine kinases (TrkA, TrkB, and TrkC) and the p75 receptor, a member of the tumor necrosis factor receptor superfamily. Ligand binding results in activation of the tyrosine kinases. Activated receptors in general are capable of triggering a number of signal transduction cascades including the MAPK pathway and the phosphatidylinositol 3-kinase (PI3K) pathway. These signals then pass on to the nucleus to activate transcription factors that alter gene expression. For excellent review on neurotrophin regulation and mechanisms, please refer to Lu (2003) and Poo (2001).

Brain-derived neurotrophic factor (BDNF), one of the most active proteins, helps to support the survival of existing neurons, and encourages the growth and differentiation of new neurons and synapses. It plays an important role in the survival of differentiated neural stem cells through the MAPK/ERK-dependent and PI3K/Akt-dependent Bcl-2 up-regulation (Lim et al., 2008). Also, it has been proven to accelerate the maturation of the synaptic vesicle protein synapsin-1 at developing neuromuscular junctions in cell cultures (Poo, 2001). It plays a novel role in the mobilization and docking of synaptic vesicles to presynaptic active zones (Pozzo-Miller et al., 1999). BDNF has emerged as a major regulator of synaptic plasticity and a key target in disorders such as major depression and Alzheimner's disease (Kuipers and Bramham, 2006). Animal models have been applied to test the effects of BDNF on synapse development (Sanchez et al., 2006). After treatment of mutant hippocampus slices with BDNF, quantitative analysis of CA1 synapses revealed a significant increase in synaptophysin expression level and the number of vesicles docked at presynaptic active zones.

Thus, BDNF has been often added in neural stem cell differentiation media (Johnson et al., 2007).

2.9 Small Molecules Against Mental or Neurodegenerative Disorders: Rg1 and Rb1

Ginseng, the root of Panax ginseng C.A. Meyer (Araliaceae), has been extensively used in traditional oriental medicine for over 2000 years. *In vivo* and *in vitro* studies have shown its beneficial effects in cardiovascular diseases, cancer and immune deficiency. A recent study has suggested that some of ginseng's active ingredients also exert beneficial effects on aging and neurodegenerative diseases (Radad et al., 2006). Ginsenosides such as Rb1 (MW1109.29 Da) and Rg1 (MW801.02 Da) are the major pharmacologically active ingredients of ginseng and their anti-aging and anti-neurodegeneration effects have been well proven (Cheng et al., 2005). Cell-based studies have shown that ginsenosides promoted NSC proliferation *in vitro* and enhanced cell survival (Shen and Zhang, 2004). Mechanisms may involve decreasing NO content and NOS activity, reducing intracellular calcium concentration, by up-regulating Hes1 expression, enhancing superoxide dismutase (SOD) activity and enhancing the ratio of Bcl-2 to Bax protein and inhibiting activation of caspase-3 (Cheng et al., 2005; Zhuang et al., 2009). Ginsenosides Rg1 and Rb1 also promoted neurite outgrowth in PC12 cells (Rudakewich et al., 2001), enhanced astrocyte differentiation from NSCs (Shi et al., 2005), increased neurotransmitter release (Xue et al., 2006), and increased synapse number and the density of synaptophysin, which is the morphological basis for explaining Rb1 and Rg1 induced facilitation of learning and memory (Mook-Jung et al. 2001).

2.10 References

Albrecht DR, Underhill GH, Wassermann TB, Sah RL, Bhatia SN. Probing the role of multicellular organization in three-dimensional microenvironments. Nat. Methods 2006;3(5):369-375.

Arnhold S, Andressan C, Angelov DN, Vajna R, Volsen SG, Hescheler J, Addicks K. Embryonic stem-cell derived neurones express a maturation dependent pattern of voltage gated calcium channels and calcium binding proteins. Int. J. Devl. Neurosci. 2000;18:201-212.

Bain G, Kitchens D, Yao M, Huettner JE, Gottlieb DI. Embryonic Stem Cells Express Neuronal Properties in vitro. Developmental Biology 1995;168:342-357.

Banker G, Goslin K. 1998. Culturing Nerve Cells (2nd ed.). Cambridge, MA: The MIT Press

Birgersdotter A, Sandberg R, Ernberg I. Gene expression perturbation in vitro - A growing case for three-dimensional (3D) culture systems. Seminars in Cancer Biology 2005;15:405-412.

Cheng K, Lai Y, Kisaalita WS. Three-dimensional polymer scaffolds for high throughput cell-based assay systems. Biomaterials 2008;29:2802-2812.

Cheng Y, Shen L, Zhang J. Anti-amnestic and anti-aging effects of ginsenoside Rg1 and Rb1 and its mechanism of action. Acta Pharmacologica Sinica 2005;26 (2):143-9.

Chiappalone M, Vato A, Tedesco MB, Marcoli M, Davide F, Martinoia S. Networks of neurons coupled to microelectrode arrays: a neuronal sensory system for pharmacological applications. Biosensors and Bioelectronics 2003;18: 627-34.

Chin V.I., Taupin P., Sanga S., Scheel J.,Gage F.H., Bhatia S.N.. Microfabricated platform for studying stem cell Fates. Biotechnology and Bioengineering 2004;88(3):399-415.

Chung BG, Flanagan LA, Rhee SW, Schwartz PH, Lee AP, Monuki ES, Jeon LN. Human neural stem cell growth and differentiation in a gradient-generating microfluidic device. Lab on a Chip 2005;5:401-406.

Conley BJ, Young JC, Trounson AO, Mollard R. Derivation, propagation and differentiation of human embryonic stem cells. The International Journal of Biochemistry & Cell Biology 2004;4(36):555-567.

Craighead HG, James CD, Turner AMP. Chemical and topographical patterning for directed cell attachment. Current Opinion in Solid State and Materials Science 2001;5:177-184.

Crook JM, Kobayashi NR. Human stem cells for modeling neurological disorders: accelerating the drug discovery pipeline. J Cell Biochem. 2008;105(6):1361-6.

Cukierman E, Pankov R, Stevens DR, Yamada KM. Taking cell-matrix adhesions to the third dimension. Science 2001;294:1708-12.

Cushing MC, Anseth KS. Hydrogel Cell Cultures. Science 2007;316;1133-1134.

Dreosti E, Odermatt B, Dorostkar MM, Lagnado L. A genetically encoded reporter of synaptic activity *in vivo*. Nature methods 2009;6(12):883-9

De Bank PA, Hou Q, Warner RM, Wood IV, Ali BE, MacNeil S, Kendall DA, Kellam B, Shakesheff KM, Buttery LDK. Accelerated formation of multicellular 3-D structures by cell-to-cell cross-linking. Biotechnology and Bioengineering 2007;97(6):1617-1625.

Deisseroth K, Singla S, Toda H, Monje M, Palmer TD, Malenka RC. Excitation-neurogenesis coupling in adult neural stem/progenitor cells. Neuron 2004;42:535-552.

Drury JL, Mooney DJ. Hydrogels for tissue engineering: scaffold design variables and applications. Biomaterials 2003;24:4337–4351.

Fletcher TL, Cameron P, De Camilli P, Banker G. The Distribution of Synapsin I and Synaptophysin in Hippocampal Neurons Developing in Culture. The Journal of Neuroscience 1991;1(6):1617-l 626.

Ford JM, Krystal JH, Mathalon DH. Neural Synchrony in Schizophrenia: From Networks to New Treatments. Schizophrenia Bulletin 2007;33(4):848-52

Fraichard A, Chassande O, Bilbaut G, Dehay C, Savatier P, Samarut J. In vitro differentiation of embryonic stem cells into glial cells and functional neurons. Journal of Cell Science 1995;108:3181-3188.

Gogos JA, Gerber DJ. Schizophrenia Susceptibility genes: emergence of positional candidates and future directions. Trends in Pharmacological Sciences 2006;27(4):226-233

Gottmann K, Dietzel ID, Lux HD, Huck S, Rohrer H. Development of inward currents in chick sensory and autonomic neuronal precursor cells in culture. J. Neurosci. 1988;8(10):3722-3732.

Graham CH, Kobayashi H, Stankiewics KS, Man,S, Kapitain SJ, Kerbel RS. Rapid acquisition of multicellular drug resistance after a single exposure of mammary tumor cells to anticancer alkylating agents. J. Natl. Cancer Inst. 1994;86:975-982

Griscom L, Degenaar P, LePioufle B, Tamiya E, Fujita H. Cell Placement and Neural Guidance Using a Three-Dimensional Microfluidic Array. Jpn. J. Appl. Phys. 2001;40:5485-5490.

Gross PG., Kartalov EP, Scherer A, Weiner LP. Applications of microfluidics for neuronal studies. Journal of the Neurological Sciences 2007;252(2):135-143.

Giugliano M, Darbon P, Arsiero M, Luscher H-R, Streit J. Single-neuron discharge properties and network activity in dissociated cultures of neocortex. J Neurophysiol. 2004;92:977-996.

Hung PJ, Lee PJ, Sabounchi P, Aghdam N, Lin R, Lee LP. A novel high aspect ratio microfluidic design to provide a stable and uniform microenvironment for cell growth in a high throughput mammalian cell culture array. Lab on a Chip 2005;5:44-48

James CD, Spence AJH, Dowell-Mesfin NM, Hussain RJ, Smith KL, Craighead HG, Isaacson MS, Shain W, Turner JN. Extracellular recordings from patterned neuronal networks using planar microelectrode arrays. IEEE Trans. Biomed. Eng. 2004;51(9):1640-1648.

Janz R, Sudhof TC, Hammer RE, Unni V, Siegelbaum SA, Bolshakov VY. Essential roles in synaptic plasticity for Synaptogyrin I and Synaptophysin I. Neuron 1999;24:687-700.

Jimbo Y, Robinson HPC, Kawana A. Simultaneous measurement of intracellular calcium and electrical-activity from patterned neural networks in culture. IEEE Trans. Biomed. Eng. 1993;40:804-810.

Johnson J, Nowicki MO, Lee CH, Chiocca EA, Viapiano MS, Lawler SE, and Lannutti JJ. Quantitative analysis of complex glioma cell migration on electrospun polycaprolactone using time-lapse microscopy. Tissue Engineering: Part C 2009;15(4): 531-40

Kane RS, Takayama S, Ostuni E, Ingber DE, Whitesides GM. Patterning proteins and cells using soft lithography. Biomaterials 1999;20:2363-2376

Kay AR, Alfonso A, Alford S, Cline HT, Holgado AM, Sakmann B, Snitsarev VA, Stricker TP, Takahashi M, Wu L-G. Imaging synaptic activity in intact neurotechnique brain and slices with FM1-43 in C. elegans, Lamprey, and Rat. Neuron 1999;24:809-817.

Kim T, Nakagawa T, Kita T, Higashi T, Takebayashi S, Matsumoto M, Kojima K, Sakamoto T, Ito J. Neural connections between embryonic stem cell-derived neurons and vestibular hair cells in vitro. Brain Research 2005;1057:127-133.

Koch P, Kokaia Z, Lindvall O, Brüstle O. Emerging concepts in neural stem cell research: autologous repair and cell-based disease modelling. Lancet Neurol. 2009;8(9):819-29.

Koh W-G, Pishko MV. Fabrication of cell-containing hydrogel microstructures inside microfluidic devices that can be used as cell-based biosensors. Anal Bioanal Chem. 2006;385:1389-1397.

Kuipers SD, Bramham CR. Brain-derived neurotrophic factor mechanisms and function in adult synaptic plasticity: new insights and implications for therapy. Curr Opin Drug Discov Devel. 2006;9(5):580-6.

Kunz-Schughart LA, Freyer JP, Hofstaedter F, Ebner R. The use of 3-D cultures for high-throughput screening: the multicellular spheroid model. J. Biomol. Screen. 2004;9:273-85

Levenberg S, Huang NF, Lavik E, Rogers AB, Itskovitz-Eldor J, Langer R. Differentiation of human embryonic stem cells on three-dimensional polymer scaffolds. Developmental Biology 2003;100(22):12741-12746.

Li N, Tourovskaia A, Folch A. Biology on a chip: Microfabrication for studying the behavior of cultured cells, Crit. Rev. Biomed. Eng. 2003;31:423-488.

Lim JY, Park SI, Oh JH, Kim SM, Jeong CH, Jun JA, Lee KS, Oh W, Lee JK, Jeun SS. Brain-derived neurotrophic factor stimulates the neural differentiation of human umbilical cord blood-derived mesenchymal stem cells and survival of differentiated cells through MAPK/ERK and PI3K/Akt-dependent signaling pathways. J Neurosci Res. 2008;86(10):2168-78.

Lin HJ, O'Shaughnessy TJ, Kelly J, Ma W. Neural stem cell differentiation in a cell–collagen–bioreactor culture system. Developmental Brain Research 2004;153:163-173.

Liu Q, Coulombe M, Dumm J, Shaffer KM, Schaffner AE, Barker JL, Pancrazio JJ, Stenger DA, Ma W. Synaptic connectivity in hippocampal neuronal networks cultured on micropatterned surfaces. Developmental Brain Research 2000;120:223-231

Liu XS, Zhang ZG, Zhang RL, Gregg SR, Meng H, Chopp M. Comparison of *in vivo* and *in vitro* gene expression profiles in subventricular zone neural progenitor cells from the adult mouse after middle cerebral artery occlusion. Neuroscience 2007;146:1053-61.

Lu B. BDNF and activity-dependent synaptic modulation. Learn. Mem. 2003;10:86-98.

Ma W, Liu Q, Jung D, Manos P, Pancrazio JJ, Schaffner AE, Barker JL, Stenger DA. Central neuronal synapse formation on micropatterned surfaces. Developmental Brain Research 1998;111:231-243.

Maeda E, Robinson HPC, Kawana A. The mechanisms of generation and propagation of synchronized bursting in developing networks of cultured neurons. J. Neurosci. 1995;15(10):6834-6845.

Mahoney MJ, Anseth KS. Three-dimensional growth and function of neural tissue in degradable polyethylene glycol hydrogels. Biomaterials 2006;27:2265-2274.

Mao C, Kisaalita WS. Characterization of 3-D collagen hydrogels for functional cell-based biosensing. Biosensors and Bioelectronics 2004;19:1075-1088.

Marchetto MCN, Winner B, Gage FH. Pluripotent stem cells in neurodegenerative and neurodevelopmental diseases. Human Molecular Genetics 2010 R1-R6

Martinez-Pinna J, Lamas JA, Gallego R. Calcium current components in intact and dissociated adult mouse sympathetic neurons. Brain Res. 2002;951:227-236.

Matthews JA, Wnek GE, Simpson DG, Bowlin GL. Electrospinning of collagen nanofibers. Biomacromolecules 2002;3:232-238.

Merz M, Fromherz P. Silicon chip interfaced with a geometrically defined net of snail neurons. Adv. Funct. Mater. 2005;15(5):739-744.

Meyer T, Teruel MN. Fluorescence imaging of signaling networks. Trends in Cell Biology 2003;13(2):101-106.

Migita S, Tateeishi A, Keinanen K, Haruyama T. Engineered synapse model cell: genetic construction and chemical evaluation for reproducible high-throughput analysis Anal Bioanal chem. 2009;396(3):1153-7

Moe MC, Varghese M, Danilov AI, Westerland U, Ramm-Pettersen J, Brundin L, Svensson M, Berg-John J, Langmoen IA. Multiple progenitor cells from the adult human brain: neurophysiological differentiation to mature neurons. Brain 2005;128:2189-2199.

Mook-Jung I, Hong H, Boo JH, Lee KH, Yun SH, Cheong MY, Joo I, Huh K, Jung MW. Ginsenoside Rb1 and Rg1 improve spatial learning and increase hippocampal synaptophysin level in mice. J Neurosci Res. 2001;63(6):509-15.

Morimoto T, Ohsawa I, TakamuraC, Ishiguro M. Involvement of amyloid precursor protein in functional synapse formation in cultured hippocampal neurons. Journal of Neuroscience Research 1998;51:185-195.

Mueller-Klieser W. The use of 3-D cultures for high-throughput screening: The multicellular spheroid model. Journal of Biomolecular Screening 2004;9(4):273-85.

Nicolau DV, Taguchi T, Taniguchi H, Tanigawa H, Yoshikawa S. Patterning neuronal and glia cells on light-assisted functionalized photoresists. Biosensors & Bioelectronics 1999;14:317-325.

O'Connor SM, Andreadis JD, Shaffer KM, Ma W, Pancrazio JJ, Stenger DA. Immobilization of neural cells in three-dimensional matrices for biosensor applications. Biosensors & Bioelectronics 2000a;14:871-881.

O'Connor SM, Stenger DA, Shaffer KM, Matric D, Barker JL, Ma W. Primary neural precursor cell expansion, differentiation and cytosolic Ca^{2+} response in three-dimenreional collagen gel. Journal of Neuroscience Methods 2000b;102: 187-195.

O'Donovan MJ. The origin of spontaneous activity in developing networks of the vertebrate nervous system. Curr. Opin. Neurobiol. 1999;9:94-104.

O'Shaughnessy TJ, Lin HJ, Ma W. Functional synapse formation among rat cortical neurons grown on threedimensional collagen gels. Neuroscience Letters 2003;340:169-172.

O'Tuathaigh CMP, Babovic D, O'Meara G, Clifford JJ, Croke DT, Waddington JL. Susceptibility genes for schizophrenia: Characterisation of mutant mouse models at the level of phenotypic behaviour. Neuroscience and Biobehavioral 2007;31:60-78

Park TH, Shuler ML. Integration of cell culture microfabrication technology. Biotechnol. Prog. 2003;19:243-253.

Perea G, Araque A. Astrocytes protentiate transmitter release at single hippocampla synapses. Science 2007;317:1083-1086.

Poo MM. Neurotrophins as synaptic modulators. Nature Rev. Neurosci. 2001;2:24-32.

Pozzo-Miller LD, Gottschalk W, Zhang L, McDermott K, Du J, Gopalakrishnan R, Oho C, Sheng Z, Lu B. Impairments in high-frequency transmission, synaptic vesicle docking, and synaptic protein distribution in the hippocampus of BDNF knockout mice. The Journal of Neuroscience 1999;19(12):4972-4983.

Pyle JL, Kavalali ET, Choi S, Tsien RW. Visualization of synaptic activity in hippocampal slices with FM1-43 enabled by fluorescence quenching. Neuron 1999;24:803-808.

Qu Y, Vadivelu S, Choi L, Liu S, Lu A, Lewis B, Girgis R, Lee CS, Snider BJ, Gottlieb DI, McDonald JW. Neurons derived from embryonic stem (ES) cells resemble normal neurons in their vulnerability to excitotoxic death. Experimental Neurology 2003;1(184):326-336.

Radad K, GilleG, Liu L, Rausch W. Use of ginseng in medicine with emphasis on neurodegenerative disorders. J Pharmacol Sci 2006; 100: 175-86.

Rudakewich M, Ba F, Benishin CG. Neurotrophic and neuroprotective actions of ginsenosides Rb1 and Rg1. Planta Med 2001;67(6):533-7

Sah DWY, Ray J, Gage FH. Regulation of voltage-gated- and ligand-gated currents in rat hippocampal progenitor cells in vitro. Int. J. Neurobiol. 1997;32:95-110.

Sanchez AL, Matthews BJ, Meynard MM, Hu B, Javed S, Cohen-Cory S. BDNF increases synapse density in dendrites of developing tectal neurons *in vivo*. Development 2006;133:2477-2486.

Serpinskaya AS, Feng G, Sanes JR, Craig AM. Synapse formation by hippocampal neuronsfrom agrin-deficient mice. Developmental Biology 1999;205:65-78.

Shen LH, Zhang JT. Ginsenoside Rg1 promotes proliferation of hippocampal progenitor cells. Neurol Res. 2004;26(4):422-8

Shi Q, Hao Q, Bouissac J, Lu Y, Tian S, Luu B. Ginsenoside-Rd from Panax notoginseng enhances astrocyte differentiation from neural stem cells. Life Sciences 2005; 76: 983-95.

Shi Y. Induced pluripotent stem cells, new tools for drug discovery and new hope for stem cell therapies. Curr Mol Pharmacol. 2009;2(1):15-8.

Shin S, Dalton S, Stice SL. Human motor neuron differentiation from human embryonic stem cells. Stem Cells and Development 2005;14:1-4.

Südhof TC, Jahn R. Proteins of synaptic vesicles involved in exocytosis and membrane recycling. Neuron 1991;6(5):665-677.

Suzuki I, Sugio Y, Moriguchi H, Jimbo Y, Yasuda K. Modification of a neuronal network direction using stepwise photo-thermal etching of an agarose architecture. Journal of Nanobiotechnology 2004;2:7.

Tzeng SF. Neural progenitors isolated from newborn rat spinal cords differentiate into neurons and astroglia. Journal of Biomedical Science 2002;9:10-16.

Tourovskaia A, Figueroa-Masot X, Folch A. Differentiation-on-a-chip: A microfluidic platform for long-term cell culture studies. Lab on a Chip 2005;5:14-19.

Vogt AK, Wrobel G, Meyer W, Knoll W, Offenhauser A. Synaptic plasticity in micropatterned neuronal networks. Biomaterials 2005;26:2549-2557.

Walsh K, Parks G. Changes in cardiac myocyte morphology alters properties of voltage-gated ion channels. Cadiovas. Res. 2002;55:64-75.

Wang H, Wesin L, Nong Y, Birnbaum S, Bendor J, Brismar H, Nestler E, Aperia A, Flajolet M, Greengard P. Norbin is an endogenous regulator of metabotropic glutamate receptor 5 signaling. Science 2009;326:1554-1557

Wang L, Wu Z-Z, Xu B, Zhao Y, Kisaalita WS. SU-8 microstructure for quasi-three-dimensional cell-based biosensing. Sensors and Actuators 2009;140(2):349-55

Weaver VM, Petersen OW, Wang F, Larabell CA, Briand P, Damsky C, Bissel MJ. Reversion of the malignant phenotype of human breast cells in three-dimensional culture and *in vivo* by integrin-blocking antibodies. J. Cell Biol. 1997:137(1):231-245.

Weibel DB, DiLuzio WR, Whitesides GM. Microfabrication. Nature 2007;5:209-218

Wolf K, Mazo I, Leung H, Engelke K, Andrian U, Deryugina EI, Strongin AY, Bröcker E, Friedl P. Compensation mechanism in tumor cell migration : mesenchymal–amoeboid transition after blocking of pericellular proteolysis. The Journal of Cell Biology 2003;160(2):267-277

Wu Z-Z, Zhao YP, Kisaalita WS. Interfacing SH-SY5Y human neuroblastoma cells with SU-8 microstructures. Colloids and Surfaces B: Biointerfaces 2006;52:14-21.

Xue J, Liu Z, Hu J, Chen H, Zhang J, Chen N. Ginsenoside Rb1 promotes neurotransmitter release by modulating phosphorylation of synapsins through a cAMP-dependent protein kinase pathway. Brain Research 2006; 1106(1): 91-98.

Yousaf MN, Houseman BT, Mrksich M. Using electroactive substrates to pattern the attachment of two different cell populations. PNAS 2001;98(11):5992-5996.

Zhuang P, Zhang Y, Pang T. Proliferation effect of neural stem cell of ginsenoside Rg1 in vitro. Zhongguo Zhong Yao Za Zhi 2009;34(4):443-6

Zhang S, Yan L, Altman M, Lassle M, Nugent H, Franke F, Lauffenburger DA, Whitesides GM, Rich A. Biological surface engineering: a simple system for cell pattern formation. Biomaterials 1999;20:1213-1220.

CHAPTER 3

SU-8 MICROSTRUCTURE FOR QUASI-THREE-DIMENSIONAL CELL-BASED BIOSENSING*

Keywords: SU-8 microstructure; SH-SY5Y cell; Voltage-gated calcium channel function; Three-dimensional cell-based biosensor; Fluorescence

* Wang L., Wu Z.-Z., Xu B., Zhao Y. and Kisaalita W.S., 2009. SU-8 microstructure for quasi three-dimensional cell-based biosensing *Sensors and Actuators* 140(2):349-355.
Reprinted here with permission of publisher.

3.1. Abstract

A quasi-three-dimensional (quasi-3-D) cell-based biosensor platform microfabricated from SU-8 has been developed and characterized. In this work, SH-SY5Y human neuroblastoma cells were integrated with SU-8 microfabricated microwells with diameters of 100µm. SH-SY5Y cells were differentiated with 1mM dibutyryl cAMP and 2.5 µM 5-bromodeoxyuridine. Voltage-gated calcium channel (VGCC) function of SH-SY5Y cells cultured within the microwells (quasi-3-D) versus those cultured on the SU-8 planar substrates (2-D) was evaluated by confocal microscopy with a calcium fluorescent indicator, Calcium Green-1. In response to 50 mM high K^+ depolarization, cells in microwells were less responsive in terms of increase in intracellular Ca^{2+} in comparison to cells on 2-D substrates. This study shows that VGCC function of cells within SU-8 microwells was indeed different from that of cells on planar SU-8 surfaces, suggesting that SU-8 microstructure did affect SH-SY5Y cell differentiation with respect to VGCC function and that high-aspect-ratio microstructures are not merely "folded" 2-D structures. Furthermore, these results are consistent with previous 2-D/3-D comparative studies carried out in polymer scaffolds and support the hypothesis that cell calcium dynamics on 2-D substrates may be exaggerated. Overall, this work is supportive of SU-8 micropattern as a viable platform for engineering a quasi-3-D cell culture system for cell-based biosensing against drugs for VGCCs.

3.2. Introduction

Unlike molecular biosensors which use isolated enzymes, antibodies or nucleic acids, cell-based biosensors employ the whole cell as the sensing element and thus can provide

information in terms of whole cell response [1]. In accelerated drug discovery, cell-based biosensors play an important role by providing functional and analytical information which is more accurate and physiologically relevant than what molecular biosensors can offer [2-3]. Thus, a cell-based assay can well bridge the gap between pure *in vitro* systems and *in vivo* test. With the development of fluorescence based technologies and their implementation in high-throughput screening (HTS) systems (e.g., fluorometric imaging plate reader (FLIPR) molecular device), cellular assay based on fluorescence imaging has proven to be an invaluable tool in drug discovery. However, in the application of cell-based biosensors, cells are cultured on two-dimensional (2-D) flat surfaces [4-5], which is contrary to how cells grow *in vivo* where extracellular matrix provides a three-dimensional (3-D) environment. This raises the issue of *in vivo-in vitro* differences from cell morphology to cell functions and further to gene expression. It has been hypothesized that cell function on 2-D surfaces may be an exaggeration of that *in vivo* [6], which necessitates investigating 3-D cell culture systems [7] and calls for 2-D/3-D comparative study for the purpose of biosensor application [8-9].

Polymers, such as collagen hydregels [10-12], N-(2-hydroxypropyl)-methacrylamide (HPMA) copolymer hydrogels [13], poly(lactic-co-glycolic acid) (PLGA), and poly(L-lactic acid) (PLLA) [14], have been applied as scaffolds to study cell growth, proliferation, differentiation as well as cell function in 3-D environments. To apply cell-based biosensors in screening drugs against voltage-gated calcium channels (VGCCs), Mao et al. [8] and Desai et al. [9] conducted comparative studies of VGCC function of cells in 3-D collagen and on 2-D surfaces and their results showed 2-D/3-D differences with respect to cell function. However, these polymers have several limitations. First, it is difficult to guarantee precise

control of the aspect ratio (height over width) with these structures. Second, limited mass transportation in scaffolds affects nutrient supply, waste drainage and drug exposure. Third, the properties of polymer scaffolds may limit the extent to which optical or electrical detection may be applicable.

Microfabrication, which can produce a miniaturized, inexpensive platform for "cell-culture-on-a-chip", can be an ideal way to engineer a quasi-3-D environment for cell culture [15]. In comparison with other 3-D cell culture systems formed from polymers, microfabricated patterns have many advantages. First, the technique has been well developed. The aspect ratio can be well controlled in fabrication process and the fabrication of microstructures can be scaled up to meet the need of HTS. Second, cells can be easily seeded in these patterns and integrated with optical as well as bioelectrical analytical methods [16-17]. Third, unlike cells embedded in collagen, cells cultured in microstructures are better exposed to growth media and drug supply; thus the mass transfer limitation problem can be minimized in the microfabricated patterns, which is an essential aspect in HTS. In addition, these platforms can allow precise control of the environment surrounding individual cells and they have been used to study physiologic and pharmacologic responses at the single-cell level. On-chip individual-cell-based cultivation system from Yasuda's lab has been reported to study single cell growth and division dynamics [18] as well as cell-to-cell communication effects in cell group class [19]. Microfabricated structures are gaining popularity for studies of microbiology [20] and cellular biology [21-25]. They have become powerful platforms for studying cell fate *in vitro* [26-27]. However, most of these microstructures are low-aspect

ratio, which have been considered as 2-D systems. Thus we proposed to fabricate high-aspect-ratio microstructures to mimic 3-D microenvironments for cell integration.

In this study, SU-8 was chosen to fabricate microwells with diameters of 100 µm. These micropatterns provided high-aspect-ratio structures for cell culture. SU-8, which is epoxy based negative photoresist, can form a film with a thickness from 1µm to 200µm with the spin coating processes. Films can be processed with photolithography to pattern high-aspect-ratio (>20) structures with high optical transparency, straight sidewalls, and excellent thermal stability. SU-8 is wildly used in fabrication of microfluidics and microelectromechanical system (MEMS) parts [28-30]. Also, SU-8 microstructure is considered a novel platform for integrating with cell culture and studying cell fate *in vitro* [22, 31]. In the present work, SH-SY5Y human neuroblastoma cells were integrated with SU-8 microwells and differentiated with 1mM dibutyryl cAMP and 2.5 µM 5-bromodeoxyuridine. Because of their importance in the central nervous and cardiovascular systems, VGCCs are becoming popular drug targets in the drug discovery. The measurement of intracellular calcium fluxes in real time is widely applied within the pharmaceutical industry to measure the activation of VGCCs. For the development of a cell-based biosensor toward screening drugs against VGCC targets, we evaluated VGCC response of SH-SY5Y cells by confocal microscopy with a calcium fluorescent indicator, Calcium Green-1. Intracellular Ca^{2+} dynamics of SH-SY5Y cells cultured in microwells versus on 2-D substrates as a control group were compared. The goal was to explore the effects of the microstructure on cell function with respect to VGCC functionality and provide a proof-of-concept for quasi-3-D cell-based assay for VGCCs.

3.3. Materials and methods

3.3.1. Fabrication of SU-8 microstructure

Flat SU-8 substrates and microwell structures were fabricated on 25-mm coverslips (Fisher Scientific, Pittsburgh, PA, USA). Before fabrication, the coverslips were cleaned with 20% sulfuric acid and then baked at 110 ◦C for at least 3 h. SU-8 (2025, MicroChem, Newton, MA, USA) was spun onto the glass substrate at a speed of 1000 rpm for 30 s. 25% (w/v) photoresist was used to achieve flat SU-8 surfaces, and the coating thickness was approximately 1.5 µm [15]. 69% (w/v) SU-8 was used for fabricating microwell structures and the resulting coating thickness was about 70–150 µm [15], depending on the processing conditions. Then the SU-8 coated coverslips were soft baked, first at 65 ◦C for 3 min and then at 95 ◦C for up to 30 min. After baking, SU-8 was exposed in soft contact mode with a Karl Suss MJB 3 HP Mask Aligner using 365 nm UV at 10 mW for four successive 15 s, interrupted for at least 20 s. No mask was used to expose the whole surface area of the flat SU-8 substrates while a chromium mask was used to fabricate the microwell patterns. Patterns and their nominal structure dimensions used in this study included 100 µm wells with a center-to-center spacing of 110 µm, and 100 µm wells with 10 µm wide channel connection. After exposure, the SU-8 coating was baked again, first at 65 ◦C for 3 min and then at 95 ◦C for 9 min before development. Patterns were developed with SU-8 developer (MicroChem, Newton, MA) for 14 min and then briefly immersed in isopropyl alcohol (Fisher Chemicals, Fairlawn, NJ) before drying with nitrogen. Finally, the patterns were hard baked at 120 ◦C for at least 30 min. Samples were sterilized by immersion in 70% ethanol in

distilled water (DI) under a UV germicidal lamp overnight, rinsed in sterile DI water 3 times and stored wet until need.

3.3.2. Atomic force microscopy

To characterize SU-8 surface topography and confirm the poly-L-lysine coating on the substrates, we used a PicoPlus-SPM (Agilent-Molecular Imaging) system for AFM imaging of the planar SU-8 surface itself as well as the bulk region of poly-L-lysine coating of the 2-D substrates. Silicon tips were used. Acoustic AC mode (AAC) was applied to obtain high resolution topographic images to overcome problems due to friction, adhesion and electrostatic forces that are normally experienced with Contact mode AFM. In AAC mode, cantilever oscillation is accomplished by indirect vibration, in which the cantilever is excited by high frequency acoustic vibration from a piezoelectric transducer attached to the cantilever holder. Tip-sample force interactions cause changes in amplitude, phase and the resonance frequency.

3.3.3. Cell line and cell culture

SH-SY5Y human neuroblastoma cells were obtained from ATCC and routinely cultured in 75-cm^2 tissue culture flasks (Costar, Corning, NY) with the growth medium in a 10% CO_2 humidified air at 37 ◦C. The growth medium was made with Eagle Minimum Essential Medium (MEM) containing 10% heat inactivated fetal bovine serum (FBS), 2.2 g/L sodium bicarbonate, 2 mM l-glutamine and 1 mM sodium pyruvate [8-9]. At 75% confluence, the cells were detached by mechanically pipetting and re-suspended in growth medium for plating. Before plating, SU-8 microwell patterns and flat substrates were coated with poly-L-lysine for at least 1 hour to enhance the cell attachment. Then these flat substrates and

microstructure pattens were washed with growth media twice. Approximately 5×10^5 cells were plated on each patterned substrate or flat substrate in growth medium, which was contained in a 35 mm Petri dish (FALCON, Becton Dickinson Labware, NJ). On the second day after plating, referred to as day 0 into differentiation hereafter, the medium was changed from growth medium to differentiation medium. The differentiation medium was comprised of MEM with 5% FBS, 2.2 g/L sodium bicarbonate, 2 mM l-glutamine, 1 mM sodium pyruvate, 1 mM dibutyrylcAMP (dcAMP) and 2.5 µM 5-bromodeoxyuridine (BrdU) [8-9]. Differentiation medium was changed daily.

3.3.4. Fluorescence staining and fluorescent microscopy

SH-SY5Y cells were stained with calcein AM (Biotium, Hayward, CA). This fluorescent dye stains living cells and their extensions by the presence of intracellular esterase activity, which converts the non-fluorescent cell-permeant calcein AM to intensely fluorescent calcein. Cells were washed with 2 mL phosphate-buffered saline (PBS) three to five times. Then cells were exposed to 2 ml 2-µM calcein AM in PBS and incubated for 30 min at 37 ˚C before the staining solution was replaced. Samples were washed with PBS 3 times. Sample fluorescence was captured with a B-2E/C FITC filter block (Nikon, Melville, NY, USA), which has an excitation bandwidth of 465-495 nm and a filter pass range of 515-555 nm.

3.3.5. Scanning electron microscopy (SEM)

Cells on SU-8 patterns were fixed with 2% glutaraldehyde in 0.1M sodium cacodylate buffer, pH 7.2 for 1 h before rinsing in cacodylate buffer (without glutaraldehyde) three times, 15 min each. This was followed by post-fixing with 1% OsO_4 in 0.1M sodium cacodylate

buffer for 1 h and rinsing in cacodylate buffer (without OsO4) three times, 5 min each. The samples were then dehydrated successively in 30, 50, 70, 80, 95 and 100% ethanol for 10 min each and dried in a SAMDRI-780A critical point drier (Tousimis Research Corporation, Rockville, MD, USA). Patterns were sputter-coated with gold for 60 s to achieve a coating thickness of about 15.3 nm. SEM images were captured with LEO 982 scanning electron microscope (LEO Electronenmikroskopie GmbH Korporation, Germany) with an acceleration voltage of 5 kV, using either the regular detector or in-lens detector.

3.3.6. Evaluation of the VGCC functionality

VGCC functionality was evaluated with the dynamics of calcium influx in response to high K^+ (50 mM) depolarization. The membrane permeable fluorescent dye, Calcium Green-1, acetoxymethylester (AM) (Molecular Probes, Eugene, OR), was used to visualize the calcium influx dynamics. The fluorescent intensity was measured by a confocal imaging system (PCM-2000, Nikon) linked to an inverted (TE300, Nikon) microscopy and a 60× Aprochromat, oil –immersion, high-numerical aperture (1.4) objective lens. On days 2 and 8 into differentiation, cells on either flat substrates or in microwell structures were washed with HBS twice and loaded with 5 µM Calcium Green-1 AM in 1 ml of HBS containing 3% heat inactivated FBS and 0.02% Pluronic F-127 (Molecular Probes, Eugene, OR) for 1 h at 37 ◦C in a 10% CO_2 humidified incubator. Cells were then washed twice with HBS and incubated with 1 ml HBS at 37 ◦C in the 10% CO_2 humidified incubator for another hour to allow complete dye de-esterification. Calcium Green-1 was excited with 488 nm argon laser and the emission was captured through a 515 nm long-pass filter. Confocal images were continuously captured at a rate of 1 frame per 3 s. While images were being captured, cells were

depolarized by adding 100 µl of high K^+ HBS (500 mM) to achieve a final K^+ concentration of 50 mM (along with 130 mM Na^+ in HBS). Functional VGCCs were demonstrated by cytosolic calcium concentration increase upon depolarization. This intracellular calcium dynamics was reflected by changes in relative intracellular Calcium Green-1 fluorescence intensities, which were plotted as average gray level units.

3.3.7. Data analysis and statistics

Student's t-test was used for statistical comparisons of calcium response magnitudes.

3.4. Results and discussion

3.4.1. SU-8 structures for culturing cells

In the present study, planar SU-8 substrates were used to culture SH-SY5Y cells in monolayer, as a 2-D control for the SU-8 microwells. Both the planar surfaces and the microwells were coated with poly-L-lysine. Fig. 3.1 (a) shows an AFM image of the planar SU-8 surface. The surface is smooth and no geometric structures can be observed. Poly-L-lysine has been applied to patten silicon surface for directing neural cell growth [32] and deposization of poly-L-lysine has been observed on mica surface with Au-nanoparticles [33]. Fig. 3.1 (b) shows an AFM image of the bulk region of poly-L-lysine coating of the 2-D substrates. This image shows that poly-L-lysine covered the substrate homogeneously and uniformly with a felt-like structure of deposited molecules. Detailed structure of coating can be viewed from the geometric coating image (Fig. 3.1 (c)). In Fig. 3.1 (c), poly-L-lysine molecule nanoparticles randomly deposited on the substrate.

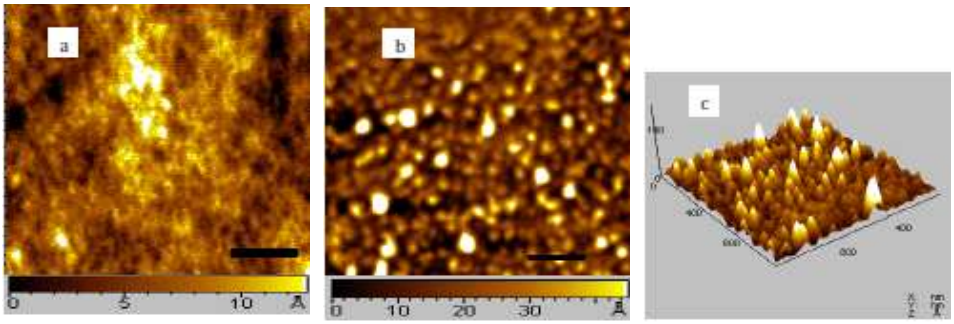

Figure 3.1. AFM images of SU-8 surface (a) and SU-8 surface coated with poly-L-lysine (b) with its geometric structure (c). In (c), the units for X and Y axes are in nanometers, while for Z axis the units are in anstrons. Bar = 200 nm.

For SH-SY5Y cell integration, SU-8 patterns with a diameter of 100 µm were used in this study. Fig. 3.2 (a) shows the representative microwell structure without channels and Fig. 3.2 (b) shows SH-SY5Y cells cultured in a 100 µm (diameter) pattern on day 8 into differentiation. Fig. 3.2 (c) and 3.2 (d) showed SH-SY5Y cells in microwells on day 2 into differentiation. Cells attached to the sidewalls, and they formed cellular clusters in the wells. In the phase contrast images (Fig. 3.2 (b) and 3.2 (c)), some of the cells seem out-of-focus because they were not in the same plane; instead, they were distributed in the 3-D space. These observations were confirmed by SEM in Fig. 3.3 (b) and 3.3 (c). For some cells, neurite outgrowth can be observed. The neurite shown in Fig. 3.2 (b) was from one cell which grew in the well, and it extended to the adjacent well. From the network-like cell patterning (Fig. 3.3 (a)) in microwell structures with channels, neurites were observed along the channels (Fig. 3.3 (c)).

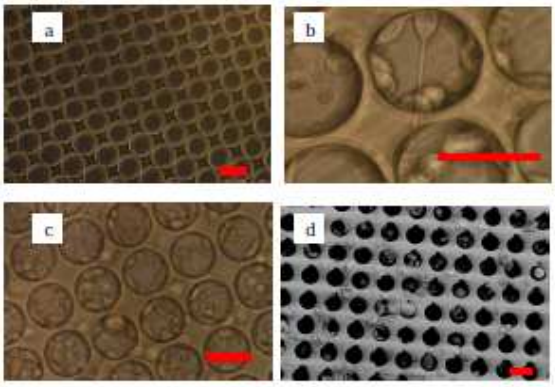

Figure 3.2. Phase contrast and SEM images of 100 µm SU-8 microwell patterns: (a) phase contrast image of patterns without cells; (b) phase contrast image of patterns with SH-SY5Y cells on day 8 into differentiation; (c) phase contrast image of pattern with SH-SY5Y cells on day 2 into differentiation; (d) SEM micrograph of patterns with SY-SY5Y cells on day 2 into differentiation . Bar = 100 µm.

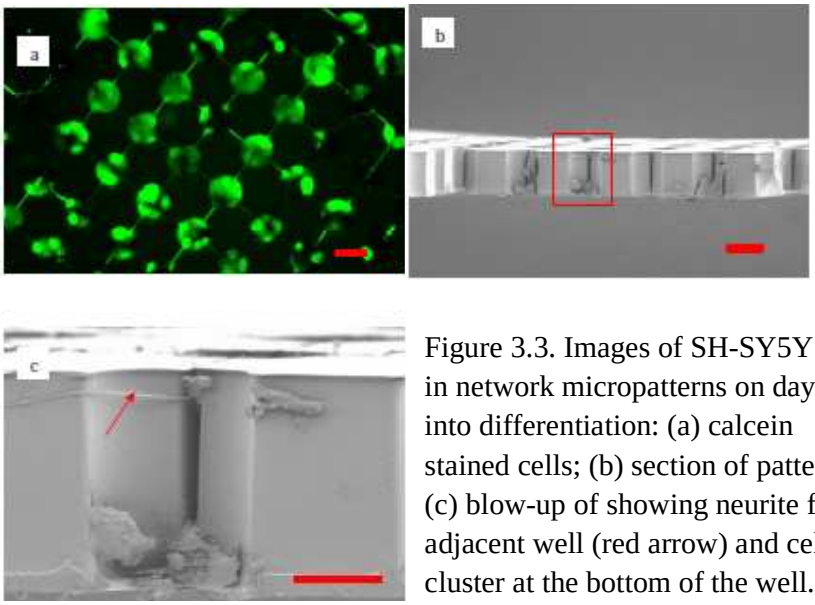

Figure 3.3. Images of SH-SY5Y cells in network micropatterns on day 8 into differentiation: (a) calcein stained cells; (b) section of patterns; (c) blow-up of showing neurite from adjacent well (red arrow) and cell cluster at the bottom of the well. Bar = 100 µm in (a) and (b), bar = 50 µm in (c).

3.4.2. VGCC responsiveness evaluation

We evaluated the VGCC function of SH-SY5Y cells cultured in microwells and on 2-D substrate with the dynamics of calcium influx in response to high K^+ (50 mM) depolarization. The membrane permeable fluorescent dye, Calcium Green-1, acetoxymethylester (AM) was used to visualize the calcium influx dynamics. Functional VGCCs were demonstrated by

cytosolic calcium concentration increase upon depolarization. This intracellular calcium dynamics was reflected by changes in relative intracellular Calcium Green-1 fluorescence intensities, which were plotted as average gray level units. Fig. 3.4 shows a typical cell and time course of the change in Calcium Green-1 fluorescent intensity for responsive and non-responsive cells upon stimulation with high K^+. The insets are confocal images showing the fluorescence changes in the stimulation process. Fig. 3.5 shows representative plots of response to high K^+ stimulation on day 8 into differentiation for cells cultured on 2-D substrates (Fig. 3.5 (a)) versus cells in microwells (Fig 3.5 (b)). Fig 3.5 qualitatively shows that cells on 2-D substrates had a larger response magnitude than cells in microwells.

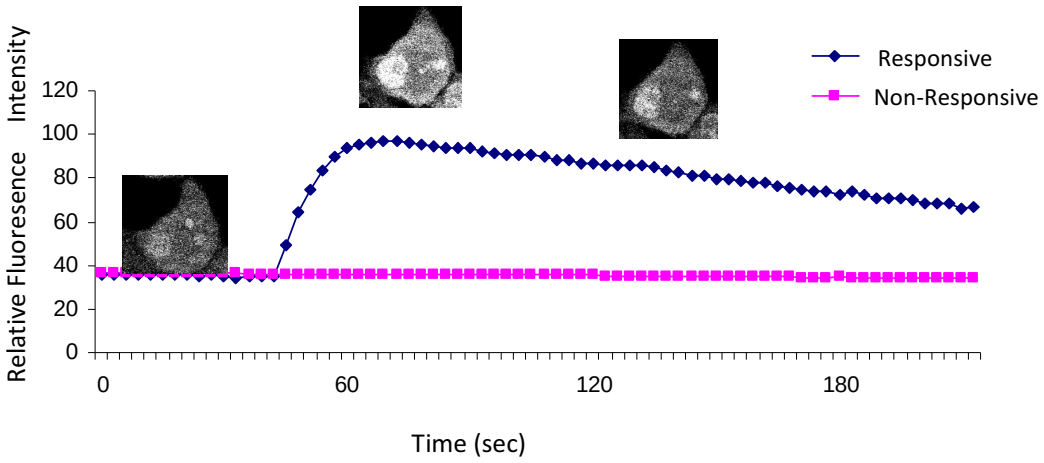

Figure 3.4. High K^+ evoked calcium transients in SH-SY5Y cells. Typical plot of changes in relative intracellular Calcium Green-1 fluorescence intensities for responsive and non-responsive cells on 2-D SU-8 substrates at day 2 into differentiation. The responsive cell was from the data pool of 67 cells measured in Table 1. Inset: Confocal images of the cell on 2-D SU-8 substrates at day 2 into differentiation. Images show fluorescence intensity changes before depolarization, 20 s and 100 s after depolarization.

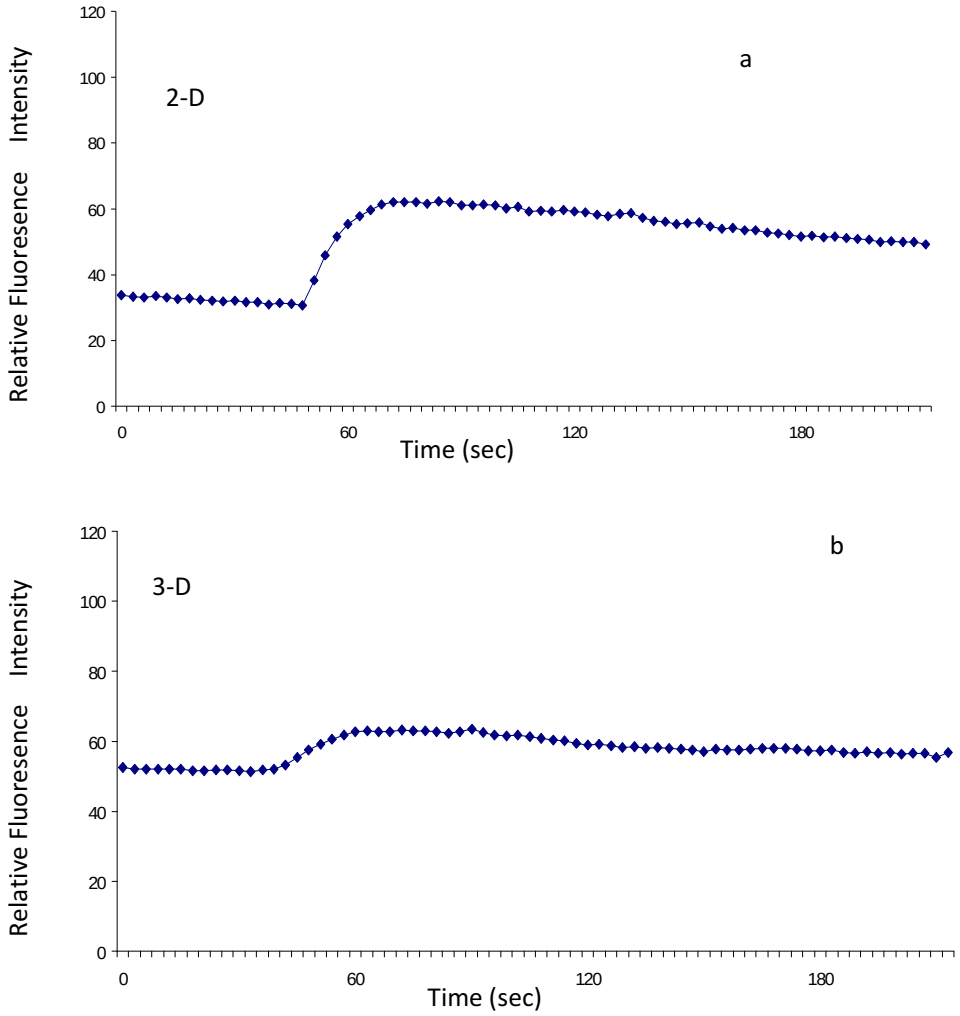

Figure 3.5. Typical plots of changes in relative intracellular Calcium Green-1 fluorescence intensities for cells on 2-D SU-8 substrate (a) and 3-D microwell (b) at day 8 into differentiation. The cells in (a) and (b) are from the data pool of 67 and 23 cells, respectively (Table 1). Cells were stimulated by high K^+ depolarization with HBS containing 50 mM K^+. Qualitatively, cells on 2-D SU-8 substrates had a higher response magnitude than cells in 3-D SU-8 microwells. Baseline drift is an indication that cells were not at "steady state", which is common.

A cell was only considered responsive when it showed an increase in Calcium Green-1 fluorescent intensity of 15% or higher over the basal fluorescent intensity level. The magnitude of the response from each cell was expressed as a peak fractional increase over basal fluorescence intensity. Table 3.1 summarizes the percentage of responsive cells and magnitudes of VGCC responsiveness (intracellular Ca^{2+} increase) to high K^+ HBS in

SH-SY5Y cells cultured in microwells versus on 2-D substrates. As shown in Table 1, it is clear that 100% of the cells on 2-D SU-8 substrates were responsive to high K^+ HBS on days 2 and 8 into differentiation. For cells in microwells, the percentage of responsive cells was 35% on day 2 and decrease to 31% on day 8. Also, cells on 2-D substrates had a larger VGCC response magnitude than cells in microwells on both days 2 and 8 into differentiation ($p < 0.05$). As shown, cells on 2-D substrates had a response magnitude of approximately 1. For cells in microwells, the response magnitude was approximately 1/3. In addition, a similar decrease of the response magnitudes was observed from day 2 to day 8 into differentiation for cells on 2-D SU-8 substrates as well as in microwells ($p < 0.05$).

Table 3.1 Percentage of responsive cells and magnitude of VGCC responsiveness to 50 mM K^+ stimulation in dcAMP and BrdU differentiated SH-SY5Y cells

	3-D SU-8 Microwells coated with poly-L-lysine		2-D SU-8 Substrates coated with poly-L-lysine	
	Percentage	Magnitude (mean±S.D.)	Percentage	Magnitude (mean±S.D.)
Day2	14/40=35%	0.32±0.11(n=14)*	67/67=100%	1.40±0.50(n=67)
Day8	9/29=31%	0.24±0.06(n=9)* #	23/23=100%	1.01±0.31(n=23)#

A cell was only considered responsive when it showed an increase in Calcium Green-1 fluorescent intensity of 15% or higher over the basal fluorescent intensity level. The percentage is expressed as: (number of responsive cells)/(total number of cells measured) = percentage of responsive cells.

* Values that are significantly different from those for cells on 2-D SU-8 substrates ($p<0.05$).
# Values that are significantly different from those for cells on day 2 into differentiation ($p < 0.05$)

These results are at odds with the suggestion that microwells are merely “folded” 2-D structure and are not likely to affect cellular function. So this study provides evidence that

VGCC function of cells in SU-8 microwells was indeed different from that of cells on planar SU-8 surfaces, which suggest that SU-8 microstructure did affect SH-SY5Y cell differentiation with respect to VGCC function. It has been speculated that cellular function in 2-D is probably an exaggeration of that in 3-D and probably *in vivo* situation [34]. Results in the present study and previous studies in our lab [8,9, 31] are consistent with this speculation. In a previous study with SH-SY5Y cells in collagen hydrogels and Cytodex microbead arrays, the magnitudes of VGCC response of differentiated cells on 2-D substrates were higher than those of cells in 3-D scaffolds. Thus this work is supportive of SU-8 micropattern as a viable platform for engineering quasi-3-D cell culture systems.

The differences between the VGCC function of cells in 3-D pattern and on 2-D surfaces may be due to the cell shape change which is introduced through microstructure. Though, the mechanism by which cells transduce changes in cell geometry into different biochemical responses remains unclear, it is known that cell morphology affects cell growth, cell differentiation as well as cell function and cell death [35-38]. Lascola et al. [35] observed cell morphology dependent whole-cell chloride currents in rat astrocytes. To control the cell shape, Parker et al. [37] and McBeath et al. [38] cultured cells on extracellular matrix coated adhesive islands of defined shape and size at the micrometer scale. However, these relatively simple geometric systems only provided a 2-D surface for controlling cell shape and imposed only limited strain on cell shape and dimension. To probe the extent of shape control, it is necessary to challenge cells with a more demanding geometry. Circular 3-D micropatterns fabricated in polymethylmethacrylate were applied to study fibroblasts growth and showed that the patterns in cellular dimention effectively retard fibroblasts invasion [39]. A packed

Cytodex 3 microbead array was fabricated for SH-SY5Y cells [31]. In these studies, not only cell shape change was observed, but also cell function change was observed.

Even a neural network-like patterning was achieved by integrating SH-SY5Y cells in the SU-8 microwells with microchannels, SH-SY5Y cells do not form synaptic connection, which suggests that more appropriate candidate cells are needed. In follow-up studies, we will extend our investigation to neural stem cells to engineer 3-D neural networks.

3.5. Conclusion

Microwell structures were fabricated using SU-8 photoresist for cell-based biosensing application. The microfabrication technique has been well developed and the microstructures' architecture can be well-controlled. The SU-8 platform is transparent and stable, which enables it to be well integrated with optical, biochemical and electrical measurement techniques. SH-SY5Y human neuroblastoma cells were successfully integrated into SU-8 microwells and VGCC function of SH-SY5Y cells on 2-D substrates and in microwells were evaluated. The responsiveness to high K^+ depolarization for cells on quasi-3-D scaffolds was significantly lower than that on 2-D substrates. This result shows that SU-8 microstructure did affect SH-SY5Y cell differentiation with respect to VGCC function and also shows that high-aspect-ratio microstructure is not merely "folded" 2-D structure. This is in agreement with previous 2-D/3-D comparative studies carried out in polymer scaffolds, and supports the speculation that 2-D cell functions may represent an exaggeration of those *in vivo*. Overall, this work demonstrates the feasibility of using SU-8 microfabricated pattern as a platform for the development of quasi-3-D cell-based biosensors.

3.6 References:

[1] J. J. Pancrazio, J. P. Whelan, D. A. Borkholder, W. Ma, D. A. Stenger, Development and Application of Cell-Based Biosensors, Annals of Biomedical Engineering 27(1999) 697-711.

[2] L. Bousse, Whole cell biosensors, Sensors and Actuators B, 34(1996) 270-275.

[3] K. Durick, P. Negulescu, Cellular biosensors for drug discovery, Biosensors and Bioelectronics 16(2001) 587-592.

[4] G.W. Gross, A. Harsch, B.K. Rhoades, W. Gopel, Odor, drug and toxin analysis with neuronal networks in vitro: extracellular array recording of network responses. Biosensors and Bioelectronics 12 (1997) 373-393.

[5] J.J. Pancrazio, P.P. Bey Jr, D.S. Cuttino, J.K. Kusel, D.A. Borkholder, K.M. Shaffer, G.T.A. Kovacs, D.A. Stenger, Portable cell-based biosensor system for toxin detection, Sensors and Actuators B 53 (1998) 179-185.

[6] E. Cukierman, R. Pankov, K.M. Yamada, Cell interactions with three-dimensional matrices, Current Opinion in Cell Biology 14(2002) 633-639.

[7] D.A. Stenger, G.W. Gross, E.W. Keefer, K.M. Shaffer, J.D. Andreadis, W. Ma, J.J. Pancrazio, Detection of physiologically active compounds using cell-based biosensors, Trends in Biotechnology 19(2001) 304-309.

[8] C. Mao, W.S. Kisaalita, Characterization of 3-D collagen hydrogels for

functional cell-based biosensing, Biosensors and Bioelectronics 19(2004) 1075-1088.

[9] A. Desai, W.S. Kisaalita, C. Keith, Z.-Z. Wu, Human neuroblastoma (SH-SY5Y) cell culture and differentiation in 3-D collagen hydrogels for cell-based biosensing , Biosensors and Bioelectronics, 21(2006) 1483-1492.

[10] S.M. O'Connor, J.D. Andreadis, K.M. Shaffer, W. Ma, J.J. Pancrazio, D.A. Stenger, Immobilization of neural cells in three-dimensional matrices for biosensor applications, Biosensors and Bioelectronics 14(2000) 871-881.

[11] H.J. Lin, T.J. O'Shaughnessy, J. Kelly, W. Ma, Neural stem cell differentiation in a cell-collagen-bioreactor culture system, Developmental Brain Research 153(2004) 163-173.

[12] D.R. Albrecht, G.H. Underhill, T.B. Wassermann, R.L. Sah, S.N. Bhatia, Probing the role of multicelllular organization in three-dimensional microenvironments, Nature Methods 3(2006) 369-375.

[13] S. Woerlya, G.W. Plant, A.R. Harvey, Cultured rat neuronal and glial cells entrapped within hydrogel polymer matrices: a potential tool for neural tissue replacement, Neuroscience Letters 205(1996) 197-201.

[14] S. Levenberg, N.F. Huang, E. Lavik, A.B. Rogers, J. Itskovitz-Eldor, R. Langer, Differentiation of human embryonic stem cells on three-dimensional polymer scaffolds, Developmental Biology 100 (2003) 12741-12746.

[15] Z.-Z. Wu, Y.P. Zhao, W.S. Kisaalita, Interfacing SH-SY5Y human neuroblastoma cells with SU-8 microstructures, Colloids and Surfaces B: Biointerfaces 52 (2006) 14-21.

[16] S.Y. Li, J.J. Ramsden, J.E. Prenosil, E. Heinzle, Measurement of Adhesion and Spreading Kinetics of Baby Hamster Kidney and Hybridoma Cells Using an Integrated Optical Method, Biotechnology Progress 10(1994) 520-524

[17] J.J. Ramsden, S.Y. Li, E. Heinzle, J.E. Prenosil, Optical Method for Measurement of Number and Shape of Attached Cells in Real Time, Cytometry 19(1995) 97-102.

[18] Y. Wakamoto, J. Ramsden, K. Yasuda, Single-cell growth and division dynamics showing epigenetic correlations, The Analyst 130(2005) 311-317.

[19] Y. Wakamoto, K. Yasuda, Quantitative evaluation of cell-to-cell communication effects in cell group class using on-chip individual-cell-based cultivation system, Biochemical and Biophysical Research Communications 349(2006) 1130-1138.

[20] D.B. Weibel, W.R. DiLuzio, G.M. Whitesides, Microfabrication, Nature 5(2007) 209-218.

[21] T.H. Park, M.L. Shuler, Integration of Cell Culture and Microfabrication Technology, Biotechnology Progress 19(2003) 243-253.

[22] V.I. Chin, P. Taupin, S. Sanga, J. Scheel, F.H. Gage, S.N. Bhatia, Microfabricated Platform for Studying Stem Cell Fates, Biotechnology and Bioengineering. 88 (2004) 399-415.

[23] Tourovskaia, A., Figueroa-Masot, X., Folch, A., Differentiation-on-a-chip: A microfluidic platform for long-term cell culture studies, Lab on a Chip 5(2005) 14-19.

[24] P.J. Hung, P.J. Lee, P. Sabounchi, N. Aghdam, R. Lin, L.P. Lee, A novel high aspect ratio microfluidic design to provide a stable and uniform microenvironment for cell growth in a high throughput mammalian cell culture array, Lab on a Chip 5(2005) 44-48.

[25] C.J. Bettinger, E.J. Weinberg, K.M. Kulig, J.P. Vacanti, Y. Wang, J.T. Borenstein, R. Langer, Three-Dimensional Microfluidic Tissue-Engineering Scaffolds Using a Flexible Biodegradable Polymer, Advanced Materials 189(2006) 165-169.

[26] N.D. Evans, E. Gentleman, J.M. Polak, Scaffolds for stem cells, Materialstoday 9 (2006) 26-33.

[27] P.G. Gross, E.P. Kartalov, A. Scherer, L.P. Weiner, Applications of microfluidics for neuronal studies, Journal of the Neurological Sciences 252(2007) 135-143.

[28] V. Seidemann, J. Rabe, M. Feldmann, S. Buttgenbach, SU8-micromechanical structures with in situ fabricated movable parts, Microsystem Technologies 8(2002) 348-350.

[29] Y.J. Chuang, F.G. Tseng, J.-H. Cheng, W.K. Lin, A novel fabrication method of embedded micro-channels by using SU-8 thick-film photoresists, Sensors and Actuators A 103(2003) 64-69.

[30] G. Voskericiana, M.S. Shivea, R.S. Shawgoc, H. Recumd, J.M. Andersona, M.J. Cimac, R. Langer, Biocompatibility and biofouling of MEMS drug delivery devices, Biomaterials 24(2003) 1959-1967.

[31] Z.-Z. Wu, Y.-P. Zhao, W.S. Kisaalita, A packed Cytodex microbead array for three-dimensional cell-based biosensing, Biosensors and Bioelectronics 22(2006) 685-693.

[32] F. Patolsky, B.P. Timko, G. Yu, Y. Fang, A.B. Greytak, G. Zheng, C.M. Lieber, Detection, stimulation, and inhibition of neuronal signals with high-denstiy nanowire transistor arrays, Science 313(2006) 1100-1104.

[33]F. Patolsky, Y. Weizmann, O. Lioubashevski, I. Willner, Au-Nanoparticle Nanowires Based on DNA and Polylysine Templates, Angewandte Chemie International Edition 41 (2002) 2323-2327.

[34] E. Cukierman, R. Pankov, D.R. Stevens, K.M. Yamada, Taking cell-matrix adhesions to the third dimension. Science 294(2001) 1708-1712.

[35] C.D. Lascola, R.P. Kraig, Whole-cell chloride currents in rat astrocytes accompany changes in cell morphology, The Journal of Neuroscience 16 (1996) 2532-2545.

[36] C. S. Chen, M. Mrksich, Geometric control of cell life and death, Science 276 (1997) 1425-1428.

[37] K.K. Parker, A.L. Brock, C. Brangwynne, R.J. Mannix, N. Wang, E. Ostuni, N.A. Geisse, J.C. Adams, G.M. Whitesides, D.E. Ingber, Directional control of lamellipodia extension by constraining cell shape and orienting cell tractional forces, The FASEB Journal 16(2002) 1195-1204.

[38] R. McBeath, D.M. Pirone, C.M. Nelson, K. Bhadriraju, C.S. Chen, Cell Shape, Cytoskeletal tension, and RhoA regulate stem cell lineage commitment, Developmental Cell 6(2004) 483-495.

[39] F. Sun, Geometric control of fibroblast growth on proton beam-micromachined scaffolds, Tissue Engineering 10 (2004) 267-272.

CHAPTER 4

MICROWELL STRUCTURE-NEURAL STEM CELL PLATFORM FOR SCREENING COMPOUNDS AGAINGST CONNECTIVITY-RELATED TARGETS*

Keywords: Neural stem cell; SU-8; 3D cell culture; Neural network; Cell locomotion; Schizophrenia

* Wang L., Mumaw J., Wu Z.-Z., Xu B., Stice S., Kisaalita W.S.. Microwell structure-neural stem cell platform for screening compounds against connectivity-related targets. *Acta Biomaterialia* (Submitted)

4.1. Abstract

We are interested in developing a cell-based assay platform for screening compounds against neural network connectivity. We first studied the relationship between SU-8 crosslinking reaction and associated cytotoxicity, and established SU-8 microstructure fabrication and surface modification procedures that yielded a biocompatible microsubstrate for human neural stem cell (hNSC) culture. Then hNSCs' interaction with SU-8 microwells was studied. Cell locomotion was studied by time-lapse recording; hNSCs in the microstructures tended to interact with curved well sidewalls or well openings in the absence of other cells, or interact with cells in the neighboring wells in the presence of other cells, and cell-cell interaction was guided by microstructure architecture (e.g. presence of microchannel and microwell). Combining fluorescent dyes and confocal microscopy, cell morphology, cytoskeleton organization and V_m were measured for cells on two-dimensional (2D) flat surface and within SU-8 microstructures. Unlike cells on 2D surface with a spread cell morphology and stress fibers, cells within 50 µm microwells were more round and did not present stress fibers within. Cells within 50 µm microwells developed a more negative V_m than cells on 2D before differentiation. Taken together, microwell architecture affected hNSC morphology, cytoskeleton organization as well as V_m establishment in a quasi-3D manner, which is consistent with other 2D/3D comparison studies. This study moves one step forward in combining hNSCs and microwell structures to form a quasi-3D neural network for drug screening.

4.2. Introduction

Mental and/or neurodegenerative disorders, such as schizophrenia, are among the most devastating illnesses in western society; however, there are few effective drugs for such diseases [1]. Currently used drugs for schizophrenia still have shortcomings [2]; for example, Ziprasidone, a FDA approved drug for treating schizophrenia since 2001, may cause severe side effects such as seizures, irregular heartbeat and so on. Effective drug discovery against these disorders is in great demand, which calls for novel assays for high throughput screening (HTS) of available molecular libraries to identify more effective small molecules as drug leads.

Synaptic function and neurotransmission system (e.g. presynaptic proteins such as synaptophysin, postsynaptic proteins such as MAP2, and N-methyl-D-aspartic acid receptors (NMDARs)), which underlie neural network connectivity, are involved in biological mechanisms for mental and neurodegenerative disorders [3-6]. Studies have shown that distance between the neuronal assemblies communicating with each other affect network oscillation frequency [7], which is an important biomarker for schizophrenia. Susceptible genes for schizophrenia, such as *Dysbindin* [8] and *DISC1* [9, 10] have been associated with network connectivity. Neural networks, which can recapitulate these crucial targets (e.g. synaptophysin, MAP2, NMDARs, *Dysbindin*, and *DISC1*) may act as an effective platform for screening available molecular libraries. Upon drug exposure, the changes in network connectivity are usually compound and concentration specific [11, 12] and depend on the number of synapses per cell, as well as the state of cell maturation [13, 14]. The ability to genetically engineering synaptical model cells [15, 16] and the use of optical detection

methods in most HTS formats makes neural networks formed *in vitro* attractive in drug discovery [17]. However, *in vitro* screening of drugs that affect neural network function *in vivo* is still primitive as current assays rely on single cellular responses from two-dimensional (2D) cell cultures [18]. Three-dimensional (3D) cell-based assays may yield physiologically more relevant results [19-22], and thus have the potential to bridge the gap between 2D assays and preclinical animal testing, saving time and cost by reducing compound attribution. Thus, engineering a 3D neural network platform is an ideal first step in moving toward 3D neural-network-based assay.

Commonly used methods to form neural networks *in vitro* can be categorized into the following three forms: random forming, chemical patterning, and structural guiding. Though randomly formed neural networks provide a useful method for studying the physiology of neurons in a simplified environment, they are not easy to manipulate. Microcontact printing [23] and self-assembled monolayer forming [24] are chemical techniques mainly used to tailor the properties of the substrates for neural network patterning. However, these cells are maintained on 2D substrates. Topographical structures can provide physical guidance for neural network formation *in vitro* and microstructured substrates have long been considered a promising approach for the creation of defined neuronal networks *in vitro.* Unlike chemical patterning, high-aspect-ratio microstructures are thought to provide quasi-3D microenvironments for neural network formation [25, 26]. Microstructures made of polydimethylsiloxane (PMDS) [27] and SU-8 (epoxy-based negative photoresist) [28] have been reported to control neural network formation *in vitro.*

Microstructures provide a novel and powerful cell culture environment for several reasons. Microstructure architecture can be well controlled in the fabrication process, thus providing a reproducible microenvironment for cell culture. In these miniaturized systems, consumption of cells and reagents can be reduced, saving cost in comparison to macroscale assays. In addition, transparent microstructures such as those made from SU-8, are also compatible with both optical and electrical readouts. SU-8 has been wildly used in fabrication of microfluidics and microelectromechanical system (MEMS) parts with high-aspect-ratio, high optical transparency and excellent thermal stability [29, 30]. However, cytotoxicity from SU-8 has limited its applications in cell-based assays [31]. Also, in the few studies using SU-8 microstructures for cell behavior *in vitro*, only primary cells and tumor-derived cells have been successfully integrated in SU-8 microstructures [25, 26, 28, 32].

Our long term goal is to develop a cell-based HTS drug discovery platform comprised of quasi-3D stem cell-derived neural networks housed in interconnected microwells amenable to optical and electrical readout. As a first step, our goal was to answer the question whether 3D microstructure architecture can be used to achieve optimal quasi-3D microenvironment for neural stem cell culture. To answer this question, we first studied the relationship between SU-8 crosslinking reaction and associated cytotoxicity, to establish SU-8 microstructure fabrication and surface modification procedures that yield a biocompatible microstructure suitable for human neural stem cell culture. Next, neural stem cells were integrated with SU-8 microwells, and the cell-microstructured SU-8 material interaction was studied with respect to morphology, cytoskeleton organization and cell locomotion during the first 24

hours of plating to provide a better understanding of the relationship between microstructure architecture and the resultant quasi-3D neural network formation.

4.3. Materials and methods

4.3.1. Fabrication of SU-8 substrates

Flat SU-8 substrates and SU-8 microstructures were fabricated on 25 mm coverslips (Fisher Scientific, Pittsburgh, PA, USA). Before fabrication, the coverslips were cleaned with 20% sulfuric acid and then baked at 110 ◦C for at least 3 h. SU-8 (SU-8 2025, MicroChem, Newton, MA, USA) was spun onto the glass substrate at a speed of 2000 rpm to achieve a thickness of 40 µm. The SU-8 coated coverslips were soft baked, first at 65 ◦C for 3 min and then at 95 ◦C for 9 min. After soft baking, SU-8 was exposed in vacuum contact mode with a Karl Suss MJB 3 HP Mask Aligner using 365 nm UV at 10 mW for 60 s. A chromium mask was used to fabricate the microwell patterns; no mask was used for flat SU-8 substrates when exposed to UV light. Microstructure dimensions used in this study included 50 µm and 100 µm in well diameter; the connecting channels were 50 µm long and 10 µm wide. After exposure, the SU-8 coating was baked (postexpsoure baking) first at 65 ◦C for 3 min and then at 95 ◦C for 9 min. Processed SU-8 film were then developed with SU-8 developer (MicroChem, Newton, MA) for 7 min and briefly immersed in isopropyl alcohol (Fisher Chemicals, Fairlawn, NJ) before drying with nitrogen. Formed microstructures were hard baked at 160 ◦C for 30 min. Prepared flat and microstructured SU-8 substrates were etched with oxygen plasma for 20 min (PLASMOD^{TM} Oxygen Plasma System, TEGAL Corporation, Richmond, CA). Samples were sterilized by immersion in 70% ethanol in distilled water (DI)

overnight and rinsed in sterile DI water 3 times. The substrates were then coated with poly-ornithine (Sigma, St. Louis, MO) in water at a concentration of 40 μg/ml for at least 1 hour. This was followed by coating with laminin (Sigma, St. Louis, MO) at a concentration of 5 μg/ml. These dishes were stored at 4 ˚C until use.

4.3.2. Scanning electron microscopy (SEM) and atomic force microscopy (AFM)

SU-8 microstructures (without cells) were sputter-coated with gold for 60 s to achieve a coating thickness of about 15.3 nm. SEM images were captured with Zeiss 1450EP environmental scanning electron microscope. To characterize SU-8 surface topography and bulk coating on SU-8 surfaces, we used a PicoPlus-SPM (Agilent-Molecular Imaging) system for AFM imaging of the planar SU-8 surface before and after oxygen plasma treatment [26]. Briefly, silicon tips were used and Acoustic AC mode (AAC) was applied to obtain high resolution topographic images. AAC mode overcomes problems associated with friction, adhesion, electrostatic forces, and other difficulties that contact mode AFM is usually confronted with. In AAC mode, driving the cantilever into oscillation is accomplished by indirect vibration, in which the cantilever is excited by high frequency acoustic vibration from a piezoelectric transducer attached to the cantilever holder. Tip-sample force interactions cause changes in amplitude, phase and the resonance frequency of the oscillation.

4.3.3. Surface energy and contact angle measurement

Contact Angle System OCA (Future Digital Scientific. Corp., USA) with analysis software (SCA20) was used to determine the surface contact angles on the SU-8 samples.

Distilled water was used as a contacting solvent. All data were obtained 5 s after placing the droplet on the surfaces under ambient conditions. The surface energy of the contacting surface (E_s) was calculated according to $E_s=E_{lv}\cos\theta$. E_{lv} is the surface energy between the water and air, which is 72.8 mJ/m^2 at 20◦C for pure water; θ is the static contact angle [33].

4.3.4. Characterization of SU-8 crosslinking reaction by differential scanning calorimetry (DSC).

We investigated different process conditions outlined in Table 1. Samples with different thicknesses (40 μm and 80 μm) were used. The Thermal Analysis Instrument DSC 823[e] (Mettler-Toledo Inc., Columbus, OH) was operated in standard mode using an aluminum pan reference with a nitrogen purge rate of 50.0 mL/min. The standard mode DSC heating program was equilibrated at 20°C and the ramp temperature was set at 10°C/min to 350°C. The relationship between extent of crosslinking and DSC readout on residual reaction exotherm was systematically established [34]. Briefly, the enthalpy (ΔH) was obtained in units of Joules/gram (J/g) by integrating the area under the reaction exotherm peaks using STAR[e] software. The extent of crosslink reaction was defined as $((\Delta H_{\text{least treated}} - \Delta H_{\text{treated}})/\Delta H_{\text{least treated}})\times 100\%$.

4.3.5. Cell line and cell culture

Human neural stem cells (ENStem-A[TM]) were purchased from Millipore (Billerica, MA). Cells were maintained in 35 mm Petri dishes with 2 mL growth medium in a 5% CO_2 humidified atmosphere at 37 ˚C. ENStem-A[TM] expansion media supplemented with penicillin/streptomycin, L-glutamine and basic fibroblast growth factor (bFGF) was used.

The medium was half changed every other day. The cells were passaged by mechanically pipetting when cells reached 90% to 100% confluence and approximately 1.2×10^6 cells were seeded into each new dish. For cell differentiation, expansion media was replaced with differentiation media. Differentiation media was similar to expansion media, except that bFGF was not added. The differentiation medium was half changed every other day.

4.3.6. Fluorescence staining and fluorescent microscopy

Neural stem cells were stained with calcein AM (Biotium, Hayward, CA) [35]. This fluorescent dye stains living cells and their extensions by the presence of intracellular esterase activity, which converts the non-fluorescent cell-permeant calcein AM to intensely fluorescent calcein. Briefly, cells were washed with 2 mL Neurobasal without phenol red (Invitrogen, Carlsbad, CA) three times and covered with 2 ml of 2 μM calcein AM in Neurobasal and incubated for 30 min at 37 ˚C. Samples were then washed with Neurobasal 3 times. Fluorescent micrographs were viewed and captured with a B-2E/C FITC filter block (Nikon, Melville, NY, USA), which has an excitation bandwidth of 465-495 nm and a filter pass range of 515-555 nm. Cell morphological roundness measurements were done with Simple PCI image software (Compix Inc., Cranberry Township, PA). Roundness is defined as $4*\pi*\text{area}/(\text{perimeter})^2$.

4.3.7. Cell adhesion and proliferation

To establish the relationship between the extent of SU-8 crosslinking and associated substrate cytotoxicity, cell adhesion and proliferation were evaluated for neural stem cells on SU-8 substrates with different extents of crosslinking. SU-8 flat substrates were fabricated

according to Table 1. Polystyrene Petri dishes were used as the control substrates. Neural stem cells (5×10^5 cells) were seeded on each sample (corresponding cell density of 10^3 cells/mm^2). Samples were stained with calcein AM as described above (Biotium, Hayward, CA) at 4 h, 24 h, 48 h and 72 h. Fluorescent images were taken, cells were counted and cell densities were calculated. To characterize cell proliferation, cell culture's doubling time was derived according to the cell growth equation below [36]:

$$Y = Ae^{kt} \qquad (1)$$

where k is the growth rate, A is the cell number at the start of the experiment and Y is the cell number at time t.

4.3.8. Cell-substrate interaction observation by time-lapse recording.

Time-lapse recording is a frequently used tool for studying cell dynamic activity *in vitro*. We used time-lapse video microscopy to study how neural stem cells interact with microstructures within the first 24 hours of plating. Microstructures with cells were kept in an environmental chamber to maintain proper conditions while recording. The WaferGen Smart Slide-100 system (WaferGen, Fremont, CA, USA) was used. This small environmental chamber is based on a 6-well dish. It uses heated glass to maintain tissue temperature even at the spot being observed, and regulates CO_2 flow and provides for rapid media exchange at selectable intervals via a computer interface. Phase contrast images were taken every minute using Leica DFC300 FX camera mounted on a Leica Z16 APO A microscope. Data were analyzed by ImageJ (NIH). Image sequences and trajectory plots for cell movement within microstructures and on 2D surface were compared.

4.3.9. Actin cytoskeleton distribution examination.

Actin cytoskeleton distribution of neural stem cells within these microstructures and on 2D surfaces was studied 24 hours after cell plating. Briefly, cells were rinsed once with phosphate-buffered saline (PBS), fixed with 4% paraformaldehye in PBS (15 min), washed twice with wash buffer (PBS containing 0.05% Tween-20), treated with 0.1% Triton X-100 in PBS (5 min), washed with wash buffer, blocked with blocking solution (1% BSA in PBS), incubated with TRITC-conjugated Phalloidin (1:200, Millipore, Billerica, MA) for 1 h, and washed with wash buffer (3 times, 5 min per wash). Fluorescence images were viewed with a Nikon ECLIPSE TE2000-S inverted microscope with a fluorescence attachment using a 60× objective. Actin cytoskeleton organizations in neural stem cells cultured in SU-8 microwells and on flat surfaces were compared.

4.3.10. Resting membrane potential (V_m) measurement

We combined the use of a potentiometric dye, tetramethylrhodamine methyl ester (TMRM) and confocal microscopy to measure the V_m of neural stem cells [37]. The concentration of the dye (D_{in} and D_{out}) is proportional to the fluorescent intensity (F_{in} and F_{out}); the black gain was set to 0 and all gray level data were corrected by deducting background values (B). The final working equation for determining the V_m of individual cells was:

$$V_m = -58\log_{10}\left(\frac{F_{in}-B}{F_{out}-B}\right)\ \text{mV} \qquad (2)$$

A calibration of the linearity of the relation between the dye concentration and the gray level reading of confocal images has ascertained that the gray level reading was linearly proportional to TMRM concentration within the range from 5 nM to 100 μM (R^2= 0.9962) [38].

4.4. Results and discussions

4.4.1. Fabrication, surface modification, and characterization of SU-8 microstructures

Figures 4.1 (a) to 4.1 (d) show the flow diagram of the fabrication process and Figure 4.1 (e) shows a scanning electron microscopy (SEM) image of 50 μm microwell patterns. The center-to-center distance is 100 μm and the width of the channel is 10 μm. Channel width was chosen as in a previous study [25]. These channels provide guidance for neurite extention within microstructures. These microwells and microchannels together created a nondegradable network pattern. In contrast to conventional chemical micropatterning methods, this type of topographical patterning did not rely on integrin-mediated selective adhesion. In addition, these microstructures provide protection for cells within microwells from shear forces caused by fluid flow in media change preocesses.

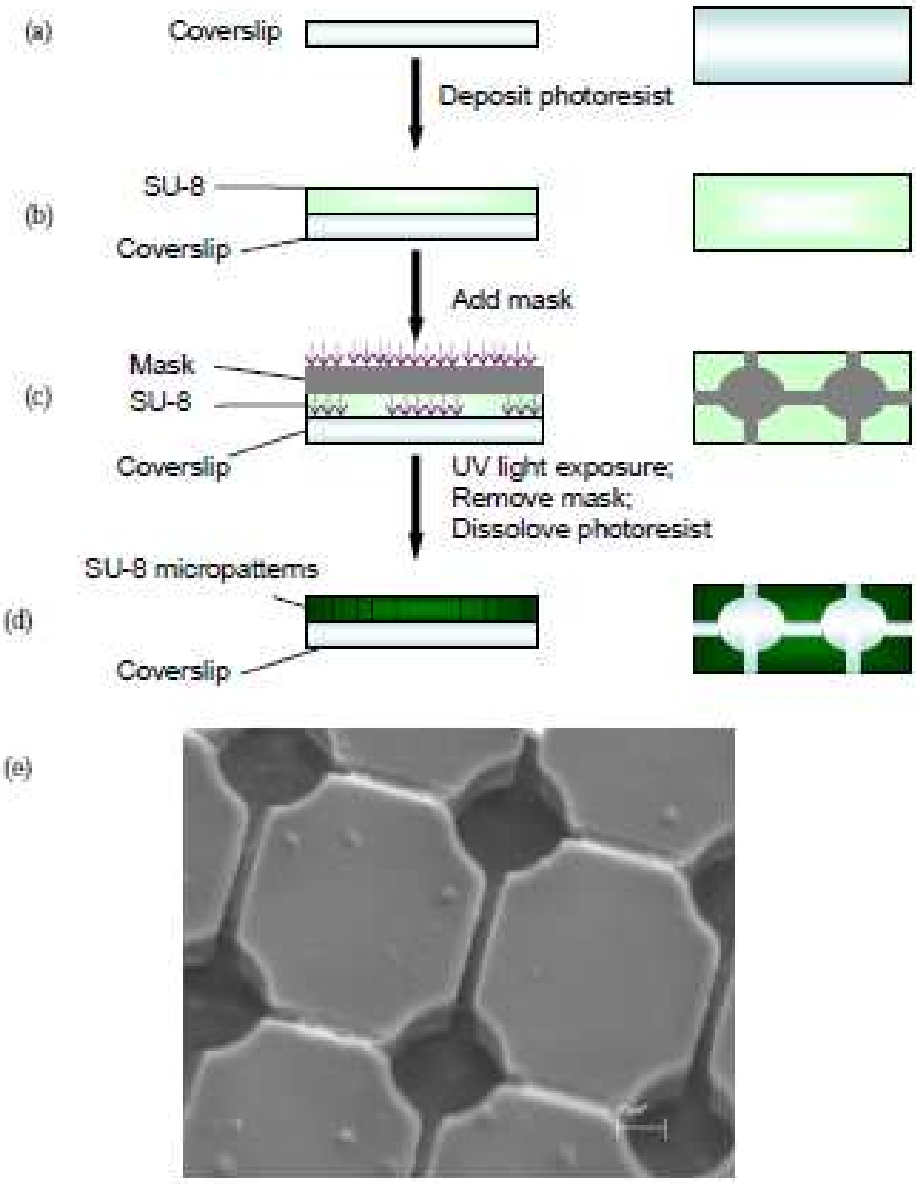

Figure 4.1. (a) - (d) show a flow diagram for the fabrication process; the right column shows the top view. Photoresist is spin-coated on a coverslip (a - b). A mask is placed in contact with the layer of photoresist (b - c). These opaque patterns shield the photoresist from ultraviolet (UV) light. Illumination with UV light results in SU-8 crosslinking. An organic solvent dissolves and removes the photoresist that is not crosslinked (c - d). (e) shows a scanning electron microscopy (SEM) image of the 50 µm microwells with interconnected channels. The center-to-center distance is 100 µm and the width of the channel is 10 µm.

SU-8 surfaces are typically hydrophobic. To change surface characteristics, SU-8 microstructures were etched with oxygen plasma, yielding hydrophilic SU-8 microstructures [39]. Figure 4.2 shows a significant increase in surface roughness as a result of oxygen plasma etching. Before etching, SU-8 surface was quite smooth (Figure 4.2 (a)); after etching, the surface became rough (Figure 4.2 (b)). The inset images in Figure 4.2 (a) and Figure 4.2 (b) present the shape of water drop on SU-8 surface before and after oxygen plasma etching, representatively. The contact angle decreased from 85.1◦ to 35.8◦ after etching. Correspondingly, the surface energy increased from 6.27 mJ/ m^2 to 57.94 mJ/ m^2. Oxygen plasma etching is an effective way to change the surface roughness; also it renders the surface hydrophilic. In addition, etched SU-8 surface enhanced poly-ornithine and laminin coating; the thickness of coated material increased on etched SU-8 surface (Figure 4.2 (c) and 4.2 (d)).

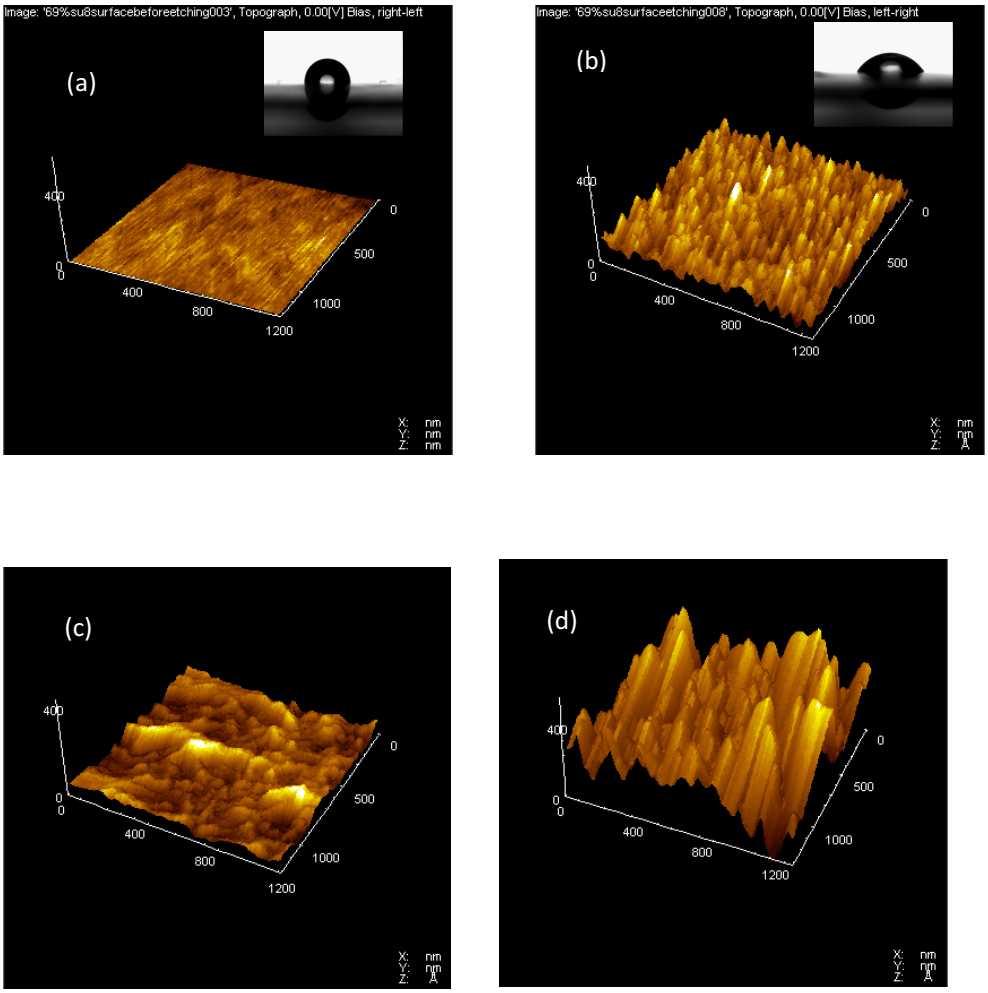

Figure 4.2. Atomic force microscopy (AFM) images showing the topographical features of SU-8 surfaces before (a) and after (b) oxygen plasma etching, and the bulk coating of poly-ornithine and laminin on unetched SU-8 surface (c) and on etched surface (d). The inset images in (a) and (b) show the shape of a water drop on SU-8 surface before and after oxygen plasma etching, representatively; a more spread drop in (b) indicates higher hydrophilicity. The units for X and Y axes are in nanometers, while the Z axis units are in angstrons.

4.4.2 Cell attachment and proliferation on SU-8 substrates with different extents of crosslinking

The cytotoxicity problem observed with SU-8 limited its application in cell-based studies [31]. This cytotoxicity has been hypothesized to be due to poorly crosslinked samples [26,

40], as the crosslinking of a polymer matrix influences physical and chemical properties of the material [34]. To study the relationship between the extents of SU-8 crosslinking and its cytotoxicity to human neural stem cells, we start with SU-8 crosslinking characterization. SU-8 substrates were fabricated following the conditions outlined in Table 4.1 and SU-8 crosslinking reaction was characterized by DSC. SU-8 films with different thicknesses (40 μm and 80 μm) were fabricated to see how the thickness affects crosslinking reaction. Figure 4.3 presents the typical DSC curves for 40 μm SU-8 films under different fabrication conditions. The sample before exposure was characterized by DSC as negative control. The partly crosslinked sample (Condition 1) showed a different exotherm reaction profile in comparison to the non-crosslinked sample (negative control). The decrease in the integrated reaction exotherm from the partly crosslinked sample (Condition 2) to completely crosslinked sample (Condition 3) reflected the significantly advanced polymerization of the film resulting from the thermal reaction in high-dosage exposure (60 s) and hard baking. Table 4.2 summarizes the extent of crosslinking for each fabrication condition. We found that fabrication process and film thickness affected the extent of crosslinking. Thicker film resulted in less crosslinking. For example, after high-dosage exposure and hard baking, the reaction exotherm of 40 μm SU-8 substrate was 0 J/g and the corresponding crosslinking extent was 100%; however, at the same fabrication condition, 80 μm SU-8 substrate had a reaction exotherm of 32.07 J/g and was only 80.61% crosslinked. These results indicated that our protocol yielded completely polymerized 40 μm thick SU-8 substrates. To make thicker completely crosslinked films would require adjusting fabrication conditions.

Table 4.1. List of sample process conditions.

Process condition		Softbaking (65°C 3 min, 95°C 6 min)	Exposure (15 s)	Exposure (60 s)	Postexposure Baking (65°C 3 min, 95°C 9 min)	Hard Baking (160°C 30 min)
Negative control		+	—	—	—	—
40 μm	Condition 1	+	+	—	—	—
	Condition 2	+	—	+	+	—
	Condition 3	+	—	+	+	+
80 μm	Condition 1	+	+	—	—	—
	Condition 2	+	—	+	+	—
	Condition 3	+	—	+	+	+

"+": procedure implemented; "—": procedure not implemented; Fabrication process followed the sequence from the left to the right, one sample was prepared under each condition.

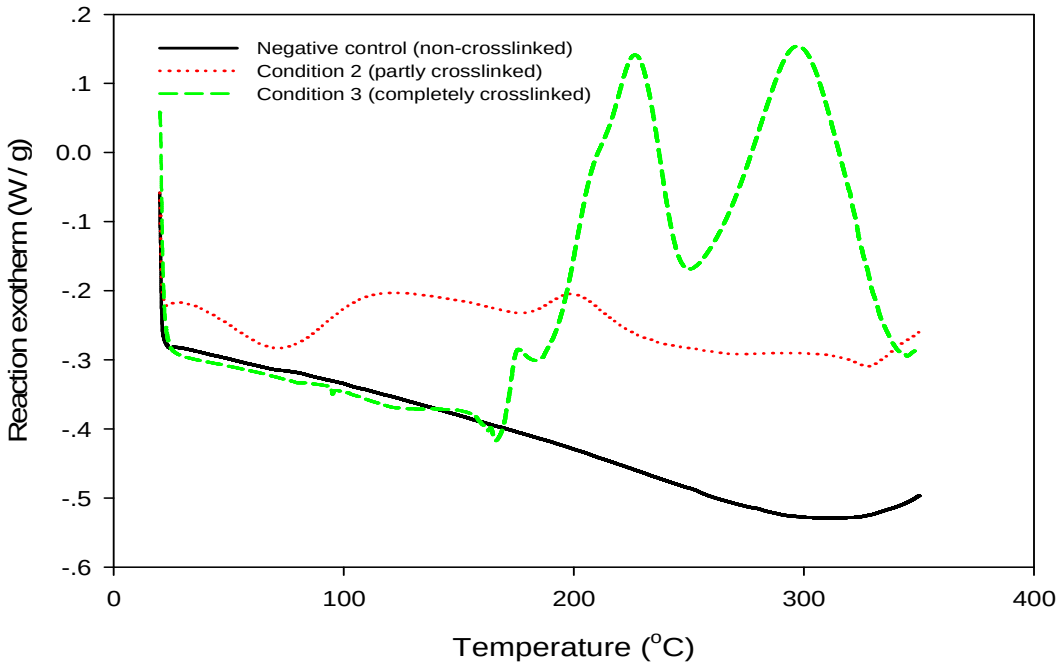

Figure 4.3. Plots of DSC data from SU-8 samples (40 um thick) that were processed under different process conditions: negative control sample without crosslinking; partly crosslinked sample under Condition 2 (softbaking + exposure + postexposure baking); completely crosslinked sample under Condition 3 (softbaking + exposure + postexposure baking + hard baking). X axis represents temperature in degrees ◦C; Y axis represents normalized heat flow in W/g.

Table 4.2. Summary of extent of cross linking reaction at each process step

	Condition 1		Condition 2		Condition 3	
	80 μm	40 μm	80 μm	40 μm	80 μm	40 μm
Enthalpy (J/g)	165.43	129.46	96.02	63.44	32.07	0
Extent of Crosslink Reaction	0	21.74%	41.96%	61.65%	80.61%	100%

To study the relationship between the extents of SU-8 crosslinking and its cytotoxicity, human neural stem cells were plated onto SU-8 substrates with different extents of crosslinking. All these SU-8 substrates were treated by oxygen plasma etching and then coated with poly-ornithine and laminin to enhance cell adhesion. SU-8 substrates without etching were hydrophobic and not suitable for cell adhesion. Neural stem cells formed spheres or clusters after plating and few cells were observed on the surface (data not shown). As a positive control, polystyrene Petri dishes coated with poly-ornithine and laminin were used for cell plating. Figure 4.4 presents cell densities at different time points on different substrates. Cell attachment was evaluated 4 hour after cell plating. As shown in Figure 4.4, more cells were observed on Petri dish surfaces and on completely crosslinked SU-8 substrates than on less crossslinked SU-8 substrates at hour 4. On Petri dish surfaces and completely crosslined SU-8 substrates, cells proliferated with doubling time of 2.2 days and 2.8 days, respectively. The difference in cell proliferation rate between cells on the polystyrene substrates and completely crosslinked SU-8 substrates may be due to the different substrate moduli. Studies have shown the effects of substrate modulus on cell proliferation [41-43]. Polystyrene's Young's modulus is around 3 GPa, SU-8's Young's modulus is around 4 GPa [44, 45]; both are far larger than the brain tissue's modulus (around

1000 Pa [41]). Neural stem cells have a higher proliferation rate on substrates with a modulus comparable to brain tissue; when substrate modulus increases, cell proliferation rate decreases [41]. On less crosslinked SU-8 substrates, cell density decreased after 24 h, which suggested that incompletely crosslined SU-8 substrates were cytotoxic to neural stem cells. These results suggested that in application of SU-8 for long-term cell culture, it is important to completely polymerize the material. As shown above, the thicker the film, the more difficult it is to completely polymerize the material. Thus, when fabricating high-aspect-ratio SU-8 microstructures for cell culture purpose, it is critical to make SU-8 film fully crosslinked to avoid material cytotoxicity. The results in this study provide an explanation for our previous observations, in which human neuroblastoma cells SH-SY5Y survived in the 97 μm thick but not in the 146 μm thick microstructures [25].

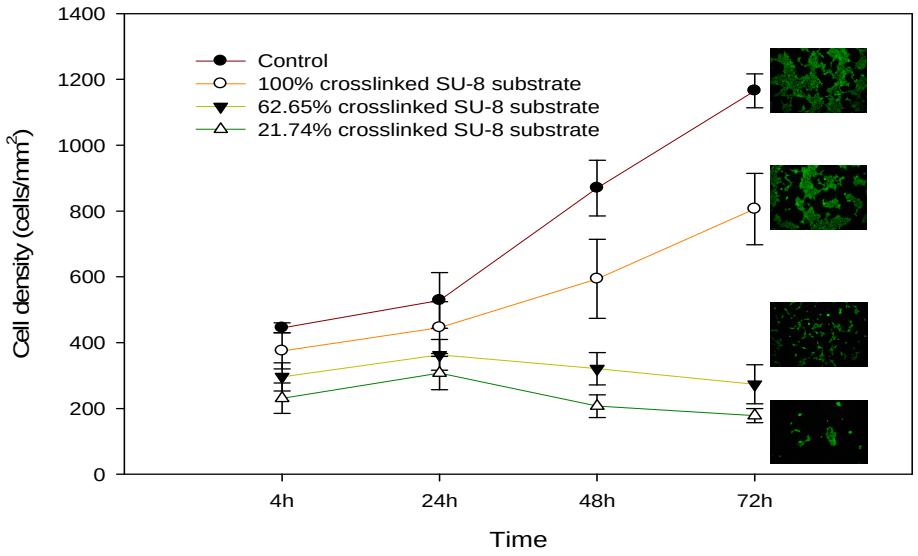

Figure 4.4. Neural stem cell density on control Petri dish and flat SU-8 substrates with different extents of crosslinking. Inset: fluorescent images showing neural stem cells on different substrate, 72 h after plating. Cells were stained with live cell indicator calcein AM.

Our results clearly established the relationship between the extents of SU-8 crosslinking and its cytotoxicity, and provide SU-8 surface modification methods for human neural stem cell culture. Even though SU-8 has been wildly used in microelectromechanical system (MEMS) parts with high-aspect-ratio, high optical transparency and excellent thermal stability [29, 30], the fabrication procedures limited its integration with currently used HTS systems (e.g. 96-well plates) for neural network activity readout. As an alternative, similar microwell structures were fabricated in nanofibrous poly-L-lactic acid (PLLA) film, which was compatible with 96-well plates [35]. PLLA scaffolds are opaque, which is unfavorable for optical detection methods. Methods have been reported to improve light transmittance at the positions with microstructures. However, because of its excellent optical transparency, SU-8 microwell structures were used in the following studies for cell integration and cell-microstructure interaction to provide the proof-of-concept for microwell-stem cell platforms.

4.4.3. Integration of neural stem cells with SU-8 microstructures

In this study, human neural stem cells were selected for the neural network platform development. Current cell sources for cell-based assays include primary cells, tumor-derived cell lines and stem cells. The process of primary cell harvesting is time consuming and requires animal sacrifice. Although tumor-derived cells can be maintained easily and passaged unlimitedly, results derived from such cells are usually questioned due to cell abnormalities. As an alternative, stem cells provide unlimited cell sources and these cells are considered normal; furthermore, stem cells are pluripotential – they can be differentiated into any cell type *in vitro*. For example, neural stem cells, which are derived from embryonic

stem cells are partially differentiated, multipotent and can develop into any type of neural cells, such as neurons and astrocytes. Neural stem cells in culture appeared normal morphologically and displayed normal features of immunoreactivity when tested for neuron-specific elements [47, 48]. In drug discovery, cell-based assays involving neural stem cells have great potential for screening compounds against many targets.

Human neural stem cells were seeded onto microstructures with different well sizes. One day after plating, live cells were observed within microstructures (Figure 4.5). Cell distribution was random on 2D flat surface (Figure 4.5 (a)); while within microstructures, cell growth was patterned by microwells and channels (Figure 4.5 (b) and (c)). These results attest to successful integration of human neural stem cells in SU-8 microstrucutres. In previous studies, not too many live cells could be observed within SU-8 microwell structures [49]. Through intensified exposure and hard baking, SU-8 was completely crosslinked, which eliminated its cytotoxicity. After surface modification by oxygen plasma etching, SU-8 surface was made hydrophilic, making it suitable for neural stem cell culture. Compared to high-aspect-ratio SU-8 microstructures used for neuronal cell culture reported by Choi et al. [50], SU-8 microwell structures in this study provided patterning for cell growth and neural network formation. One day after cell plating, growth media was changed to differentiation media. Neurite extension appeared by day 7 into differentiation (Figure 4.6); differentiated neural stem cells formed random neural network-like connectivity on flat surface (left); while within microstructures, network-like formation was guided by structures (right). Neurites grew along microchannels to cells in the neighboring microwells. Merz and Fromherz [28] also reported a geometrically defined network of snail neurons using SU-8 microstructure. In

the few studies using SU-8 microstructures for cell behavior *in vitro*, only primary cells and tumor-derived cells have been successfully integrated in SU-8 microstructures [25, 26, 28, 32]. Even though patterned SU-8 microstructures have been designed for neural implant, these strucutures were still low-aspect-ratio [51]. Our results proved that high-aspect-ratio SU-8 microwell structures provide an effective tool for guiding neural stem cell-derived neural network-like organization.

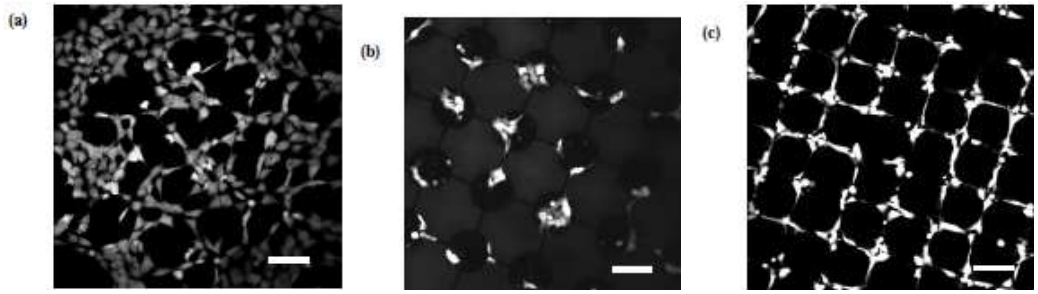

Figure 4.5. Confocal images showing neural stem cells cultured on flat SU-8 surfaces (a) and within micropatterns (b and c). The diameters of micropatterns in (b) and (c) are 100 µm and 50 µm, respectively. Cells were stained with calcein AM one day after plating. Bar = 100 µm.

In Figure 4.5 (b and c) and Figure 4.6 (a, right), some cells were observed on the sidewalls of microwells, typically at the position of channel opening; neurite extensions were also observed along the channels or at the opening of channels even before differentiation. Similar observations were reported by Wang et al. [35]. In addition, some cells were observed in the channels which are 10 µm wide. However, at a lower microwell diameter of 15 µm, which is comparable to the diameter of cell body in suspension, no cells were observed in the microwells. These findings raised questions of how cells got into channels and whether the channel opening location had attractive architectural features. To answer

these questions, we used time-lapse microscopy to study cell locomotion within 24 hours after plating.

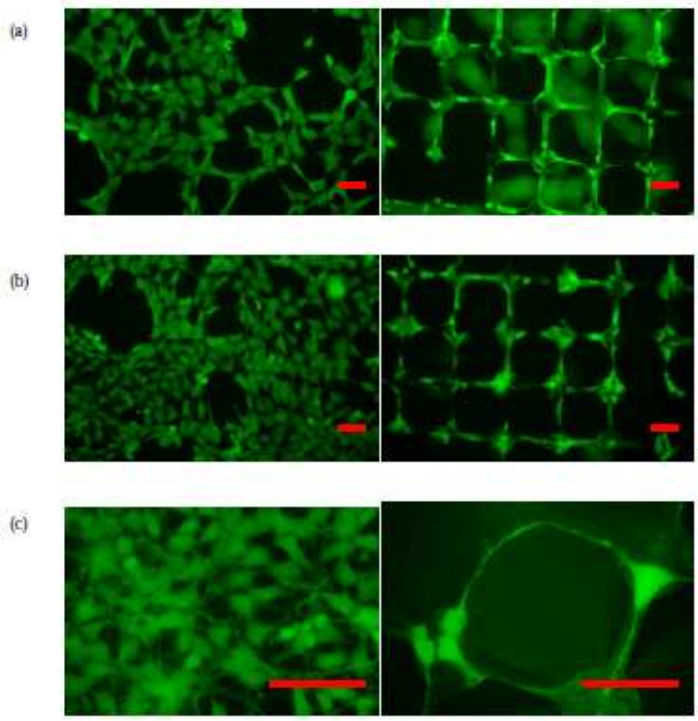

Figure 4.6. Fluorescence images showing neural stem cells cultured on flat SU-8 surfaces (left column) and within microwells with a diameter of 50 µm (right column) on day 0 (a), day 2 (b) and day 7 (c) into differentiation. Cells were stained with calcein AM. At day 7 (c), differentiated neural stem cells formed random neurite extension on flat surfaces; while within microstructures, network-like formation was guided by structures. Bar = 50 µm.

4.4.4. Cell-microstructure interaction study

4.4.4.1. Cell locomotion study by time-lapse recording

Figure 4.7 shows trajectory plots (a and b) and image sequences (c and d) for cell movement on 2D surface. In absence of other cells to interact with, cells on 2D surface moved randomly in confined areas (Figure 4.7 (a)), extending neurites, stretching their cell body, and changing their cell bodies' orientation (Figure 4.7 (c)). In the presence of other cells, cell movement pattern was the same; however, cell movement area became wider (Figure 4.7 (b)). Cells migrated around to get connected and formed cellular clusters (Figure 4.7 (d)). During differentiation, they extended neurites to form neural network-like

interaction (data not shown). Thus, neural stem cells tended to form interactions with other cells and cellular locomotion was driven by the need for interaction, which is consistent with previous studies [52]. Kulesa and Fraser [52] reported that cell-cell interaction played an important role in neural crest cell migration *in vivo*. To study neural stem cell locomotion within microstructures, the seeding cell density was controlled at a low level ($6x10^4$ cells/cm^2) so that single cell activity could be observed.

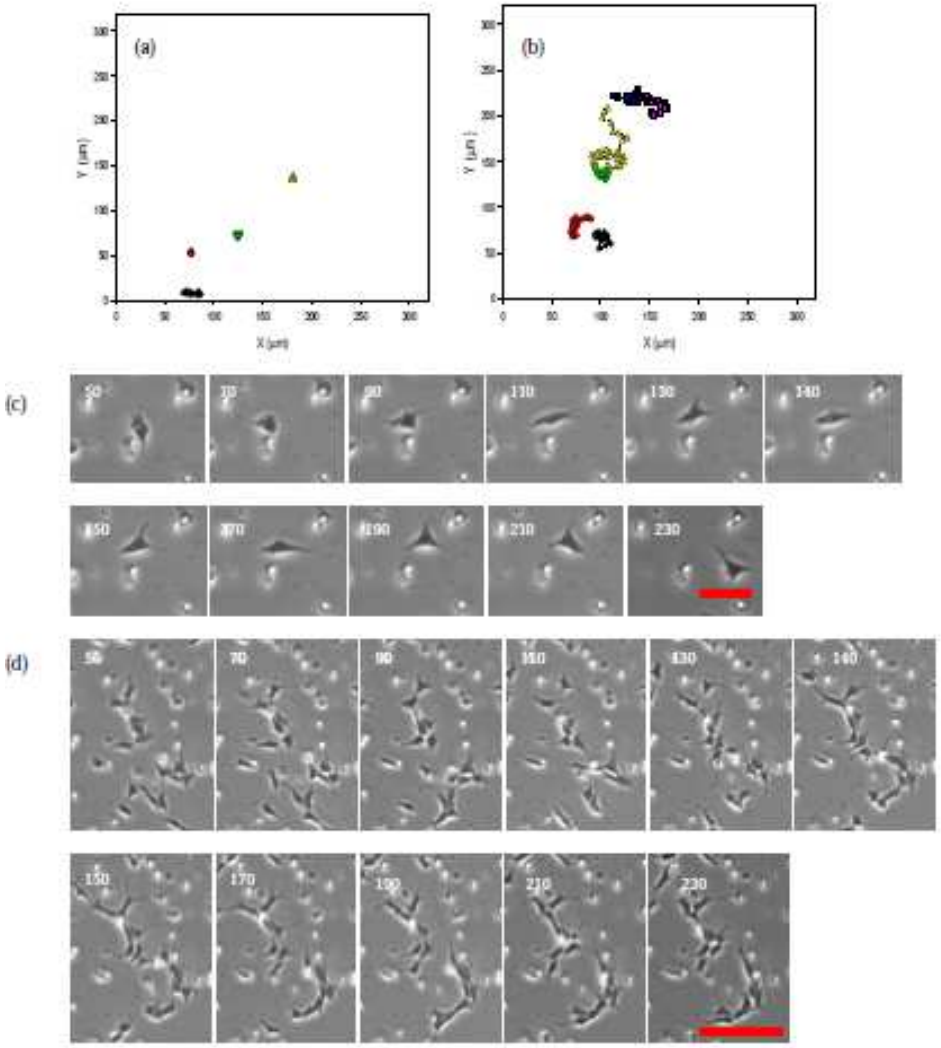

Figure 4.7. Trajectory plots (a and b) and image sequences (c and d) of neural stem cell movement on 2D surface. (a) and (c): in absence of other cells to interact with, cells on 2D surface moved randomly in a confined area, projecting out neurite-like structure, stretching and changing their cell bodies' orientation. (b) and (d): in the presence of other cells to interact with, the cell movement pattern was the same while the cell movement area became larger; cells moved around to get connection and formed cellular clusters. Bar = 50 µm in (b) and 100 µm in (c).

At the beginning of the recording, cells were observed to fall into microwells randomly (Figure 4.1S). Some cells fell onto the bottom in the microwell (Figure 4.1S (a) – (e)); some cells attached to the sidewalls in the microwell (Figure 4.1S (f)). With 15 µm microwell, which was comparable to the diameter of cell body in suspension, no cells were observed in

the microwells; while with 30 µm microwell, cells were observed in microwells. Thus, for neural stem cell integration, microwell size should be larger than the size of a suspended cell to facilitate the ability of the cell to be incorporated into the well. More cells were observed in the 100 µm microwells; they formed cellular clusters easily. Thus, the microwell diameter is an important factor in the design of microwell structures for neural stem cell integration.

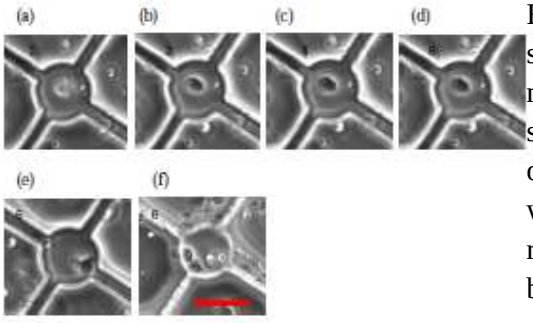

Figure 4.1S. Phase contrast images showing neural stem cells falling into microwells randomly. (a-d): image sequence of cell falling onto the bottom of a microwell; the process took place within 6 min at the beginning of recording. (e and f): Cells fell to the bottom or attached to the sidewalls of the microwells at 6 min of recording. Bar = 50 µm.

Cells within microstructures, in absence of other cells, had a limited active movement area (Figure 4.8 (a)) which was confined by microwells (Figure 4.8 (b)). As shown in Figure 4.8 (b), all the seven cells on the microwell bottom interacted with the sidewall; at the end of the recording, six cells were observed at the opening of microchannels, but none moved into these channels. According to these trajectories, some cells first fell on the bottom in the center of the well, but moved towards the sidewall; some cell moved along the sidewall. Figure 4.9 (a) presents a typical image sequence of single cell interaction with microstructures. Images were obtained by focusing at the bottom of microwells; some of these images showed cells out of focus, suggesting that cells crawled onto the sidewall. Cells on the top of the microstructures, in absence of other cells, interacted with the microwell opening edges (Figure 4.8 (c-d) and Figure 4.9 (b)); some cells moved towards the opening edges, and some cells moved along the curved opening edges in a limited area. These

observations suggested that single cell movement within microstructures was confined, which is similar to single cell movement on 2D surface. In addition, cells tended to interact with curved sidewalls of microwell structures either within the microwell or on top of the structure, the mechanism behind which is still not known.

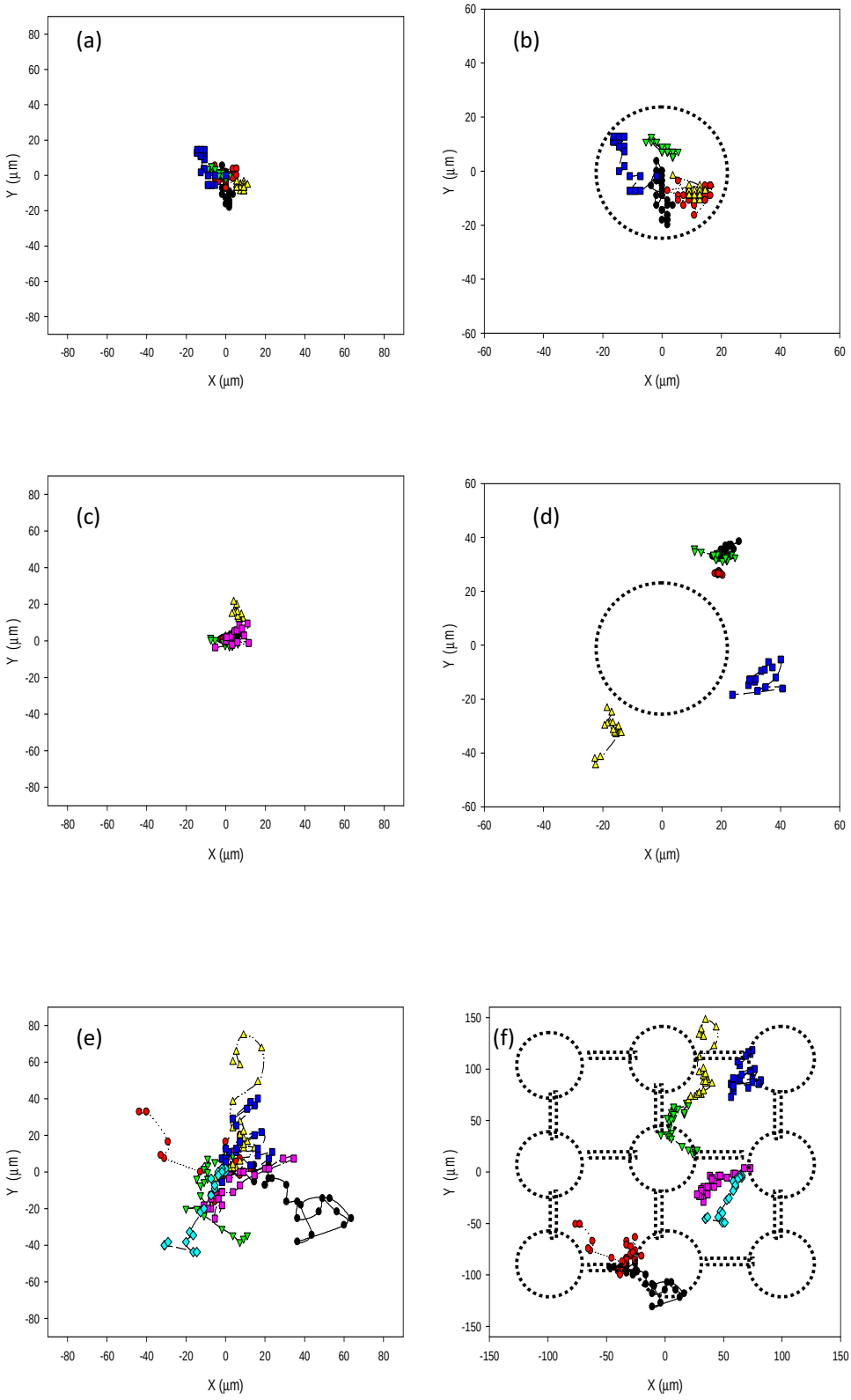
(a)
(b)
(c)
(d)
(e)
(f)
Y (µm)
X (µm)

Figure 4.8. Trajectory plots of neural stem cell movement within 3D microstructures. (a-d): Single cell interaction with micropatterns was limited and cell active movement area was confined. Even though single cells could be observed at the opening of microchannels, none moved into these channels. (a-b): Cells within microwells interacted with sidewalls. (c-d): On the top of the micropattern, cells moved towards microwell opening edges. (e and f): In the presence of other cells to interact with, neural stem cells formed connections with other cells; cell locomotion was more active with a larger movement area (e), and cell movement was affected (guided) by microstructures (f).

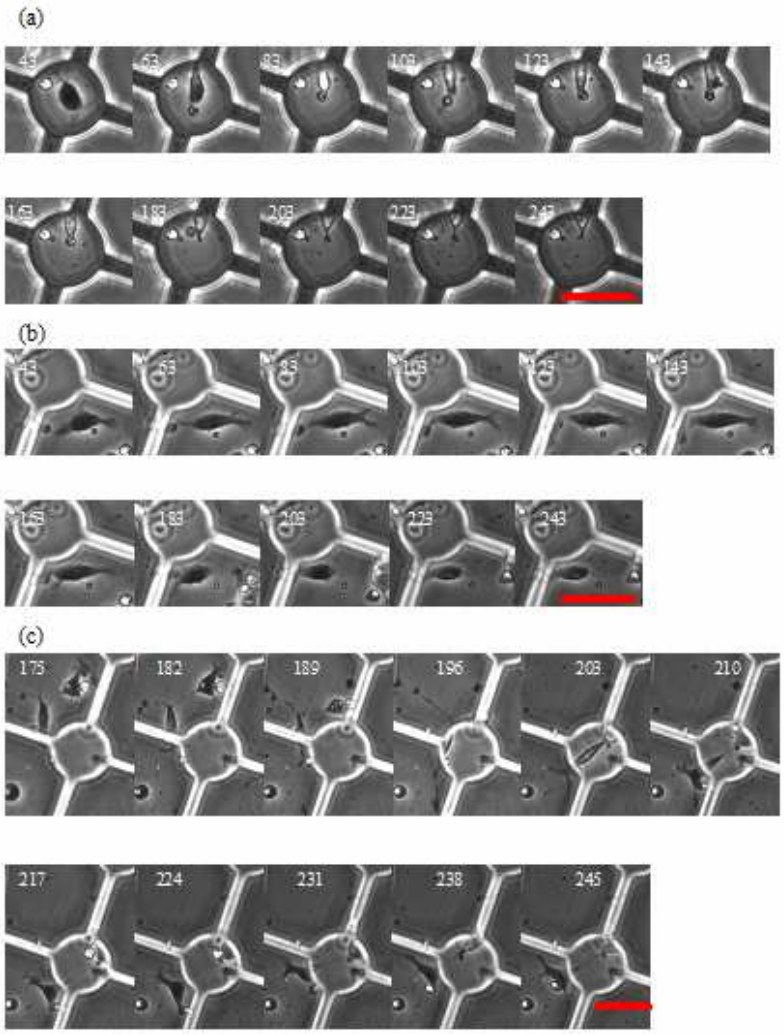

Figure 4.9. Image sequences of neural stem cell movement within 3D microstrcutures during the first 4 hours after cell plating. (a): Single cell movement at the bottom of microwell. (b): Single cell movement on the top of micropattern. (c): Cell moved into the well from the top (at the position of channel opening or along the channel); and formation of neurite-like structure across the microwell was observed. Bar = 50 μm.

In the presence of other cells, neural stem cells in microwell structures formed interconnections. Cell locomotion was more active (Figure 4.8 (e)), which is consistent with 2D cell locomotion (Figure 4.7 (b)). Figure 4.8 (f) presents trajectory plots for cells on the top of microwell structure. In Figure 4.8 (f), some cells moved towards the microwell opening edges and ended up at the opening of channels; some moved along the channel edges and the microwell opening edges; and some moved into the well along the sidewall as shown in Figure 4.9 (c). Cells, which fell onto the top of microstructures, moved into the well from the top at the position of channel opening or along the channel (Figure 4.9 (c)); and neurites across the microwell were observed in the recording. Even though cells did not fall into microchannels, cells were observed to move along the sidewalls of microwell and channel in the presence of other cells (Figure 4.2S). Taken together, cells tended to interact with cells in neighboring wells; and cell-cell interaction was affected (guided) by microstructures.

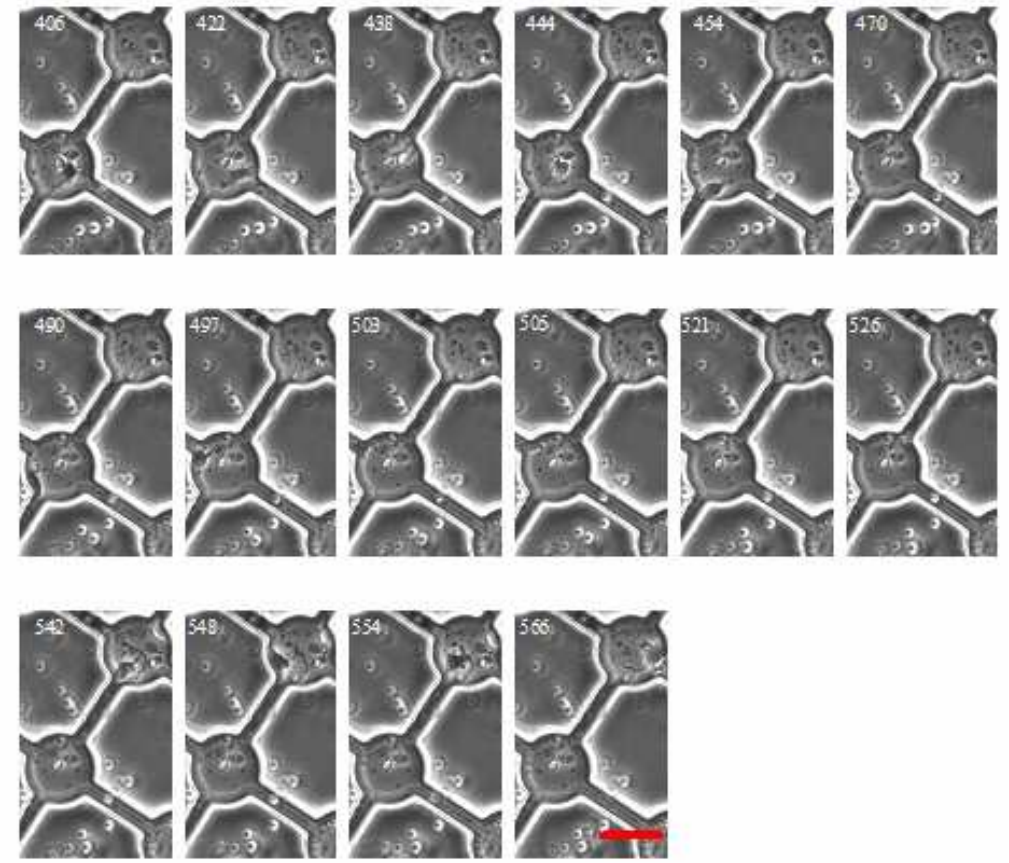

Figure 4.2S. Image sequences of neural stem cell movement within 3D micropatterns during the first 24 hours after cell plating; cells moved along the sidewalls of microwells and channels. Bar = 50 µm.

In-vitro studies of cell dynamics have been carried out with substrates textured with grooves and ridges at both micro- and nanoscale levels [53, 54]. Recently, Johnson et al. [55] reported glioma cell migration on electrospun polycaprolactone using time-lapse analysis. However, there are few studies on human neural stem cell dynamic locomotion *in vitro*. For the first time, our results showed dynamic neural stem cell locomotion within microwell structures during the first 24 hours after plating. These studies have provided information on how neural stem cells get into microwell structures and how neural stem cells reacted to microwell structures. Microstructure architecture could be applied to guide connectivity

driven cell locomotion (e.g. presence of microchannels guided neural stem cell migration). In microstructure/scaffold design for stem cell integration, microwell size control and microchannel presence could be engineered for microenvironment architecture optimization. Neural stem cell migration plays an important part in neurogenesis in adult neural tissue [56, 57]; our microwell structure may also provide a platform for studying neural stem cell migration *in vitro*.

Based on time-lapse recording, microwell structures provided a 3D microenvironment for neural stem cells integration; unlike cell locomotion on 2D surface, cells within microwell structures crawled onto sidewalls of microwells, or moved into microwells and moved down along sidewalls. In implementing the resulting platform (neural stem cells integrated with microwell structures) in HTS, cells onto the walls or cells on the bottom or both can be used. This raised the question of whether there were any differences in cells based on location within the microwell. To explore this question, we focused on similarity or difference with respect to dimensionality as suggested by cytoskeleton organization. Cells cultured on "physiologically relevant" substrates have exhibited different cytoskeleton distribution from that of cells on 2D surface [58, 59]. Cells on 2D surface spread out and exhibited actin stress fibers, while cells cultured in 3D microenvironment had round shape and did not present actin stress fibers within.

4.4.4.2. Effects of microstructure on cellular morphology and function

Effect of microstructure architecture on cellular morphology was studied by examing actin distribution (Figure 4.10). Cells on 2D surface had actin distribution along cell bodies,

especially in the neurites (Figure 4.10 (a1-a2)). Stress fibers were observed within cell bodies (Figure 4.10 (a3)). Within100 μm and 50 μm microwells, some cells spread on the bottom surface and had a similar actin distribution pattern as cells on 2D surface (Figure 4.10 (b1-b2), Figure 4.10 (c1)); but these cells were less spread out within microwells than cells on 2D surface. Within 100 μm microwells, cells formed cellular aggregates (Figure 4.10 (b3)); actin was observed along the cell body and no stress fibers were observed within cell body; a similar pattern was observed for cells along the sidewalls of 50 μm microwells (Figure 4.10 (c2)). Confocal image sections for cells within these microwells showed the aggregates of actin protein within cell bodies (Figure 4.10 (c3)). These results suggested that 50 μm microwell structure affected cellular actin distribution in a 3D manner. Studies have shown that stress can lead to the formation of actin stress fibers, which may result in an autoinflammatory condition [60, 61]. Cells along the sidewalls of 50 μm microwells presented no stress fibers within; thus, it is possible that microwell structures affected cell cytoskeleton organization in an autoregulatory manner to avoid inducing inflammation and cells had the tendency to reside in a more comfortable microenvironment to avoid inflammation. This may also partly explain why cells tended to interact with curved well openings, or move towards curved sidewalls.

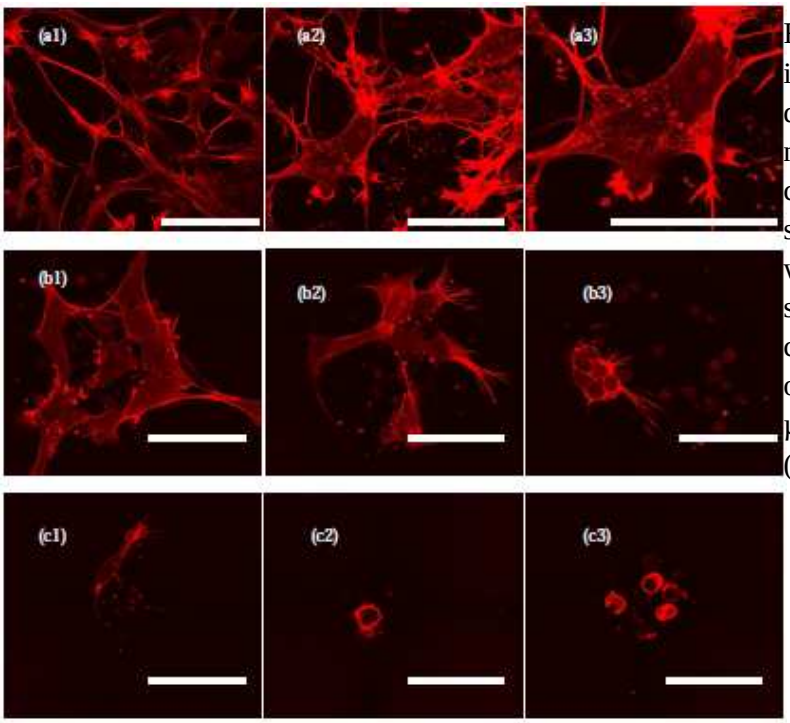

Figure 4.10. Confocal images showing actin distribution within neural stem cells cultured on flat SU-8 surface (a1-a3) and within microwell structures (b1-b3, c1-c3). The diameters of microwells are 100 µm (b1-b3) and 50 µm (c1-c3). Bar = 50 µm.

Table 4.3 summarized morphological measurements of neural stem cells on flat surface and within microstructures at different well sizes, one day after cell plating. Cells within microwells were less spread than cells on flat surface; as well size changed from 100 µm to 50 µm, cell spreading area also changed significantly ($P < 0.01$). Morphological roundness of cells on flat surface was not significantly different from that of cells within 100 µm microwells; but with 50 µm microwells, cellular roundness was significantly larger ($P<0.01$). Neural stem cells were also integrated with microstructures with a diameter of 30 µm. Morphological measurements showed even less spreading area and larger roundness in 30 µm microwells than 50 µm microwells (data not shown). This finding, in agreement with previous work [62], confirmed that microstructure architecture affects cell morphology.

Table 4.3. Summary of morphological measurements for human neural progenitor cells on flat surfaces and microstructures before differentiation

	Flat surface	3D SU-8 Microwells with D = 100 μm	3D SU-8 Microwells with D = 50 μm
Area (μm^2) (mean±S.D.)	480±113	345±112*	212±57*#
Perimeter (μm) (mean±S.D.)	98±14	85±18*	62±11*#
Roundness (mean±S.D.)	0.63±0.11	0.61±0.13	0.69±0.10*#
Cell number	n=50	n=52	n=48

* Values that are significantly different from those for cells on 2D SU-8 substrates ($p<0.01$).
# Values that are significantly different from those for cells within microwells with D = 100 μm ($p < 0.01$).

Changes in cell morphology may lead to changes in cell functionality [25, 26, 62-64]. For example, human neuroblastoma cells (SH-SY5Y) integrated in SU-8 microstructures have been characterized with respect to cell morphology, resting membrane potential and voltage-gated calcium channel function; and cells within microstructures responded significantly differently from cells on flat surface [25, 26, 62]. Resting membrane potential (V_m) establishment is an important electrophysiological property of neural cells that marks functional differentiation; maintenance of an appropriate V_m is vital for maintaining physiological functions such as action potential propagation, cell signaling and ion channel gating. The fluorescence method for V_m measurement was used in this study. Comparing the means of the intra/extracellular fluorescence intensity ratios (R), it was found that ratio for neural stem cells on flat substrates (75.71 ± 40.32, n=237) was significantly different ($P<0.01$) from the ratio for cells in the 50 μm microwell structures (109.65 ± 80.43, n=70). Figure 4.11

presents the frequency distribution of the estimated V_m values for neural stem cells on flat substrates and in 50 μm microwell structures. The nonparametric Two-sample Kolmogorov-Smirnov test was used to test whether the V_m distributions were identical between cells on 2-D surface and within 3-D microstructure. It was found that more negative V_m values were established for cells in the 50 μm microwell network structures than for cells on flat substrates ($P < 0.05$).

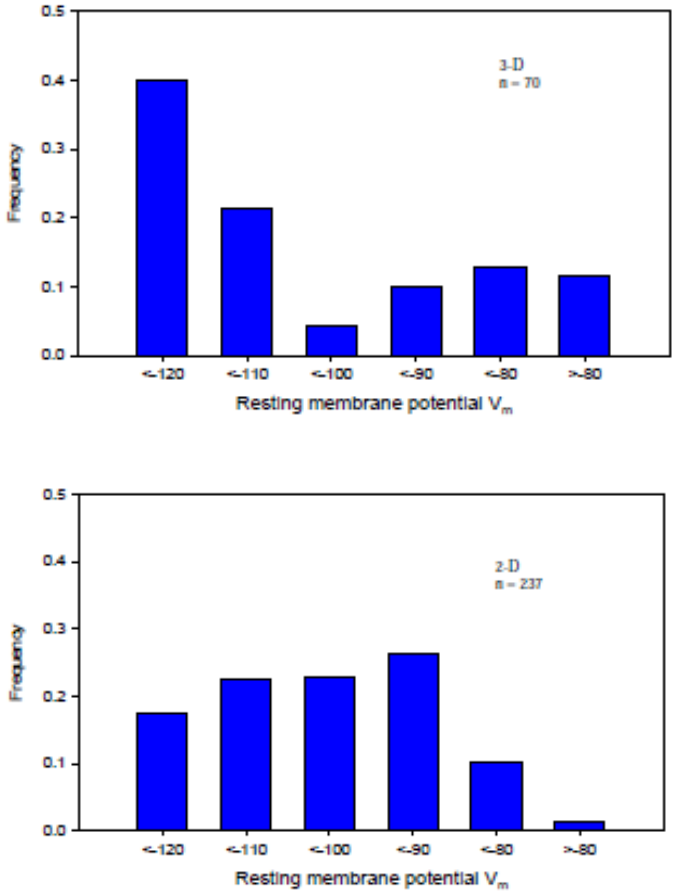

Figure 4.11. Frequency distribution of the estimated neural progenitor resting membrane potentials on flat SU-8 substrates and in the microwell network structures. The nonparametric Two-sample Kolmogorov-Smirnov test was used to test whether the V_m distributions were identical between 2-D and 3-D cells on day 2. The test was based on the null hypothesis H0: the two histograms are identically distributed versus the alternative hypothesis H1: the two histograms are not identically distributed, and H0 is rejected at 5% level. Results indicated that more negative V_m values were established for cells in the microwell network structures than for cells on flat substrates ($P < 0.05$).

These results indicated that cells cultured in microstructured scaffolds exhibited more negative V_m establishment than on flat substrates, which is consistent with our previous studies, in which SH-SY5Y cells in collagen hydrogels [38] or within SU-8 microwells [25] developed a higher ratio than those on flat surface. Even though V_m values around -90 mV have been documented for neural stems or precursor derived neural cells [65], the negative V_m values in this study may be overestimated due to nonpotentiometric binding. According to Mao and Kisaalita [38], a procedure for correcting using valinomycin is necessary for more accurate V_m estimation. Since the neural stem cells were extremely sensitive to treatment with valinomycin, that procedure was not followed in the present study. However, this does not compromise the conclusions reached, because the V_m values have been employed in a strictly comparative context. The V_m difference between 2D and 3D cells may be partly due to the altered cytoskeleton organization [66, 67]. Cytoskeleton changes may affect stretch-activated ion channels, which could affect neuronal responses and regulate cell differentiation.

Taken together, these results showed that microwell structures affected neural stem cell morphology as well as functionality with respect to resting membrane establishment, providing evidence that these high-aspect-ratio microstructures are not “folded-2D” and can provide quasi-3D microenvironments for cell culture. In our preliminary 2D/3D transcriptomic comparative study [68], Human Whole Genome U133A 2.0 Plus GeneChip Expression Analysis (Affymetrix, Santa Clara, CA) was performed for neural stem cells. The set of genes related to neural network connectivity in schizophrenia, discussed in the Introduction, were found to be upregulated in 3D in comparison to 2D cultures (Figure 4.3S (a)). Furthermore, these genes were upregulated in differentiation at day 14 compared to

those before differentiation (Figure 4.3S (b)). There results were further confirmed by immunostaining for some synaptic makers' expression ((Figure 4.3S (c)), suggesting that neural stem cells have the potential for creating the proposed platform with physiologically relevant neural network. In the next step, we will confirm the synaptic connectivity in the platform followed by validating the platform with drugs known to treat schizophrenia.

a

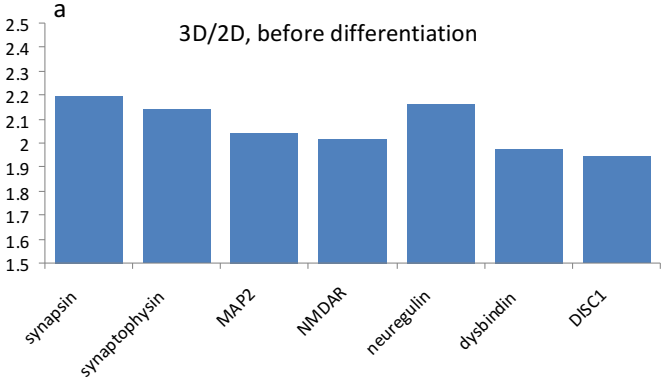
3D/2D, before differentiation
2.5
2.4
2.3
2.2
2.1
2
1.9
1.8
1.7
1.6
1.5
synapsin
synaptophysin
MAP2
NMDAR
neuregulin
dysbindin
DISC1

b

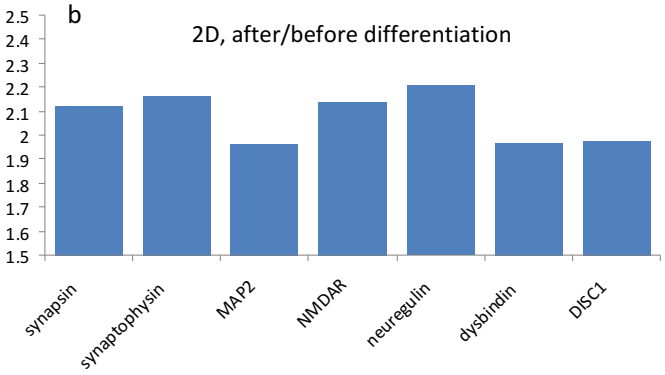
2D, after/before differentiation
2.5
2.4
2.3
2.2
2.1
2
1.9
1.8
1.7
1.6
1.5
synapsin
synaptophysin
MAP2
NMDAR
neuregulin
dysbindin
DISC1

c

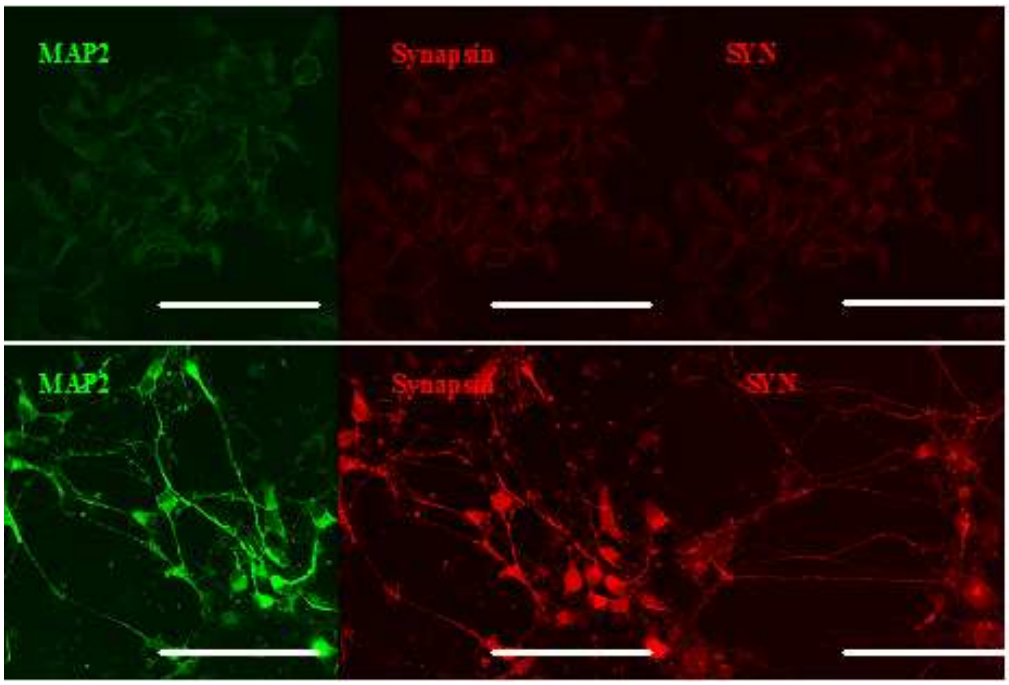
MAP2
Synapsin
SYN
MAP2
Synapsin
SYN

Figure 4.3S. (a-b): Microarray gene analysis results; listed genes are related to neural network connectivity and schizophrenia as discussed in the Introduction. Neural stem cells were cultured under three conditions (neural stem cells on 2D before differentiation, in 3D before differentiation, and on 2D after differentiation); four biological samples were tested in each group. Total RNA was isolated from all these samples using Qiagen RNeasy Kits (Qiagen, Valencia, CA) according to the manufacturer's standard protocol. Pure RNA samples were sent to Affymetrix Core facility at Medical College of Georgia for Human Whole Genome U133A 2.0 Plus GeneChip Expression Analysis (Affymetrix, Santa Clara, CA). The expression value of each gene was obtained by Expression Console (Affymetrix) with the probe logarithmic intensity error (PLIER) algorithm. Expression values were then normalized using the Quartile Normalization technique as suggested by Affymetrix. Average values from each group were used for ratio calculation. (a): ratios of listed genes' expression levels are presented for cells before differentiation in 3D porous polystyrene scaffolds (Cheng et al., 2008) over 2D surface (2D). (b): ratios of listed genes' expression levels are presented for cells on 2D surface at day 14 after differentiation over before differentiation. (c): Confocal images of neural stem cells on 2D glass surface before differentiation (top row) and at day 21 in differentiation (bottom row), stained with MAP2 (green), synapsin (red) and synaptophysin (SYN, red). Scale bar = 100 μm.

4.5. Conclusion

This study constitutes the first step toward a cell-based HTS drug discovery platform comprised of quasi-3D stem cell-derived neural networks housed in interconnected microwells. The results support the following conclusions.

1) SU-8 material associated cytotoxicity to cells can be avoided by process conditions that ensure completely crosslinking. Relationship between SU-8 crosslinking and cytotoxicity has been established; SU-8 microstructure fabrication and surface modification procedures have been established to yield a biocompatible microenvironment for human neural stem cell culture.

2) SU-8 microwell structures can be used to pattern neural stem cell growth and neural network formation. Human neural stem cells have been successfully integrated and patterned with SU-8 microwell structures and patterned neural network-like formation was observed for differentiated neural stem cells within microstructures.

3) Microstructure architecture (e.g. presence of microchannel and microwell) can be applied to guide interaction-driven activity of neural stem cells within a 3D microenvironment. Cellular morphology, cytoskeleton organization and resting membrane potential establishment of cells within microstructures were statistically significantly different from those of cells on flat 2D surface; microwell structures can provide 3D microenvironments for cell integration, offering the opportunity for engineering quasi-3-D neural network connectivity.

4.6 References:

[1] Seow D, Gauthier S. Pharmacotherapy of Alzheimer's disease. Can. J. Psychiatry 2007;52(10): 620-29.

[2] Javitt DC, Spencer KM, Thaker GK, Winterer G, Hajós M. Neurophysiological biomarkers for drug development in schizophrenia. Nature reviews: drug discovery 2008;7:68-83.

[3] Cutler NR, Sramek JJ. Review of the next generation of Alzheimer's disease therapeutics: challenges for drug development. Prog Neuropsychopharmacol Biol Psychiatry 2001; 25(1): 27-57.

[4] Law AJ, Weickert CS, Hyde TM, Kleinman JE, Harrison PJ. Reduced spinophilin but not microtubule-associated protein 2 expression in the hippocampal formation in schizophrenia and mood disorders: molecular evidence for a pathology of dendritic spines. Am J Psychiatry. 2004;161(10):1848-55.

[5] Meador-Woodruff JH, Clinton SM, Beneyto M, McCullumsmith RE. Molecular abnormalities of the glutamate synapse in the thalamus in schizophrenia. Ann N Y Acad Sci. 2003;1003:75-93.

[6] Hashimoto R, Tankou S, Takeda M, Sawa A. Postsynaptic density: a key convergent site for schizophrenia susceptibility factors and possible target for drug development. Drugs Today (Barc) 2007;43(9):645-54.

[7] Ford JM, Krystal JH, Mathalon DH. Neural Synchrony in Schizophrenia: From Networks to New Treatments. Schizophrenia Bulletin 2007;33(4): 848-52

[8] Dickman DK and Davis GW. The schizophrenia susceptibility gene dysbindin controls synaptic homeostasis. Science 2009;326:1127-30

[9] Kim JY, duan X, Liu CY, Jang MY, Guo JU, Pow-anpongkul N, Kang E, Song H, Ming GL. DISC1 regulates new neuron development in the adult brain via modulation of AKt-mTOR signaling through KIAA1212. Neuron 2009;63:761-73

[10] Enomoto A, Asai N, Namba T, Wang Y, Kato T, Tanaka M, Tatsumi H, Taya S, Tsuboi D, Kuroda K, Kaneko N, Sawamoto K, Miyamoto R, Jijiwa M, Murakumo Y, Sokabe M, Seki Y, Kaibuchi K, Takahashi M. Roles of Disrupted-In-Schizophrenia 1-intefracting protein girdin in postnatal development of the dentate gyrus. Neuron 2009;63(6):774-87

[11] Gross GW, Rhoades BK, Azzazy HME, Wu M. The use of neuronal networks on multielectrode arrays as biosensors. Biosensors & Bioelectronics 1995;10:553-67.

[12] Gross GW, Harsch A, Rhoades BK, Gopel W. Odor, drug and toxin analysis with neuronal networks in vitro: extracellular array recording of network responses. Biosensors & Bioelectronics 1997;12(5):373-93.

[13] Maeda E, Robinson HPC, Kawana A. The mechanisms of generation and propagation of synchronized bursting in developing networks of cultured neurons. J. Neurosci. 1995;15(10): 6834-45.

[14] O'Donovan MJ. The origin of spontaneous activity in developing networks of the vertebrate nervous system. Curr. Opin. Neurobiol. 1999;9:94-104.

[15] Dreosti E, Odermatt B, Dorostkar MM, Lagnado L. A genetically encoded reporter of synaptic activity in vivo. Nature methods 2009;6(12):883-9

[16] Migita S, Tateeishi A, Keinanen K Haruyama T. Engineered synapse model cell: genetic construction and chemical evaluation for reproducible high-throughput analysis Anal Bioanal chem. 2009;396(3):1153-7

[17] Chiappalone M, Vato A, Tedesco MB, Marcoli M, Davide F, Martinoia S. Networks of neurons coupled to microelectrode arrays: a neuronal sensory system for pharmacological applications. Biosensors and Bioelectronics 2003;18: 627-34.

[18] Jordan S, Johnson JL, Regardie K, Chen R, Koprivica V, Tadori Y, Kambayashi J, Kitagawa H, Kikuchi T. Dopamine D2 receptor partial agonists display differential or contrasting characteristics in membrane and cell-based assays of dopamine D2 receptor signaling. Progress in Neuro-Psychopharmacology & Biological Psychiatry 2007;31:348-56

[19] Cukierman E, Pankov R, Stevens DR, Yamada KM. Taking cell-matrix adhesions to the third dimension. Science 2001;294:1708-12.

[20] Kunz-Schughart LA, Freyer JP, Hofstaedter F, Ebner R. The use of 3-D cultures for high-throughput screening: the multicellular spheroid model. J. Biomol. Screen. 2004;9:273-85

[21] Mueller-Klieser W. The use of 3-D cultures for high-throughput screening: The multicellular spheroid model. Journal of Biomolecular Screening 2004;9(4):273-85.

[22] Liu XS, Zhang ZG, Zhang RL, Gregg SR, Meng H, Chopp M. Comparison of in vivo and in vitro gene expression profiles in subventricular zone neural progenitor cells from the adult mouse after middle cerebral artery occlusion. Neuroscience 2007;146:1053-61.

[23] Vogt AK, Wrobel G, Meyer W, Knoll W, Offenhauser A. Synaptic plasticity in micropatterned neuronal networks. Biomaterials 2005;26:2549-57.

[24] Yousaf MN, Houseman BT, and Mrksich M. Using electroactive substrates to pattern the attachment of two different cell populations. PNAS 2001;98(11):5992-96.

[25] Wu Z-Z, Zhao YP, Kisaalita WS. Interfacing SH-SY5Y human neuroblastoma cells with SU-8 microstructures. Colloids and Surfaces B: Biointerfaces 2006;52:14–21.

[26] Wang L, Wu Z-Z, Xu B, Zhao Y, Kisaalita WS. SU-8 microstructure for quasi-three-dimensional cell-based biosensing. Sensors and Actuators 2009;140(2):349-55

[27] Griscom L, Degenaar P, LePioufle B, Tamiya E, and Fujita H. Cell placement and neural guidance using a three-dimensional microfluidic array. Jpn. J. Appl. Phys. 2001; 40: 5485-90.

[28] Merz M and Fromherz P. Silicon chip interfaced with a geometrically defined net of snail neurons. Adv. Funct. Mater. 2005;15(5):739-44.

[29] Chuang YJ, Tseng FG, Cheng J-H, Lin WK. A novel fabrication method of embedded microchannels by using SU-8 thick-film photoresists. Sensors and Actuators A 2003;103:64-9.

[30] Hung PJ, Lee PJ, Sabounchi P, Aghdam N, Lin R, Lee LP. A novel high aspect ratio microfluidic design to provide a stable and uniform microenvironment for cell growth in a high throughput mammalian cell culture array. Lab on a Chip 2005;5:44-8.

[31] Vernekar VN, Cullen DK, Fogleman N, Choi Y, Garcı′aA J, Allen MG, Brewer GJ, LaPlaca MC. SU-8 2000 rendered cytocompatible for neuronal bioMEMS applications. J Biomed Mater Res A 2009;89(1):138-51.

[32] Leclerc E, Furukawa KS, Miyata F, Sakai Y, Ushida T, Fujii T. Fabrication of microstructures in photosensitive biodegradable polymers for tissue engineering applications. Biomaterials 2004;25: 4683-90

[33] Liu X, Lim JY, Donahue HJ, Dhurjati R, Mastro AM, Vogler EA. Influence of substratum surface chemistry/energy and topography on the human fetal osteoblastic cell line hFOB 1.19: phenotypic and genotypic responses observed in vitro. Biomaterials 2007;28:4535-50.

[34] Dudley CN, Schöberl B, Sturgill GK, Beckhamb HW, Rezac ME. Influence of crosslinking technique on the physical and transport properties of ethynyl-terminated monomer/polyetherimide asymmetric membranes. Journal of Membrane Science 2001;191:1-11.

[35] Wang L and Kisaalita WS. Characterization of micropatterned nano-fibrous scaffolds for neural network activity readout for high-throughput screening. Journal of Biomedical Material Research Part B: Applied Biomaterials 2010 (in press)

[36] Desai A, Kisaalita WS, Keith C, Wu Z-Z. Human neuroblastoma (SH-SY5Y) cell culture and differentiation in 3-D collagen hydrogels for cell-based biosensing. Biosensors and Bioelectronics 2006;21:1483-92.

[37] Mao C and Kisaalita WS. Determination of resting membrane potential of individual neuroblastoma cells (IMR32) using a potentiometric dye (TMRM) and confocal microscopy. J Fluorescence 2004;14:739-43.

[38] Mao C, Kisaalita WS. Characterization of 3-D collagen hydrogels for functional cell-based biosensing. Biosensors and Bioelectronics 2004;19:1075-88.

[39] Mahlberg R, Niemi HE-M, Denes F, Rowell RM. Effect of oxygen and hexamethyldisiloxane plasma on morphology, wettability and adhesion properties of polypropylene and lignocellulosics. In. J. Adhension Adhesives 1998;18:283-97.

[40] Hennemeyer M, Walther F, Kerstan S, Schürzinger K, Gigler AM, Stark RW. Cell proliferation assays on plasma activated SU-8. Microelectronic Engineering 2008;85(5-6):1298-301

[41] Saha K, Keung AJ, IrwinE F, Li Y, Little L, Schaffer DV, Healy KE. Substrate modulus directs neural stem cell behavior. Biophysical Journal 2008;95(9): 4426-38.

[42] Wells RG. The role of matrix stiffness in regulating cell behavior. Hepatology 2008;47(4):1394-400.

[43] Kim S, English AE, Kihm KD. Surface elasticity and charge concentration-dependent endothelial cell attachment to copolymer polyelectrolyte hydrogel. Acta Biomaterialia 2009;5:144-51.

[44] Tay FEH, van Kan JA, Watt F, Choong WO. A novel micro-machining method for the fabrication of thick-film SU-8 embedded micro-channels. J. Micromech. Microeng. 2001;11:27-32.

[46] Miyake K, Satomi N, Sasaki S. Elastic modulus of polystyrene film from near surface to bulk measured by nanoindentation using atomic force microscopy. Appliled Physics Letters 2006;89:031925.

[47] Tzeng SF. Neural progenitors isolated from newborn rat spinal cords differentiate into neurons and astroglia. Journal of Biomedical Science 2002;9:10-6.

[48] O'Connor SM, Stenger DA, Shaffer KM, Matric D, Barker JL, Ma W. Primary neural precursor cell expansion, differentiation and cytosolic Ca^{2+} response in three-dimenreional collagen gel. Journal of Neuroscience Methods 2000;102:187-95.

[49] Chin VI, Taupin P, Sanga S, Scheel J, Gage FH, Bhatia SN. Microfabricated platform for studying stem cell fates. Biotechnol. Bioeng. 2004;88:399-415.

[50] Choi Y, Powers R, Vernekar V, Frazier AB, LaPlaca MC, Allen MG. High aspect ratio SU-8 structures for 3-D culturing of neurons. Proceedings of IMECE2003: 2003 ASME International Mechanical Engineering Congress and RD&D Expo November 12 – 21, 2003, Washington, D.C., USA

[51] Spratley JPF, Ward MCL, Hall PS, Thursfield C. Flexible SU-8 microstructures for neural implant design. Sensors and Actuators A 2008;147:324-31

[52] Kulesa PM and Fraser SE. In ovo time-lapse analysis of chick hindbrain neural crest cell migration shows cell interactions during migration to the branchial arches. Development 2000;127:1161-72

[53] Curtis A and Wilkinson C. Topographical control of cells. Biomaterials 1997;18(24):1573-83.

[54] Flamming RG, Murphy CJ, Abrams GA, Goodman SL, Nealey PF. Effects of synthetic micro- and nano-structured surfaces on cell behavior. Biomaterials 1999;20:573-88.

[55] Johnson J, Nowicki MO, Lee CH, Chiocca EA, Viapiano MS, Lawler SE, and Lannutti JJ. Quantitative analysis of complex glioma cell migration on electrospun polycaprolactone using time-lapse microscopy. Tissue Engineering: Part C 2009;15(4): 531-40

[56] Yamamoto K, Yamaguchi M, Okabe S. Direct visualization of cell movement in the embryonic olfactory bulb using green fluorescent protein transgenic mice: evidence for rapid tangential migration of neural cell precursors. Neuroscience Research 2005;51:199-214

[57] Seki T, Namba T, Mochizuki H, Onodera M. Clustering, Migration, and Neurite Formation of Neural Precursor Cells in the Adult Rat Hippocampus. The journal of comparative neurology 2007;502:275-90

[58] Beyec JL, Xu R, Lee SY, Nelson CM, Rizki A, Alcaraz J, Bissell MJ. Cell shape regulates global histone acetylation in human mammary epithelial cells. Experimental cell research 2007;313:3066-75

[59] Solon J, Levental I, Sengupta K, Georges PC, Janmey PA. Fibroblast adaptation and stiffness matching to soft elastic substrates. Biophysical Journal 2007;93:4453-61

[60] Houle F, Huot J. Dysregulation of the endothelial cellular response to oxidative stress in cancer. Mol Carcinog. 2006;45(6):362-7

[61] Verdoni AM, Smith RS, Ikeda A, Ikeda S. Defects in actin dynamics lead to an autoinflammatory condition through the upregulation of CXCL5. PLoS One. 2008;3(7):e2701.

[62] Wu Z-Z, Zhao YP, Kisaalita WS. A packed Cytodex microbead array for three-dimensional cell-based biosensing. Biosensors and Bioelectronics 2006;22:685-93.

[63] Chen CS and Mrksich M. Geometric control of cell life and death. Science 1997;276:1425-28.

[64] McBeath R, Pirone DM, Nelson CM, Bhadriraju K and Chen CS. Cell Shape, cytoskeletal tension, and RhoA regulate stem cell lineage commitment. Dev. Cell 2004;6:483-95.

[65] Hogg RC, Chipperfield H, Whyte KA, Staford MR, Hansen MA, Cool SM. Functional maturation of isolated neural progenitor cells from the adult rat hippocampus. Eur J Neurosci 2004;19:2410-20.

[66] Ratushnyak AS, Zapara TA, Zharkikh AA, Ratushnyak OA. Effects of changes in dynamic equilibrium in microtubule and microfilament systems on the plastic responses of neurons. Neurosci. Behav. Physiol. 1997;27(4):353-9

[67] Formigli L, Meacci E, Sassoli C, Squecco R, Nosi D, Chellini F, Naro F, Francini F, Zecchi-Orlandini S. Cytoskeleton/stretch-activated ion channel interaction regulates myogenic differentiation of skeletal myoblasts. Journal of Cellular Physiology 2007;211(2):296-306

[68] Cheng K, Lai Y., Kisaalita WS. Three-dimensional polymer scaffolds for high throughput cell-based assay systems. Biomaterials 2008;29:2802-12.

CHAPTER 5

CHARACTERIZATION OF MICROPATTERNED NANO-FIBROUS SCAFFOLDS FOR NEURAL NETWORK ACTIVITY READOUT FOR HIGH-THROUGHPUT SCREENING[*]

Key words: Nano-fibrous PLLA scaffolds; Laser micromachining; Micropatterns; Human neural stem cells; Chemical depolarization.

[*]Wang L., Kisaalita W.S. 2010. Characterization of micropatterned nano-fibrous scaffolds for neural network activity readout for high-throughput screening. *Journal of Biomedical Material Research Part B: Applied Biomaterials* (In press).

Reprinted here with permission of publisher.

5.1. Abstract

Micropatterns were fabricated in nano-fibrous poly-L-lactic acid (PLLA) films by laser micromachining and the resulting scaffolds were characterized with respect to architecture, thermal, mechanical and mass transport properties. Also, human neural stem cells were successfully cultured in these micropatterned nano-fibrous scaffolds (MNFSs). The scaffolds were incorporated in high-density well plates (e.g., 96-well plates), creating a platform for high-throughput screening (HTS) of drugs with physiologically more relevant networked neural cultures. Through mathematical modeling of the transport of model stimulants, the feasibility of stimulating neural networks cultured in MNFSs was demonstrated. More work is needed to establish biological network activity-MNFS architecture relationships.

5.2. Introduction

Mental and/or neurodegenerative disorders, such as schizophrenia and Alzheimer's disease (AD), are among the most devastating illnesses in western society. However, there are few effective drugs for such diseases[1]; for example, currently used drugs for schizophrenia still have shortcomings[2]. Drug discovery against these disorders is in great demand, which calls for effective screening of available molecular libraries to identify effective small molecules as drug leads. To quickly identify hits from diverse molecular libraries, cell-based assays together with automated high-throughput screening (HTS) are the state of the art.

Many studies have suggested that synaptic pathology and neurotransmission dysfunction underlies these biological mechanisms for mental and neurodegenerative disorders[3]. Neural

networks, which can recapitulate these crucial targets, may act as a platform for screening available molecule libraries in drug discovery. *In vitro* screening of drugs that affect neural network function *in vivo* is still primitive as current assays rely on single cellular responses from two-dimensional (2D) cell cultures. Three-dimensional (3D) cell-based assays may yield physiologically more relevant results and thus have the potential to bridge the gap between 2D assays and preclinical animal testing, saving time and cost by improving clinical efficacy predictability. Thus, engineering a platform for 3D neural network patterning *in vitro* for HTS system is an ideal first step to move to 3D neural-network-based assay.

To pattern neural networks formation *in vitro,* chemical patterning and structural guiding [4,5] are commonly used methods. Microlithographic materials and techniques[6], microcontact printing[7,8] and self-assembled monolayers[9] are mainly used to tailor the properties of the substrates for patterning neural cell growth. However, these cells are maintained on 2D substrates. Topographical structures can provide physical guidance for neural network formation *in vitro* and micropatterned substrates have long been considered a promising approach for the creation of defined neuronal networks *in vitro*. High-aspect-ratio microstructures are thought to provide quasi-3D microenvironments with well-defined architectures for neural cell growth and neural network formation[10,11]. Microstructures made of polydimethylsiloxane (PMDS)[12] and SU-8 (epoxy-based negative photoresist)[13] have been reported to control neuronal outgrowth and synapse formation *in vitro*. However, these structures are devoid of natural extracellular matrix (ECM) architecture with respect to nano-fibrous structures.

To best mimic the architecture of the natural ECM, nano-fibrous scaffolds have been fabricated using phase separation[14], electrospinning[15] and self-assembly[16]. The nano-fibrous scaffolds are able to promote the differentiation of neural stem cells[17,18] and induce "3D matrix adhesion" as defined by Cukierman et al. [19] in human fibroblast cells. These nano-fibrous structures have been combined with microporous structures for tissue engineering[20]. In this study, we aimed to combine the effects of nano-fibrous scaffolds on neural stem cell differentiation and that of microstructures on neural network patterning, to provide micropatterned nano-fibrous scaffolds (MNFSs) for neural network formation *in vitro*. Furthermore, we aimed to integrate the MNFSs with currently used HTS systems (e.g. 96-well plates) for neural network activity readout.

To study neural network activity, depolarizing neural cells by chemicals and observing signal propagation (such as calcium wave propagation stimulated by high concentration potassium buffer) is one commonly used method[21]. With the development of fluorescence based technologies and their implementation in HTS systems, e.g., fluorometric imaging plate reader (FLIPR), neural-network-based assay combined with fluorescence imaging could be an invaluable tool in drug discovery, especially for screening drugs or compounds against neural network activity. In such an application, one main concern is to distinguish whether the signal propagation observed in the network is due to cell-to-cell connectivity or due to stimulant compound diffusion from the injection spot. Thus, the third aim was to simulate model stimulant compound transport to compare chemical diffusion to signal propagation in MNFSs with the goal of establishing the feasibility of stimulating neural networks by chemical means in this platform.

5.3. Materials and methods

5.3.1. Fabrication of nano-fibrous scaffold

The nano-fibrous scaffold was fabricated by the liquid-liquid phase separation method using poly-L-lactic acid (PLLA)[14]. Fig. 5.1 shows the flow diagram for the fabrication process. Briefly, PLLA (Sigma, St. Louis, MO), was homogeneously dissolved into tetrahydrofuran (THF) at various concentrations (1.25%-5% wt/v). Based on previous studies[14] and preliminary study in our group (data not shown), it is found that when the concentration increased (such as 9% wt/v), the solution (PLLA in THF) became very viscous and the fabricated scaffold lacked porous structure and nanofibers. When the concentration was too low (such as 1% wt/v), the formed gel was very fluffy and unstable in cold water. Thus the range 1.25%-5% wt/v was chosen in this study. 4 mL PLLA/THF solution was pre-warmed at 55 °C and then quickly cast onto a glass Petri dish (8 cm in diameter) followed by ultra-freezing at -80 °C for 2 h. The gelled PLLA/THF solution was immersed into cold double distilled water (4 °C) for 2 days to leach out the solvent (THF). Water was changed three times every day and the resultant PLLA structure was air-dried. PLLA scaffolds without nano-fibrous structures were fabricated following the same procedure but without the ultra-freezing process.

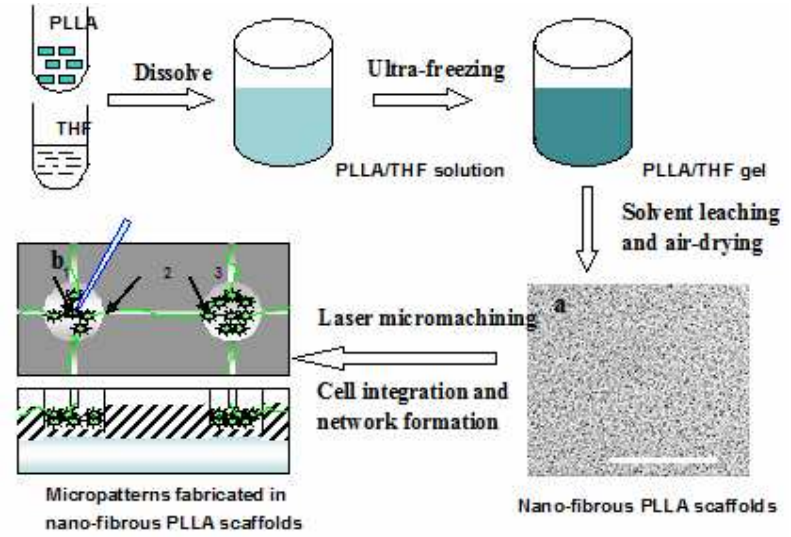

Fig. 5.1. Flow diagram of the fabrication process: (a) the resultant nano-fibrous PLLA structure; (b) the schematic of micropatterns fabricated in nano-fibrous PLLA film; the top is the top view and the bottom is the cross-section view. Assuming a neural network in the microstructure unit, stimulus would be added through a micropippet to the cell at the center of the stimulus microwell (postion 1). Cellular signal (e.g. calcium wave) would propagate from the stimulus microwell (position 1) to the neighboring well (position 3) within this neural network; meanwhile, the stimulating compound would diffuse from the stimulus well (position 1) to the neighboring well (position 3). Scale bar = 100 μm.

5.3.2. Characterization of nano-fibrous PLLA scaffolds

5.3..2.1. SEM observation. PLLA scaffolds were sputter-coated with gold for 60 s to achieve a coating thickness of about 15.3 nm. SEM images were captured with a FEI Inspect-F scanning electron microscope (FEI Company, OR, USA). Fiber diameters were measured with Simple PCI image software (Compix Inc., Cranberry Township, PA).

5.3.2.2. Porosity measurement. The porosity values of the nano-fibrous scaffold were measured by liquid displacement[22]. Ethanol was used in our procedure because it penetrated easily into the pores and did not induce shrinkage or swelling.

5.3.2.3. Diffusivity measurement by fluorescence recovery after photobleaching (FRAP). Diffusion coefficients of both small and large molecular weight compounds were measured with fluorescein sodium and FITC-dextran. Fluorescein sodium, USP (MW = 332, Allied Chemical, India) was chosen because it is similar in size to many small molecular weight drugs, such as ketamine (MW = 238). FITC-dextran (~40 kDa, Sigma-Aldrich) was selected because it is similar in size to some large molecular weight compounds in media, such as leukemia inhibitory factor (LIF, ~32-62 kDa).

All FRAP experiments were performed on a Leica DMI 6000B microscope with Leica TCS SP5 LAS AF FRAP wizard (Leica Application Suite Advanced Fluorescence). Samples were incubated with fluorescein sodium (30 μM) or FITC-dextran (30 μM) at 4 °C overnight. Before testing, samples were equilibrated at room temperature for 30 min, and all tests were performed at room temperature (25 °C). FRAP experiments were carried out in the middle of the scaffolds. The middle zone FRAP experiments were performed at approximately half of the scaffold thickness from the surface. All photobleaching was performed with an argon laser at 100% power (100 mV, 488 nm emission) for 394.5 s. Images in recovery process were performed with an argon laser at 5% power for 395.4 s (300 frames, with an interval of 1.315 s). All images were recorded with a 20×/0.5 HCX PL APO CS 0.70 DRY UV objective (Leica). Images were 512 by 512 pixels.

Diffusion coefficients were calculated from the FRAP experiments using the method described by Axelrod et al. [24]. Briefly, the mean fluorescence in the bleached region over time was converted to a normalized fractional fluorescence intensity

$$f = F(t)-F(0)/F(\infty)-F(0) \qquad (1)$$

where F(t) is the fluorescence intensity at time t, F(0) is the fluorescence intensity immediately after bleaching, and F(∞) is the fluorescence after complete recovery. The fractional fluorescence intensity was plotted versus time and fitted with a logarithmic curve. The recovery rate varied with size of the bleached area, location of the bleached area and the size of the diffusing molecule[25]. The equation for the curve was used to determine the half-recovery time ($\tau_{1/2}$) at f = 0.5. The bleaching parameter, which describes the relationship between the half-recovery time and the characteristic diffusion time, was also calculated according to Axelrod et al. [24]. The half-recovery time, $\tau_{1/2}$, the measured initial spot radius ω, and the bleaching parameter, γ_D [24], were used to determine the diffusion coefficient, D:

$$D = (\omega^2/4\,\tau_{½})\,\gamma_D \qquad (2)$$

5.3.2.4. Thermal properties. The thermal properties of air-dried PLLA scaffolds were characterized by differential scanning calorimetry (DSC). The Thermal Analysis Instruments Mettler Toledo DSC 823[e] (Mettler-Toledo Inc., Columbus, OH) was operated in standard mode using an aluminum pan reference with a nitrogen purge rate of 50.0 mL/min. The standard mode DSC heating program was equilibrated at 20°C and the ramp temperature set at 10°C /min to 200°C. Glass transition temperature (T_g), the melting temperature (T_m), and the enthalpy of melting of PLLA (ΔH_m) were determined. The degree of crystallinity (X_c) was calculated as $X_c = \Delta H_m / \Delta H_m^0$, where ΔH_m^0 is the enthalpy of melting of 100% crystalline PLLA. The calculated value of ΔH_m^0 is 93.7 J/g[14,22].

5.3.2.5. Mechanical property. The compressive modulus of the nano-fibrous PLLA scaffolds (5% wt/v) was measured at ambient temperature. The samples were tested on an Instron Model 3344 Materials Testing Machine (Instron Co., Canton, MA, USA). Scaffolds were cut into pieces (approximately 10 mm in length and 10 mm in width) for testing. Samples were compressed at a displacement rate of 0.6 mm/min. Four different samples were tested.

5.3.2.6. Optical property of micropatterns. Light transmittance of polymer scaffolds at the pattern position was measured by a microscope (BX40, Olympus) coupled with a digital camera (D100, Nikon). Images were taken with the same lamp power and exposure time. These images were processed with SimplePCI 2000 software. The light transmittance ratio was calculated by dividing the sample mean grey level from three different spots by the control grey level (plain cover slips).

5.3.2.7. Surface energy and contact angle measurement. Contact Angle System OCA (Future Digital Scientific. Corp., USA) with analysis software (SCA20) was used to determine the surface contact angles on the nano-fibrous PLLA samples both before and after NaOH treatment. Distilled water was used as a contacting solvent. All data were obtained 5 s after placing the droplet on the surfaces under ambient conditions. The surface energy of the contacting surface (E_s) was calculated according to $E_s = E_{lv}\cos\theta$. E_{lv} is the surface energy between the water and air, which is 72.8 mJ/m^2 at 20 ℃ for pure water; θ is the static contact angle[23].

5.3.3. Fabrication of MNFSs

Nano-fibrous PLLA scaffolds were micromachined with an excimer laser-based laser micromachining system Resonetics RapidX250 (Resonetics, USA). The excimer laser model coupled to this system was ATLEX-500-SI (ArF, 193 nm wavelength). The direct write approach was used as micromachining mode. Using appropriate mask sizes, channels (10-20 μm wide) and wells (up to 100 μm in diameter) were fabricated into the nano-fibrous structure, creating high-aspect-ratio MNFSs.

5.3.4. Integration of MNFSs with 96-well plates

MNFSs were cut into pieces that can fit into the wells of 96-well plates (*In Vitro* Scientific, Sunnyvale, CA) using laser micromachining with the Rapid X 250 Excimer System (Resonetics, Nashua, NH). Then PLLA pieces were glued on the bottom of these wells by MONO AQUA liquid glue which is transparent and non-toxic (American Tombow Inc., Suwanee, GA).

5.3.5. Simulation of chemical diffusion in MNFSs.

As depicted in Fig. 1(b), a stimulating compound was added through a micropippet to an imaginary cell at the center of the stimulus microwell (i.e. postion 1). If the stimulus concentration at position 1 reached the threshold value (e.g. voltage-gated calcium channel opening), cellular response at position 1 and signal propagation (e.g. calcium wave propagation) from the stimulus microwell (position 1) to the neighboring wells (i.e. position 3) would be induced. Meanwhile, the stimulating compound would diffuse from position 1 to position 3. At the time it took the signal to reach cells at position 3, the stimulus

concentration due to diffusion was compared with the threshold value for inducing cellular response; confirming that the cellular response that would be observed at position 3 would only be due to network connectivity and not the diffusing chemical.

Diffusion of small molecular weight compounds within MNFSs was simulated with COMSOL Multiphysics 3.5a (COMSOL Inc., MA, USA). Fluorescein was chosen to represent small molecular weight compounds. Fluorescein (500 mM[11]) was added through a micropippet with a tip opening of 6 μm, 20 μm or 50 μm. And the threshold value for stimulating cell response was assumed to be 50 mM[11]. Diffusivity of fluorescein in water is 640×10^{-12} m^2/s [26] and that of fluorescein in nano-fibrous PLLA scaffolds (5%) was measured as described above. Calcium waves have been observed to travel at a speed ranging from 10 μm/s to 100 μm/s [27]. A calcium wave propagating speed of 43 μm/s [21] was assumed. Microwell diameter was 50 μm and channel width was 10 μm; two channel lengths (70 μm and 100 μm) were investigated.

5.3.6. Cell line and cell culture

Human neural stem cells ENStem-A™ were purchased from Millipore (Billerica, MA) and maintained in 35 mm Petri dishes with 2 mL growth medium in a 5% CO_2 humidified atmosphere at 37 °C. ENStem-A™ expansion media supplemented with penicillin/streptomycin, L-glutamine and basic fibroblast growth factor (bFGF). The medium was changed every other day. The cells were passaged by mechanically pipetting when progenitor cells reached 90% to 100% confluence, around 1.2×10^6 cells were seeded into each new dish. Prepared nano-fibrous PLLA micropatterns were treated with 0.2 M NaOH

for 40 min at 40 °C to increase the surface hydrophility. Then samples were sterilized by immersion in 70% ethanol in distilled water (DI) under a UV germicidal lamp overnight. After sterilization, they were rinsed in sterile DI water 3 times. The substrates were then coated with poly-ornithine (Sigma, St. Louis, MO) in water at a concentration of 40 μg/mL for at least 1 hour. This was followed by coating with laminin (Sigma, St. Louis, MO) at a concentration of 5 μg/mL. These dishes were stored at 4 °C unstill use.

5.3.7. Fluorescence staining and fluorescent microscopy

Neural stem cells were stained with calcein AM (Biotium, Hayward, CA). This fluorescent dye stains live cells and their extensions by the presence of intracellular esterase activity, which converts the non-fluorescent cell-permeant calcein AM to intensely fluorescent calcein. Cells were washed with 2 mL Neurobasal without phenol red (Invitrogen, Carlsbad, CA) three to five times. Then cells were exposed to 2 mL 2 μM calcein AM in neurobasal and incubated for 30 min at 37 °C before the staining solution was replaced. Samples were washed with neurobasal 3 times. Sample fluorescence was viewed and captured with a B-2E/C FITC filter block (Nikon, Melville, NY, USA), which has an excitation bandwidth of 465-495 nm and a filter pass range of 515 - 555 nm.

5.3.8. SEM observation

Cells on PLLA patterns were fixed with 2% glutaraldehyde in 0.1 M sodium cacodylate buffer (pH 7.2) for 1 h and then rinsed in cacodylate buffer three times (15 min each). This was followed by post-fixing with 1% OsO_4 in 0.1 M sodium cacodylate buffer for 1 h and rinsing in cacodylate buffer three times (5 min each). The samples were then dehydrated in

35%, 50%, 70%, 80%, 95% and 100% ethanol successively for 10 min each and dried in Hexamethyldisilazane (HMDS, Sigma, St. Louis, MO). Scaffolds were sputter-coated with gold for 60 s to achieve a thickness of about 15.3 nm. SEM images were captured with a FEI Inspect-F scanning electron microscope (FEI Company, OR, USA).

5.3.9. Data analysis and statistics

Student's t-test was used for statistical comparisons of fiber diameter and porosity.

5.4. Results and discussions

5.4.1. Characterization of nano-fibrous PLLA scaffold

5.4.1.1. Structure, porosity and mass transfer within scaffolds. Figure 5.2 shows the SEM images of nano-fibrous PLLA scaffolds prepared at different concentrations of PLLA in THF. Fiber diameters were measured and the results are presented in Table 5.1. It was found that the fiber diameters increased significantly ($P<0.05$) when the PLLA concentration increased. These fibers were all at sub-micro scale (~ 200 - 300 nm), which is close to the size range of collagen matrix (~ 50 - 200 nm). Thus the nano-fibrous structures could mimic the architecture of the natural extracellular matrix (ECM) with respect to fiber size.

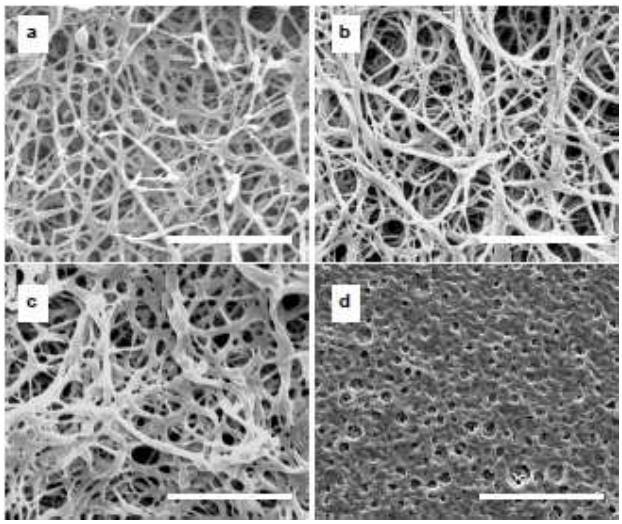

Fig. 5.2. SEM images of nano-fibrous PLLA scaffolds prepared at different concentrations of PLLA in THF (a-c): (a) 1.25% wt/v; (b) 2.85% wt/v and (c) 5% wt/v. (d) shows 5% wt/v PLLA in THF scaffolds without nano-fibrous structures. Scale bar = 5 µm in (a-c), and 20 µm in (d).

Table 5.1. Fiber size distribution of nano-fibrous scaffolds fabricated with various PLLA concentrations

Concentrations of PLLA in THF solution (wt/v%)	**1.25**	**2.85**	**5**
Fiber diameter (mean±SD) (nm)	202.8±33.9 (n = 77)	238.2±45.1* (n = 49)	293.6±49.4*# (n = 38)
Porosity (%)	92.2±3.0 (n = 3)	85.9±0.2* (n = 3)	84.9±1.2* (n = 3)

*: P<0.05. Compared with the data of 1.25% (wt/v) PLLA scaffold. #: P<0.05. Compared with the data of 2.85%(wt/v) PLLA scaffold.

The nano-fibrous PLLA scaffolds were highly porous as shown in Table 5.1. Compared with PLLA scaffolds without nano-fibrous structures which had a porosity of 53.85%, the porosities of nano-fibrous PLLA scaffolds were above 80%. As the PLLA concentration increased, the scaffold porosity decreased (Table 5.1). However, the porosity was still above 80%. These results were consistent with results for freeze-dried PLLA nano-fibrous scaffolds [14], suggesting that the drying method may not be a factor in resultant porosity.

Highly porous PLLA scaffolds allowed molecular diffusion within the scaffolds, ensuring cells in the scaffolds enough exposure to chemicals in the media. In cell culture media, compounds vary from small molecules (MW < 1kDa) to large ones (MW ~ 60 kDa). And fluorescein sodium and FITC-dextran were selected to represent these compounds. Diffusivities of fluorescein sodim and FITC-dextran in PLLA scaffolds with different PLLA concentrations in THF (2.85% and 5%) were studied by FRAP. Fig. 5.3 presents examples of fluorescence intensity recovery in the bleached region vs. time in 2.85% (wt/v) PLLA scaffolds. As expected, larger molecules diffused much slower than small molecules. In 2.85% (wt/v) PLLA scaffolds, diffusivity of fluorescent sodium was 124.38 ± 2.02 $\mu m^2/s$ (n = 3) and diffusivity of FITC-dextran was 5.26 ± 0.28 $\mu m^2/s$ (n = 3); in 5% (wt/v) PLLA scaffolds, diffusivity of fluorescent sodium was 104.31 ± 1.90 $\mu m^2/s$ (n = 3) and diffusivity of FITC-dextran was 4.21 ± 0.50 $\mu m^2/s$ (n = 3). The measured diffusion coefficient of fluorescein sodium in 5% PLLA is smaller than that in water [26,28].

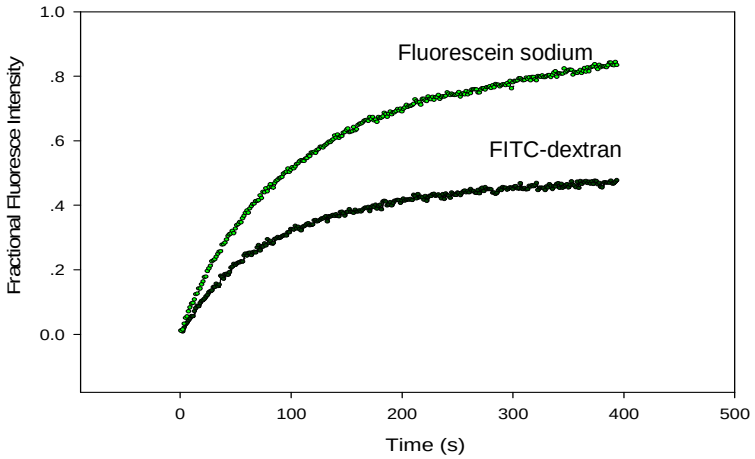

Fig. 5.3. Examples of fluorescence intensity recovery in the bleached region vs. time after bleaching in 2.85% (wt/v) PLLA in THF scaffolds.

5.4.1.2. Mechanical property and thermal property. As supportive substrates for cell culture and platforms for HTS application, sufficient mechanical strength of the scaffolds is required. The compressive modulus of the nano-fibrous PLLA scaffolds (5% wt/v) was measured. The nano-fibrous PLLA scaffolds had a compressive modulus of 9.65 ± 0.43 MPa (n = 4). Compared with the modulus of freezing-dried nano-micro-PLLA scaffolds which was within 50 kPa[29], the increase in film stiffness may be due to the air-drying process. Mechanical cues from microenvironments, such as substrate modulus, affect cell behavior, especially directing neural stem cell differentiation [30,31]. According to these studies, neural tissues preferred substrates with a modulus of the brain tissue (around 500 Pa). In our case, the nano-fibrous PLLA substrates are too stiff to provide an in-vivo like substrate for neural cell growth with respect to stiffness. However, the architecture of microwell structures promoted cellular cluster formation within the microwells (as shown in Fig. 5.5 and Fig. 5.6). Cell-cell contact within the clusters could become dominant for cell differentiation. Thus, the nano-fibrous PLLA micropatterns are still promising in providing a microenvironment which favors neural stem cell growth and differentiation.

Though PLLA has gained much interest in tissue engineering, its lower melting temperature and lower ability of crystallization limit its widespread application[32]. Thermal properties were studies by DSC and the results are presented in Table 5.2. The average glass transition temperature (T_g) and the average melting temperature (T_m) of nano-fibrous PLLA scaffolds was 65.55 °C and 175.93 °C, respectively. The average crystallinity (X_c) was found to be 56.71%. PLLA scaffolds without nano-fibrous structures (5% wt/v) were fabricated without ultra-freezing process and their thermal properties were characterized by DSC. These

PLLA scaffolds without nano-fibrous structures (5% wt/v) had a lower T_g (53.46 ℃) and a lower X_c (31.11%) than nano-fibrous PLLA scaffolds (5% wt/v), indicating that the thermal properties and crystallization properties have been improved in nano-fibrous PLLA scaffolds[32]. Thus, the nano-fibrous PLLA scaffolds have great potential as high performance polymers for HTS systems.

Table 5.2. Thermal properties of PLLA nano-fibrous scaffolds determined by DSC

Concentrations of PLLA/THF solution (wt/v%)	**T_g (℃)**	**T_m (℃)**	**X_c (%)**
1.25	67.62	175.39	56.64
2.85	64.88	176.65	56.98
5	64.14	175.74	56.52

5.4.2. Fabrication and characterization of MNFSs

Laser micromachining is a powerful tool for microstructure fabrication. It is capable of cutting, drilling, etching, stripping, and skiving materials such as polymers, plastics, glass, semiconductor materials, ceramic and thin metals. And achievable microstructure dimension ranges from 1 μm to 1mm. Fig. 5.4 shows different micropatterns fabricated in nano-fibrous PLLA films. The “direct write” approach was used as the micromachining mode. Using appropriate mask sizes, channels (around 10 μm) and wells (up to 100 μm) were fabricated into the nano-fibrous structure. The depths can be controlled by the number of laser pulses (data not shown) or energy level (which was kept constant in this study). Laser micromachining can be directly applied to different kinds of polymers using direct write approach, which provides flexibility in material choices, fabrication techniques and pattern

design. In addition, the fabrication technique avoids use of chemical reagents that may introduce undesirable effects for cell culture applications. Furthermore, using this technique, it is possible to produce microstructured units in sufficiency to meet the need in HTS.

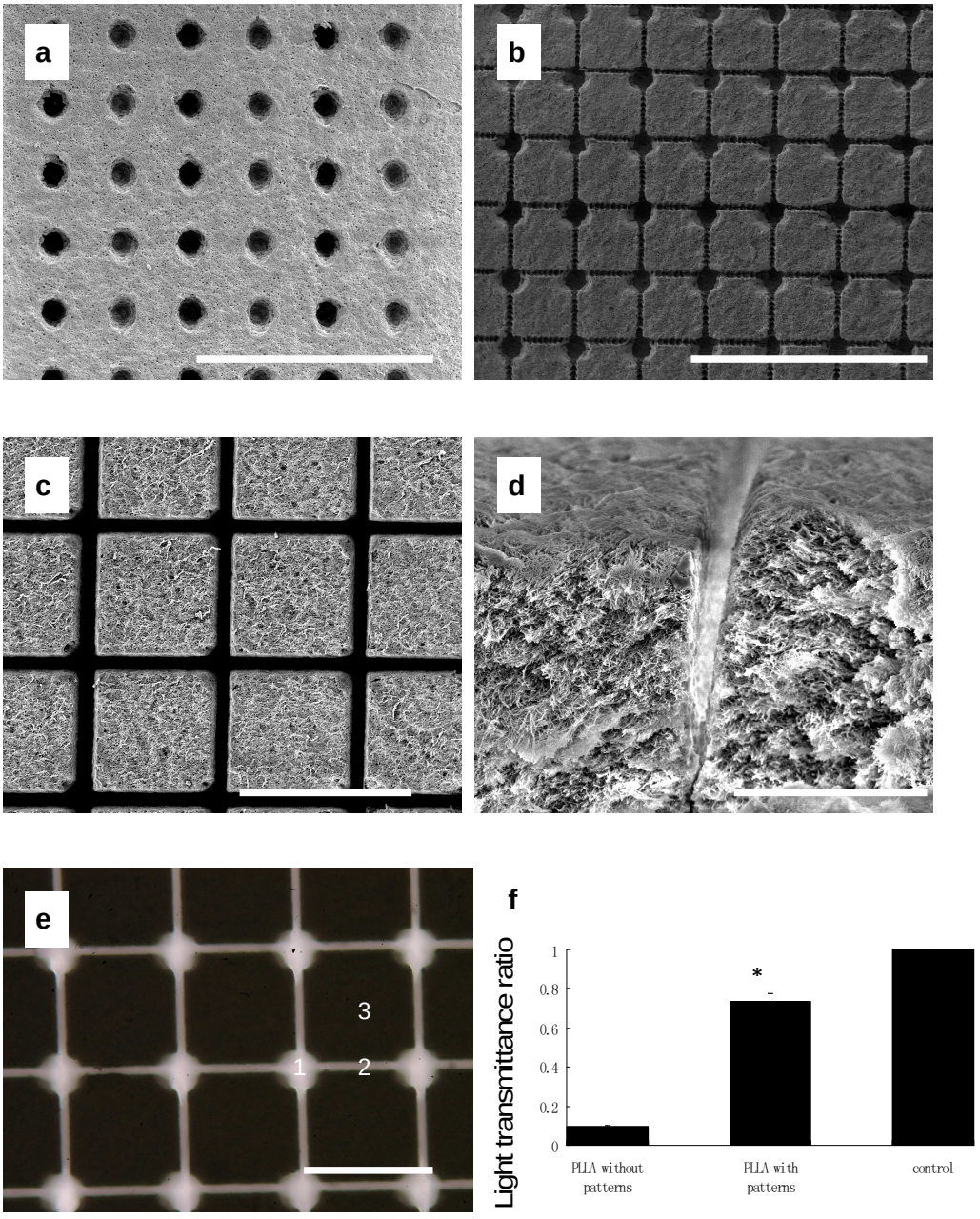

Fig. 5.4. SEM images (a-d) of micropatterns fabricated in nano-fibrous PLLA in THF scaffolds (5% wt/v). (a): a microwell array. (b): a network pattern consisting of microwells and channels. (c): a network pattern consisting of channels only, without microwells. (d): the crosssection of a channel in the scaffold. (e): phase contrast image of micropatterned nano-fibrous scaffolds (MNFSs) as in (b). (f): the light transmittance profile at the positions with micropatterns (such as position 1 and 2 in (e)) and without micropatterns (such as position 3 in (e)); * indicated that the light transmittance ratio at the position with patterns was significantly higher than that at the position without patterns. Scale bar = 500 µm in (a) and (b), 200 µm in (c) and (e), and 50 µm in (d).

Compared to microstructures derived through traditional microfabrication using SU-8 or PDMS, micropatterns based on nano-fibrous PLLA scaffolds have high porosity. Also, nano-fibrous structures provide extra cellular matrix contact for cell attachment that mimics *in vivo* extracellular collagen fibers in terms of scale. However, PLLA scaffolds are opaque, which is unfavorable for optical detection methods. To solve this problem, microwells in PLLA scaffolds were drilled through, leaving a thin film at the bottom and making cells in the wells optically accessible (Fig. 5.1 (b)). Fig. 5.4 (e) shows a phase contrast image of the MNFSs in Fig. 5.4 (b). From Fig. 5.4 (f), it is evident that the light transmittance at the positions with microstructures was improved.

Prepared MNFSs were hydrophobic, which is unfavorable for cell culture. To tailor the surface property for cell culture purpose without changing nano-fibrous structures, MNFSs were treated with 0.2 M NaOH. Studies have shown that NaOH treatment on PLLA increased material wettability and surface roughness at nanometer scale[33]. Modification of surface wettability/energy can be used to improve cell adhesion and proliferation[23, 33]. Through base hydrolysis treatment, the contact angle of PLLA film decreased from 116.4 ◦ to 46.4 ◦, and surface energy increased from -32.3 mJ/m^2 to 50.2 mJ/m^2. The modified PLLA surface would be suitable for cell attachment. Fig. 5.5 and Fig. 5.6 show cell integration with MNFSs. Cell

patterning in a network pattern consisting of microwells and channels (as in Figure 5.4(e)) can be observed in Fig. 5.5 (b). Cells attached to the inside walls of the microwells and formed clusters within the wells (Fig. 5.5 (c) and (d)). Neurite extension was also observed along the microchannels (Fig. 5.5 (c)). These observeations were confirmed by SEM images in Fig. 5.6. Thus, we successfully integrated neural stem cells with MNFSs. The nano-fibrous PLLA based micropatterns can provide physical guidance for neural network formation *in vitro*.

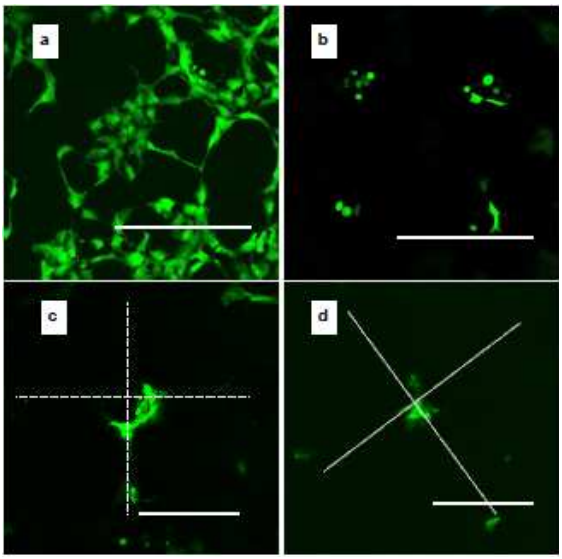

Fig. 5.5. Fluorescence images of calcein stained neural stem cells: (a): on 2-D nano-fibrous PLLA substrate. (b-d): within MNFSs; a network pattern consisting of microwells and channels (as in Figure 4(e)) was applied in this study. (c-d): cells attached to the sidewalls of microwells or formed clusters in the wells; dotted line shows the position of channels. Scale bar = 150 µm in (a) and (b), 100 µm in (c) and (d).

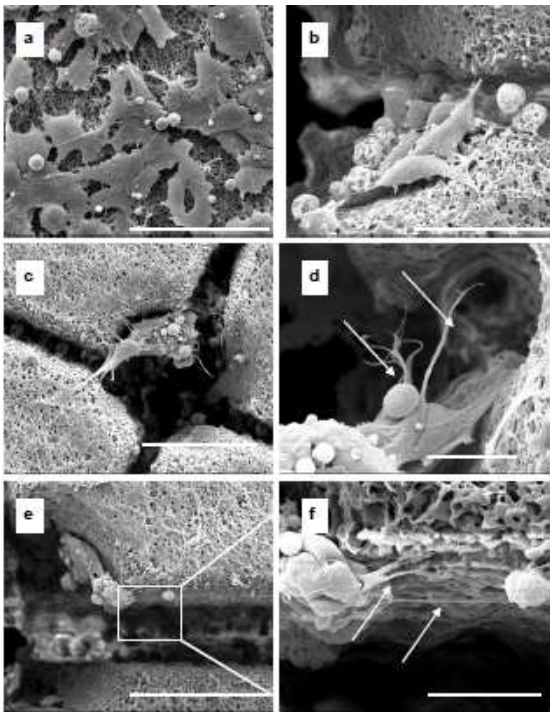

Fig. 5.6. SEM images of neural stem cells: (a): on 2-D nano-fibrous PLLA substrate. (b-f): in a network pattern consisting of microwells and channels (as in Figure 4(e)). (b-c): attached to the sidewalls of microwells or formed clusters in the wells. (d-f): neurite extensions observed in the well and along the channel (arrows). Scale bar = 50 µm in (a), (c) and (e), 30 µm in (b), and 10 µm in (d) and (f).

5.4.3. Integration of MNFSs into high-density-well plates

To demonstrate potential for MNFSs in HTS system, MNFSs were integrated with 96-well plates. These films were cut into pieces that fit 96-well plate (Fig. 5.7 (a)). The pieces were then glued on the bottom of these wells with a non-toxic glue (Fig. 5.7 (b) and (c)), which did not affect the nano-fibrous structures of PLLA scaffolds (Fig. 5.7(d)). The glue formed a thin film between PLLA scaffold and glass (Fig. 5.7(d)). The glue sealed the nano-fibrous structures only at the interface of glue film and PLLA scaffolds (Fig. 5.7(e)). The glue is transparent and the thin glue film did not block light transmission (data not shown). Combined with fluidic handing, this process can be adapted to any other currently used cell culture dishes or plates (24-well, 384-well plates), providing ready-to-use convenience and automated instrumentation compatibility. Our future study will characterize neural stem cell differentiation and network connectivity within nano-fibrous PLLA

micropatterns, which will provide a proof-of-concept for network-based platform for biosensing in drug screening.

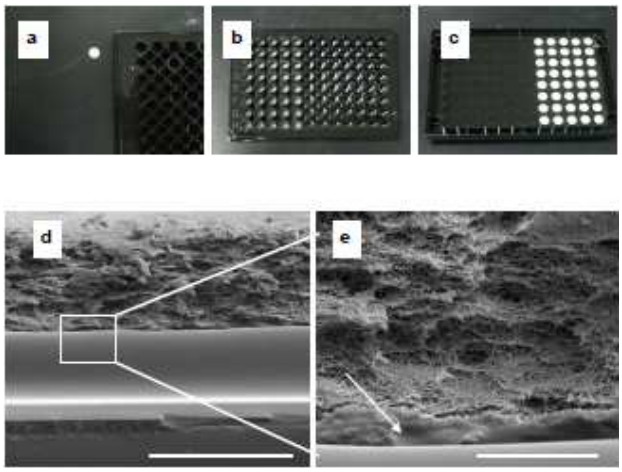

Fig. 5.7. (a): a small round piece of MNFSs which was cut by laser micromachining according to the dimension of 96-well plates; (b) and (c): the top (b) and bottom (c) views of 96-well plates after integration of MNFSs. (d) and (e): SEM images of nano-fibrous PLLA scaffolds glued onto the plate glass bottom. At the interface of PLLA scaffold and glue, the nano-fibrous structures were sealed by glue (arrow); but most of the PLLA film still kept the nano-fibrous structures as shown in (d) and (e). Scale bar = 100μm in (d) and 20 μm in (e).

5.4.4. Simulation of chemical diffusion in MNFSs

Fig. 5.8 (a) presents the fluorecein concentration profiles at different positions in MNFSs after injecting from the tip. At position 1, the stimulus concentration drops abruptly from initial 500 mM to around 16 mM at 0.1 s. Thus the concentration at position 1 reaches the threshold value of 50 mM within 0.1 s, and the cell at position 1 would get stimulated. At position 2, the concentration increases to about 4 mM and then decreases to 0 gradually, which is lower than the threshold value and could not induce cellular response. This indicates that 6 μm wide tip can be used to chemically stimulate single cell without affecting cells nearby. The concentration at position 3 increases slightly to a value above 0; and the process happens very slowly. A calcium wave propagation, traveling at 43 μm/s, takes around 3.5 s to reach the neighboring well from the stimulation spot when the channel length is 150 μm. At that time, the concentration at position 3 is still lower than the threshold value for inducing

cellular response (Table 5.3). Thus, if cellular response is observed at position 3, it would be caused by cell-cell interaction within the network rather than stimulus diffusion. Thus, using these MNFSs for studying neural network activity by chemical stimulation is feasible. Fig. 5.8 (b) shows the diffusion from the stimulus well to the neighboring wells at 1 s, 5 s and 10 s after stimulus injection.

Table 5.3 summarizes the concentration profiles at position 3 at different time points after adding the stimulus for patterns with different channel lengths. The numbers in bold are the concentrations at the time when calcium waves reach position 3. The concentrations were too low to stimulate cell response. However, the concentrations at position 3 in patterns with channel length of 70 μm were higher than that in patterns with a channel length of 150 μm. This indicates the effects of channel length on compound diffusion within microstructures. For chemical depolarization of neural network in MNFSs, channel length should be long enough to distinguish cellular response caused by stimulus from that caused by cell-to-cell communication.

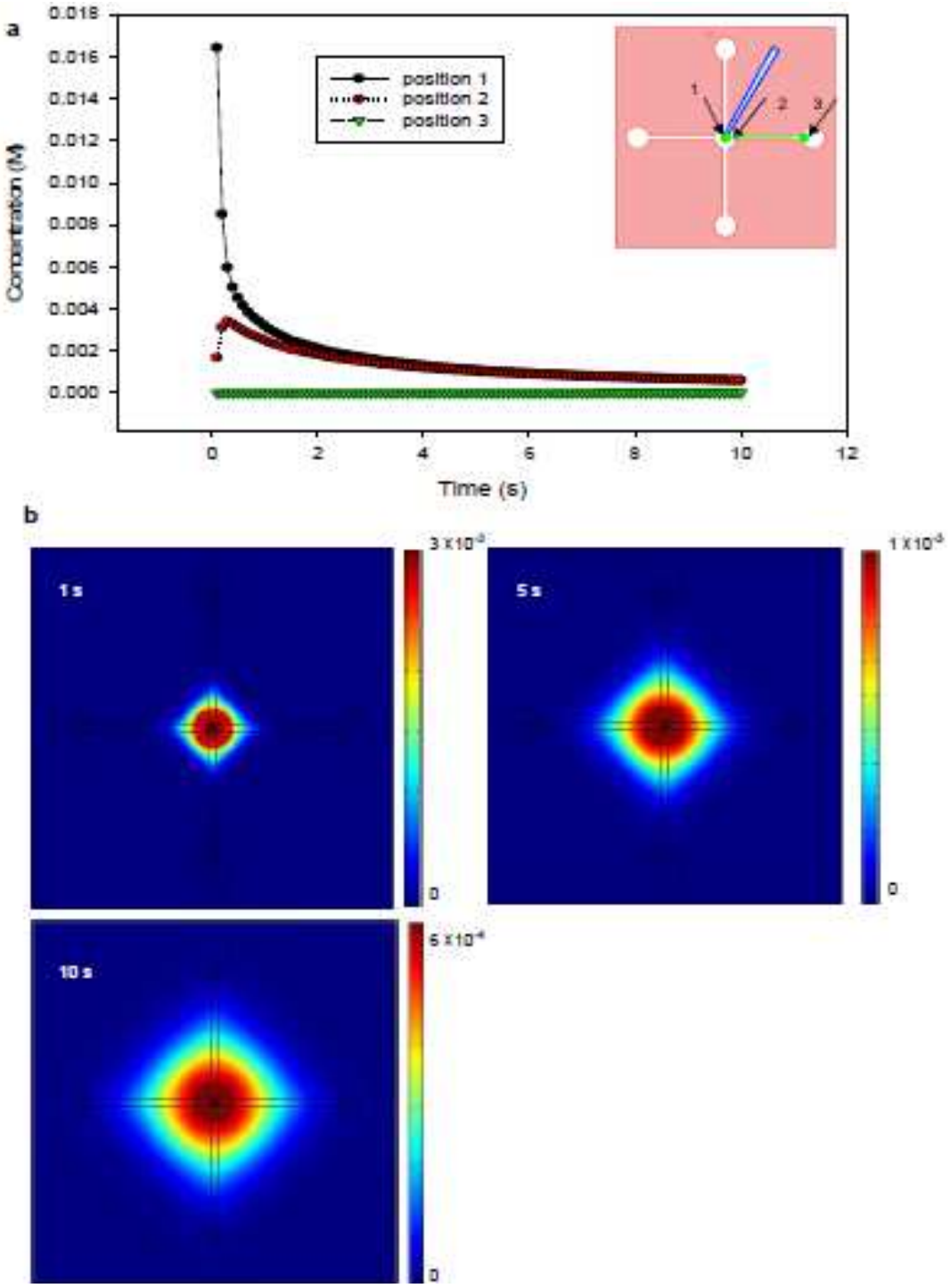

Fig. 5.8. Simulation of fluorescein diffusion in MNFSs. (a): The micropatterns had microwells of 50 µm in diameter, with channel width and length of 10 µm and 150 µm respectively. The diffusion of 500 mM fluorescein added through a micropippet with a tip diameter of 6 µm at postion 1 in the stimulus well was simulated (inset). Plots show fluorescein concentrantion profiles at positions 1, 2 and 3. (b): simulated fluorescein diffusion in the MNFSs from the stimulus well to the neighboring well at 1 s, 5 s and 10 s after fluorescein addition.

When adding stimulus with tips of different opening areas, concentration profiles at position 3 were also studied (Table 5.1S and Table 5.2S in supplementary materials). These results show that the larger the opening, the higher the concentration detected at position 3 when the calcium wave reaches the position. In HTS application, tip opening may not be fabricated to as small as 6 μm. For larger tip diameters, channel length can be increased to counteract the effects from wider openings.

Table 5.3. Fluorescein concentration (μM) at the opening of the neighboring microwell (position 3 in Fig. 5.8(a)) after injection in the stimulus well (position 1 in Fig. 5.8(a)). 500 mM fluorescein was injected with a tip of 6 μm in diameter. Two channel lengths (70 μm and 150 μm) were used in the simulation. For a calcium wave propagation, traveling at a speed of 43 μm/s, it takes around 1.6 s to reach the neighboring well (position 3) for 70 μm channel and around 3.5 s for 150 μm channel. The numbers in bold are the chemical concentrations at the time a calcium wave reaches the position.

Channel length	1 s	1.6 s	3.5 s	5 s	10 s
L = 70 μm	19.55	**41.13**	107.31	140.20	186.13
L =150 μm	0.01	0.15	**2.11**	4.93	17.76

Table 5.1S. Fluorescein concentration (μM) at the opening of the neighboring microwell (position 3 in Fig. 5.8(a)) after injection in the stimulus well (position 1 in Fig. 5.8(a)). 500 mM fluorescein was injected with tips of different diameters (D). The diameter of the microwell was 50 μm, the channel width was 10 μm and the channel length was 150 μm. For a calcium wave propagation, traveling at a speed of 43 μm/s, it takes around 3.5 s to reach the neighboring well (position 3). The numbers in bold are the chemical concentrations at the time when a calcium wave reaches the position.

Tip diameter	1 s	3.5 s	5 s	10 s
D = 6 μm	0.01	**2.11**	4.93	17.76
D = 20 μm	0.01	**16.36**	47.89	200.94
D = 50 μm	0.10	**112.49**	320.03	1266.31

Table 5.2S. Fluorescein concentration (μM) at the opening of the neighboring microwell (position 3 in Fig. 5.8(a)) after injection in the stimulus well (position 1 in Fig. 5.8(a)). 500 mM fluorescein was injected with tips of different diameters (D). The diameter of the microwell was 50 μm, the channel width was 10 μm and the channel length was 70 μm. For a calcium wave propagation, traveling at a speed of 43 μm/s, it takes around 1.6 s to reach the neighboring well (position 3). The numbers in bold are the chemical concentrations at the time when a calcium wave reaches the position.

Tip diameter	1 s	1.6 s	5 s	10 s
D = 6 μm	0.01	**41.13**	140.20	186.13
D = 20 μm	153.10	**482.73**	1675.94	2115.23
D = 50 μm	1303.08	**3354.42**	10433.25	13098.89

5.5. Conclusion

This study constitutes the first step toward a HTS platform for 3-D patterned neural network for application in drug screening as well as in basic research. The results support the following conclusions.

1）Fabricated PLLA scaffolds have nano-fibrous structures that mimic collagen fibers in ECM and exhibit higher porosity, improved thermal and mechanical properties than PLLA scaffolds without nano-fibrous structures.

2）Laser micromachined patters in the nano-fibrous PLLA films are compatible with stem cell culture and integrate easily in high-density-well plates (e.g. 96-well plates) for HTS application.

3）Mathematical simulation confirmed that it is possible to study neural network activity induced by chemical stimulation in these MNFSs, and by controlling parameters in MNFSs (such as channel), cellular responses due to cell-to-cell communication can be distinguished from those caused by chemical diffusion.

5.6 References:

1 Javitt DC, Spencer KM, Thaker GK, Winterer G, Hajós M. Neurophysiological biomarkers for drug development in schizophrenia. Nature reviews: drug discovery 2008; 7: 68-83.

2 Seow D, Gauthier S. Pharmacotherapy of Alzheimer's disease. Can. J. Psychiatry 2007; 52(10): 620-629.

3 Cutler NR, Sramek JJ. Review of the next generation of Alzheimer's disease therapeutics: challenges for drug development. Prog Neuropsychopharmacol Biol Psychiatry. 2001; 25(1): 27-57.

4 Craighead HG, James CD, Turner AMP. Chemical and topographical patterning for directed cell attachment. Current Opinion in Solid State and Materials Science 2001; 5: 177-184.

5 Kane RS, Takayama S, Ostuni E, Ingber DE, Whitesides GM. Patterning proteins and cells using soft lithography. Biomaterials 1999; 20: 2363-2376.

6 Nicolau DV, Taguchi T, Taniguchi H, Tanigawa H, Yoshikawa S. Patterning neuronal and glia cells on light-assisted functionalized photoresists. Biosensors & Bioelectronics 1999; 14: 317-325.

7 Vogt AK, Wrobel G, Meyer W, Knoll W, Offenhauser A. Synaptic plasticity in micropatterned neuronal networks. Biomaterials 2005; 26: 2549-2557.

8 Stevens MM, Mayer M, Anderson DG, Weibel DB, Whitesides GM, Langer R. Direct patterning of mammalian cells onto porous tissue engineering substrates using agarose stamps. Biomaterials 2005; 26: 7636-7641.

9 Yousaf MN, Houseman BT, and Mrksich M. Using electroactive substrates to pattern the attachment of two different cell populations. PNAS 2001; 98(11): 5992-5996.

10 Wu Z-Z, Zhao Y-P, Kisaalita WS. A pached Cytodex microbead array for three-dimensional cell-based biosensing. Biosensors and Bioelectronics 2006; 22:685-693.

11 Wang L, Wu Z-Z, Xu B, Zhao Y, Kisaalita WS. SU-8 microstructure for quasi-three-dimensional cell-based biosensing. Sensors and Actuators 2009; 140(2):349-355

12 Griscom L, Degenaar P, LePioufle B, Tamiya E, and Fujita H. Cell placement and neural guidance using a three-dimensional microfluidic array. Jpn. J. Appl. Phys. 2001; 40: 5485-5490.

13 Merz M and Fromherz P. Silicon chip interfaced with a geometrically defined net of snail neurons. Adv. Funct. Mater. 2005; 15(5): 739-744.

14 Yang F, Murugan R, Ramakrishna S, Wang X, Ma Y-X, Wang S. Fabrication of nano-structured porous PLLAscaffold intended for nerve tissue engineering. Biomaterials 2004; 25: 1891–1900.

15 Matthews JA., Wnek GE, Simpson DG, and Bowlin GL. Electrospinning of collagen nanofibers. Biomacromolecules 2002; 3: 232-238.

16 Zhang S, Gelain F, Zhao X. Designer self-assembling peptide nanofiber scaffolds for 3D tissue cell cultures. Seminars in Cancer Biology 2005; 15: 413-420

17 Yim EK, Pang SW, Leong KW. Synthetic nanostructures inducing differentiation of human mesenchymal stem cells into neuronal lineage. Exp Cell Res. 2007; 15, 313(9):1820-1829.

18 Patel S, Kurpinski K, Quigley R, Gao H, Hsiao BS, Poo M-M, Li S. Bioactive nanofibers: synergistic effects of nanotopography and chemical signaling on cell guidance. Nano Lett. 2007; 7 (7): 2122-2128.

19 Cukierman E, Pankov R, Stevens DR, Yamada KM. Taking cell-matrix adhesions to the third dimension. Science 2001; 294: 1708-1712.

20 Yang F, Murugan R, Wang S, Ramakrishna S. Electrospinning of nano/micro scale poly(L-lactic acid) aligned fibers and their potential in neural tissue engineering. Biomaterials 2005; 26: 2603-2610.

21 Wang S S-H, and Thompson SH. Local positive feedback by calcium in the propagation of intracellular calcium waves. Biophys. J. 1995; 69:1683-1697.

22 Zhang R, Ma PX. Poly(a-hydroxyl acids)/hydroxyapatite porous composites for bone-tissue engineering. I. Preparation and morphology. J Biomed Mater Res 1999; 44:446-455.

23 Liu X, Lim JY, Donahue HJ, Dhurjati R, Mastro AM, Vogler EA. Influence of substratum surface chemistry/energy and topography on the human fetal osteoblastic cell line hFOB 1.19: phenotypic and genotypic responses observed in vitro. Biomaterials 2007; 28: 4535-4550.

24 Axelrod D, Koppel DE, Schlessinger J, Elson E, and Webb WW. Mobility measurement by analysis of fluorescence photobleaching recovery kinetics. Biophys. J. 1976;16:1055–1069.

25 Leddy HA, Guilak F. Site-specific molecular diffusion in articular cartilage measured using fluorescence recovery after photobleaching. Annals of Biomedical Engineering 2003; 31: 753-760.

26 Galambos P, Forster FK. Micro-fluidic diffusion coeffeicent measurement. Presented as proceedings at the μTAS' 98 Workshop, Banff, Canada, October 13-16, 1998.

27 Jaffe LF. On the conservation of fast calcium wave speeds. Cell Calcium 2002; 32(4): 217-229.

28 Culbertson CT, Jacobson SC, Ramsey JM. Diffusion coefficient measurements in microfluidic devices. Talanta 2002; 56:365-373.

29 Chen VJ, Ma PX. Nano-fibrous poly(l-lactic acid) scaffolds with interconnected spherical macropores. Biomaterials 2004; 25: 2065-2073.

30 Engler AJ, Sen S, Sweeney HL, Discher DE. Matrix elasticity directs stem cell lineage specification. Cell 2006; 126: 677-689.

31 Saha K, Keung AJ, Irwin EF, Li Y, Little L, Schaffer DV, Healy KE. Substrate modulus directs neural stem cell behavior. Biophysical Journal 2008; 95: 4426-4438.

32 Xu H, Teng C, Yu M. Improvements of thermal property and crystallization behavior of PLLA based multiblock copolymer by forming stereocomplex with PDLA oligomer. Polymer 2006; 47: 3922-3928.

33 Wang Y-Q, Cai J-Y. Enhanced cell affinity of poly(L-lactic acid) modified by base hydrolysis: Wettability and surface roughness at nanometer scale. Current Applied Physics 2007; 7S: e108-e111.

CHAPTER 6

ADMINISTRATION OF BDNF/GINSENOSIDES COMBINATION ENHANCED SYNAPTIC DEVELOPMENT IN HUMAN NEURAL STEM CELLS[*]

Keywords: Ginsenosides; Brain-derived neurotrophic factor; Human neural stem cells; Synapse; Cell density.

[*]Wang L., Kisaalita W.S.. Administration of BDNF/ginsenosides combination enhanced synaptic development in human neural stem cells. *Journal of Neuroscience Methods* (in preparation)

6.1. Abstract

Ginsenosides Rg1 and Rb1, major pharmacologically active ingredients from Ginseng, the root of Panax ginseng C.A. Meyer (Araliaceae), were applied in the differentiation media for human neural stem cells (hNSCs), together with brain-derived neurotrophic factor (BDNF), a commonly used compound for neural stem cell (NSC) differentiation. Cell locomotion and neurite extension were observed by time-lapse microscopy and analyzed by ImageJ. The expression of synaptic formation was confirmed by immunostaining of synaptophysin (SYN) or/and the co-localization of synapsin I and microtubule associated protein-2 (MAP-2). Effects of cell density on neural differentiation were also examined. Results have shown that administration of BDNF/ginsenosides (Rg1 and Rb1) combination in differentiation medium promoted cell survival, enhanced neurite outgrowth and synaptic marker expression during differentiation. High cell density enhances synaptic marker expression in BDNF/ginsenosides combination medium. In all, this study established a condition for hNSCs synaptic development in early differentiation, which is a crucial step in applying this cell line in neural network-based assay.

6.2. Introduction

Neural stem cells (NSCs), which are derived from embryonic stem cells (ESCs) are partially differentiated, multipotent and can develop into any type of neural cells (e.g. neurons and astrocytes) *in vitro* (Zhang, 2006). Also, NSCs are capable of proliferating, thus providing an unlimited cell source. In pharmaceutical and biotechnology industries, human NSCs (hNSCs) are being considered as a promising cell source in preclinical studies (Irion et

al., 2008). While in tissue engineering and regenerative medicine, these cells are actively being investigated for neurodegenerative disease therapy (Ogawa et al., 2009). There is interest in differentiating hNSCs to mature functional neural networks for preclinical studies of drugs against connectivity related targets (e.g. N-methyl-D-aspartic acid receptors (NMDARs)) (Meador-Woodruff et al., 2003; Wang and Kisaalita, 2010).

NSC differentiation is regulated by various microenvironment cues, such as chemical and physical properties of extracelluar matrix (Little et al., 2008), and functional neural network development from NSCs has been proven to be microenvironment dependent (Illes et al., 2009). Among these effective molecules that affect neuronal fate (Schaffer and Gage, 2004), brain-derived neurotrophic factor (BDNF) is an effective modulator of hNSC differentiation and neuronal cell survival (Poo, 2001). It plays an important role in the survival of differentiated neural stem cells through the MAPK/ERK-dependent and PI3K/Akt-dependent Bcl-2 up-regulation (Lim et al., 2008). Also, it has been proven to accelerate the maturation of the synaptic vesicle protein synapsin-1 at developing neuromuscular junctions in cell cultures (Poo, 2001). Thus, BDNF has been often added in neural stem cell differentiation media (Johnson et al., 2007).

Ginseng, the root of Panax ginseng C.A. Meyer (Araliaceae), has been extensively used in traditional oriental medicine for over 2000 years. *In vivo* and *in vitro* studies have shown its beneficial effects in cardiovascular diseases, cancer and immune deficiency (Cheng et al., 2005). A recent study has suggested that some of ginseng's active ingredients also exert beneficial effects on aging and neurodegenerative diseases (Radad et al., 2006). Ginsenosides such as Rb1 (MW1109.29 Da) and Rg1 (MW801.02 Da) are the major pharmacologically

active ingredients of ginseng and their anti-aging and anti-neurodegeneration effects have been well proven (Cheng et al., 2005). Cell-based studies have shown that ginsenosides promoted NSC proliferation *in vitro* and enhanced cell survival (Shen and Zhang, 2004). Mechanisms may involve decreasing NO content and NOS activity, reducing intracellular calcium concentration, by up-regulating Hes1 expression, enhancing superoxide dismutase (SOD) activity and enhancing the ratio of Bcl-2 to Bax protein and inhibiting activation of caspase-3 (Cheng et al., 2005; Zhuang et al., 2009). Ginsenosides Rg1 and Rb1 also promoted neurite outgrowth in PC12 cells (Rudakewich et al., 2001), enhanced astrocyte differentiation from NSCs (Shi et al., 2005), increased neurotransmitter release (Xue et al., 2006), and increased synapse number and the density of synaptophysin, which is the morphological basis for explaining Rb1 and Rg1 induced facilitation of learning and memory (Mook-Jung et al. 2001).

In this study, we explored the effects of BDNF/ginsenosides (Rg1 and Rb1) combination on hNSC differentiation. Based on previous studies of BDNF and ginsenosides for neural cell survive and differentiation, it was expected that the combination could enhance synaptic development in hNSC differentiation than BDNF or ginsenosides, separately. We also studied the effects of cell density on hNSC differentiation with respect to synaptic formation. The goal was to establish a hNSC differentiation condition for neural network connectivity development, reflected by synaptic formation.

6.3. Materials and methods

6.3.1. Cell line and cell culture

hNSCs, purchased from Millipore (ENStem-A^{TM}, Billerica, MA), were derived from WA09 human ESCs using methods previously described (Shin et al., 2005). Cells were maintained as previously described (Wang and Kisaalita, 2010). Briefly, cells were cultured in 35 mm Petri dishes with 2 mL growth medium in a 5% CO_2 humidified atmosphere at 37 ˚C. ENStem-A^{TM} expansion media supplemented with penicillin/streptomycin, L-glutamine and basic fibroblast growth factor (bFGF) was used. The medium was half changed every other day. Cells were passaged by mechanically pipetting when cells reached 90% to 100% confluence and around 1.2×10^6 cells were seeded into each new dish. For cell differentiation, expansion media was replaced with differentiation media. Compared with expansion media, bFGF was withdrawn in basic differentiation media (Yan et al., 2005). Ginsenosides Rg1 (5 μM) and Rb1 (5 μM) (National Institute for the Control of Pharmaceutical and Biological Products, Beijing, China) and BDNF (10 ng/ml, Invitrogen, Carlsbad, CA) were added in basic differentiation media. The concentrations were decided based on previous studies (Shi et al., 2005; Johnson et al., 2007). There were four differentiation conditions: 1) basic differentiation media; 2) ginsenosides Rg1 (5 μM) and Rb1 (5 μM) in basic differentiation media; 3) BDNF (10 ng/ml) in basic differentiation media; 4) combination of BDNF (10 ng/ml) and ginsenosides Rg1 (5 μM) and Rb1 (5 μM) in basic differentiation media. The differentiation medium was half changed every other day. Phase contrast images were taken at different time points (before differentiation, week 2, week 3, and week 4 in differentiation) for analysis (n = 3). According to our previous studies on this cell line (data not shown), dead

cells are bright and form clusters; while live cells attach to the substrates and are darker. Thus, live cells were distinguishable and were counted. Student's t-test was used for statistical comparisons.

6.3.2. Cell locomotion observation by time-lapse recording.

We used time-lapse video microscopy as previously described (Wang et al., 2010) to study neural stem cell locomotion before differentiation and during differentiation. Briefly, cells were differentiated with basic differentiation media or combined differentiation media for 3 weeks, then cells were plated onto coverslips and their locomotion was recorded for 10 hours. The WaferGen Smart Slide-100 system (WaferGen, Fremont, CA, USA) was used to keep the cells in proper conditions while recording. This small environmental chamber is based on a 6-well dish. It uses heated glass to maintain temperature even at the spot being observed, and regulates CO_2 flow. Phase contrast images were taken every minute using Leica DFC300 FX camera mounted on a Leica Z16 APO A microscope. Image sequences and trajectory plots were generated by ImageJ (NIH). Manual analysis of cell locomotion speed (average speed within the first 10 hours after plating) and neurite outgrowth (at the end of 10 hours' recording) was carried out according to methods published by Chen et al. (2009) and Mitchell et al. (2007), respectively. Data for cell movement before and during differentiation were compared.

6.3.3. Immunostaining for synaptic markers

We used 2 sets of staining to confirm the expression of synaptic markers: staining for the expression of synaptophysin (SYN) and the co-localization of synapsin I and microtubule

associated protein-2 (MAP-2). Protocols from Aruna Biomedical Inc. (Athens, GA) were followed. Briefly, cells were rinsed twice with phosphate-buffered saline (PBS), fixed with 2% paraformaldehye in PBS (15 min), permeablized with 0.5% Tween 20 (3 times, 5 minutes each), blocked for 45 minutes in blocking buffer, which is comprised of 6% from the animal that the second antibodies were produced in. Cells were exposed to a mixture of rabbit polyclonal anti-synapsin I (1:500) (Chemicon, Temecula, CA) and monoclonal anti-MAP2 (1:500) (Sigma, St. Louis, MO), or samples were incubated with polyclonal rabbit anti-human SYN (1:200) (DakoCytomation, Denmark) overnight at 4 ˚C. After exposure to primary antibodies, samples were washed with PBS (4 times, 5 minutes each), and incubated for 1 hour at room temperature with blocking buffer containing a mixture of rhodamine-conjugated goat anti-rabbit IgG (1:500) and fluorescein-conjugated donkey anti-mouse IgG (1:500) (Jackson Immunological Research, West Grove, PA), or rhodamine-conjugated goat anti-rabbit IgG (1:500) (Jackson ImmunoResearch Laboratories, West Grove, PA). To capture fluorescence images of cells stained for SYN or synapsin I, cells were scanned with the Green HeNe laser and the resulting fluorescent signals were captured through a 565 nm long-pass filter (BA1, Nikon, Melville, NY) by a photomultiplier detector. While fluorescence images of cells stained for MAP-2 was viewed and captured with a B-2E/C FITC filter block (Nikon, Melville, NY, USA), which has an excitation bandwidth of 465-495 nm and a filter pass range of 515 - 555 nm. Fluorescence intensity was measured with Simple PCI image software (Compix Inc., Cranberry Township, PA). Student’s t-test was used for statistical comparisons.

6.4. Results and discussions

6.4.1. Combination of ginsenosides with BDNF promotes hNSC survival during differentiation.

Cells were kept in differentiation media for 4 weeks, and Figure 6.1 (a) - (d) presents phase contrast images of hNSCs at week 4 in differentiation under different conditions. Dead cells, which were brighter than the live cells attaching on the substrates, were observed in all these samples. There were more dead cells in groups under basic differentiation (a) or ginsenosides-induced differentiation (b) than in groups under BDNF-induced differentiation (c) or BDNF/ginsenosides combination-induced differentiation (d). Normalized cell densities are presented in Figure 6.1 (e). Administration of BDNF or ginsenosides did not significantly increase cell survival at week 4 in differentiation. While there were significantly more cells surviving in groups under BDNF/ginsenosides combination-induced differentiation ($P < 0.05$). By examining hNSCs in combinational group at week 2, week 3 and week 4 in differentiation (Figure 6.2 (a) - (d)), it is noticeable that cells kept proliferation during the first three weeks without significant increase in cell density ($P > 0.05$). At week 3 and week 4 in differentiation, some dead cells were observed; however, there was no significant decrease in cell density during differentiation. As shown in other studies (Saha et al., 2008), cell numbers decrease during differentiation, indicating that not all these cells could survive and differentiate to neural cells. Our results indicated that BDNF and ginsenosides could work synergically to maintain cell viability during differentiation. BDNF plays an important role in the survival of differentiated neural stem cells through the MAPK/ERK-dependent and PI3K/Akt-dependent Bcl-2 up-regulation (Lim et al., 2008). And ginsenosides promoted

neural stem cell proliferation *in vitro* and enhanced cell survival (Shen and Zhang, 2004) through mechanisms that may involve decreasing NO content and NOS activity, reducing intracellular calcium concentration, up-regulating Hes1 expression, enhancing superoxide dismutase (SOD) activity, and enhancing the ratio of Bcl-2 to Bax protein (Cheng et al., 2005; Zhuang et al., 2009). In the following studies, combination of BDNF and ginsenosides (Rg1 and Rg1) was applied in differentiation meida.

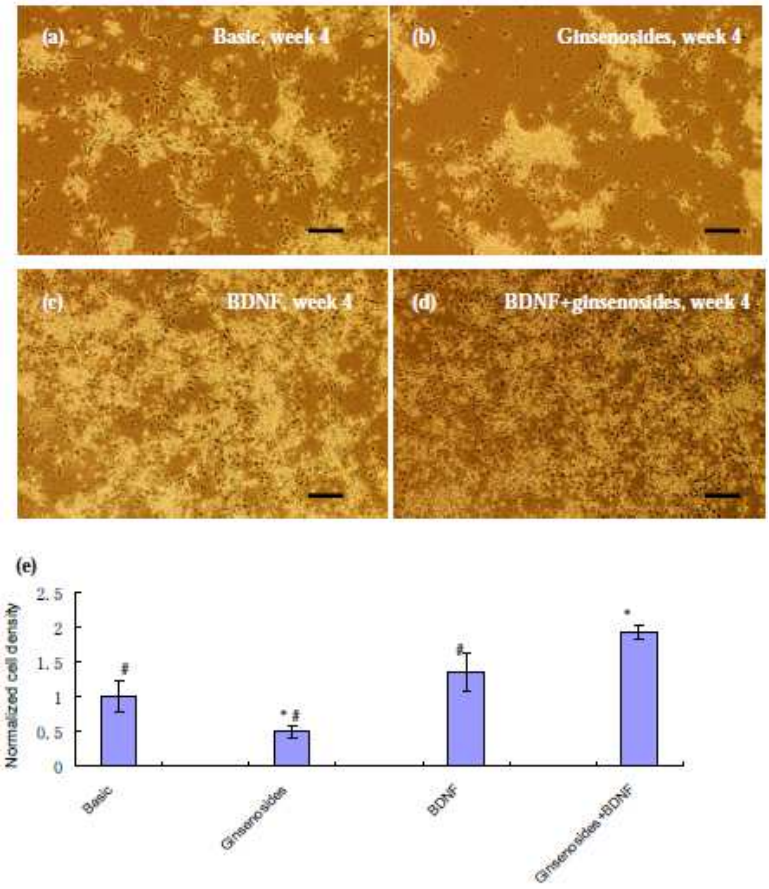

Figure 6.1. (a-d): Phase contrast images of hNSCs at week 4 in differentiation in basic differentiation media (a), basic media with ginsenosides Rg1 (5 μM) and Rb1 (5 μM) (b), basic media with BDNF (10 ng/ml) (c), basic media with combination of BDNF (10 ng/ml) and ginsenosides Rg1 (5 μM) and Rb1 (5 μM) (d). Scale bar = 100 μm. (e): Cell densities were normalized by dividing with the density from the basic differentiation media group. *: $P < 0.05$, compared to the group with basic differentiation media; #: $P < 0.05$, compared to the group with the combinational differentiation media.

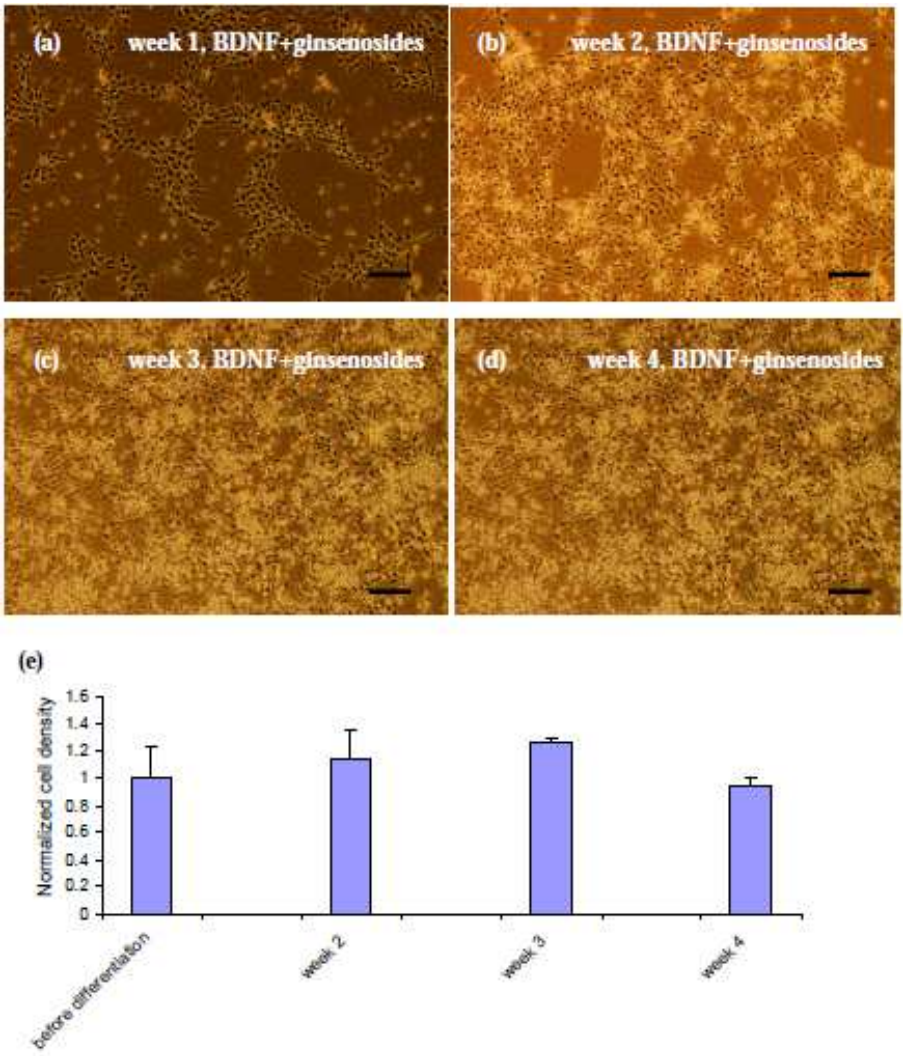

Figure 6.2. Phase contrast images of neural stem cells before differentiation (a), during differentiation at week 2 (b), week 3 (c), and week 4 (d). Differentiation media contained BDNF (10 ng/ml) and ginsenosides Rg1 (5 μM) and Rb1 (5 μM). Scale bar = 100 μm. (e): Cell densities were normalized by dividing with the density from the group before differentiation. Cell densities did not change significantly during differentiation ($P > 0.05$).

6.4.2. Combination of ginsenosides and BDNF promotes neurite outgrowth during differentiation.

Time-lapse recording was used to study hNSC locomotion before and after differentiation. To explore the effects of combinational differentiation media on hNSC differentiation with respect to neurite outgrow, cells in basic differentiation media were used as a control for cells

in combinational differentiation media,. Figures 6.3 and 6.4 show image sequences and trajectory plots, respectively, for hNSCs before differentiation and at week 3 in differentiation. Before differentiation, cells moved randomly at a speed of 5.86 ± 4.57 µm/h (Figure 6.4 (d)) and interacted with other cells and formed cellular clusters (Figure 6.3 (a) and Figure 6.4 (a)). Cells moved at significantly lower speeds of 1.01 ± 0.53 µm/h and 0.83 ± 0.31 µm/h in basic and combination differentiation media, respectively. Our results confirmed the active hNSC locomotion before differentiation. hNSC migration *in vivo* plays a crucial role in the early phase of histogenesis in the embryonic striatum (Hamasaki et al., 2003). Recent studies have shown NSC migration and invasion in 3D tumor cell aggregates *in vitro* (Heese et al., 2005). Cell-cell contact, as well as extra-cellular matrix (ECM) components and soluble proteins secreted into microenvironment by intermediate or final target cells, underlies the mechanisms for hNSC locomotion both *in vivo* and *in vitro* (Hamasaki et al., 2003; Heese et al., 2005). In our study, active hNSC locomotion may be driven by cell-cell contact to form connection with other cells.

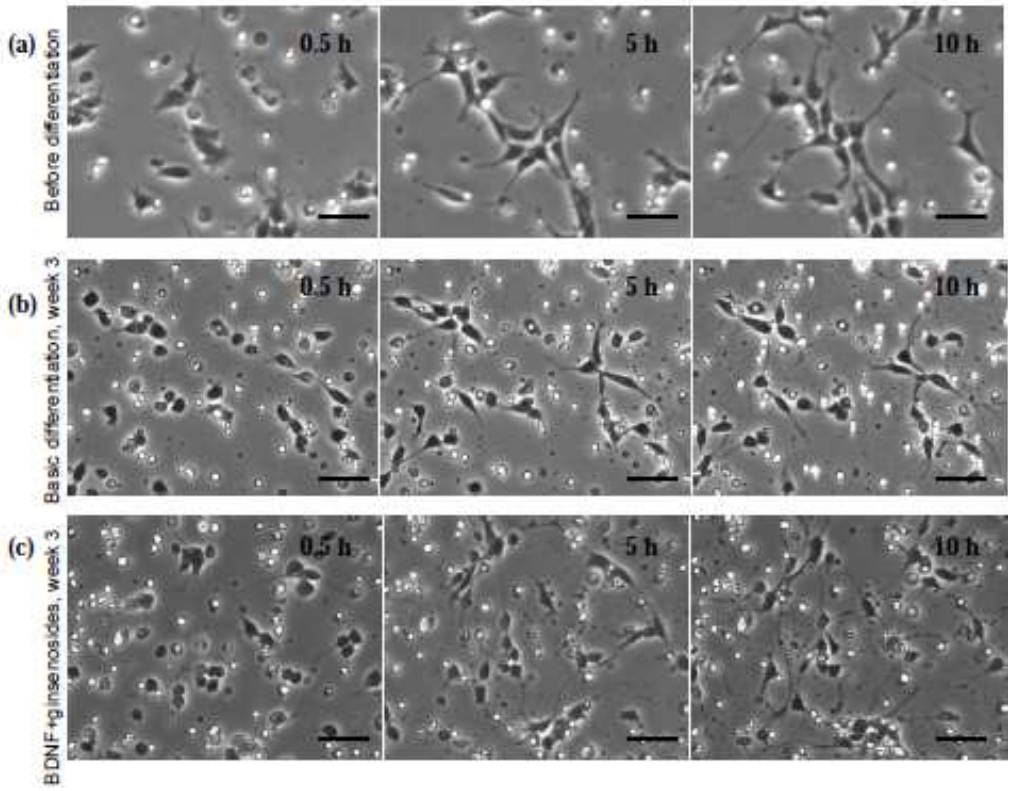

Figure 6.3. Image sequences of cell locomotion before differentiation (a) and at week 3 in differentiation (b and c). Images showed cells on 2D flat surface after plating at 0.5 h, 5 h and 10 h. (a): Cells were kept in proliferation media. (b): Cells were differentiated in basic differentiation media. (c): Cells were differentiated in combinational differentiation media (BDNF (10 ng/ml) and ginsenosides Rg1 (5 μM) and Rb1 (5 μM)). Before differentiation, cells interacted with other cells, moved and formed cellular clusters (a). In differentiation, cell bodies moved in a confined area, and extended out neurites to get connection with other cells (b and c). Scale bar = 50 μm.

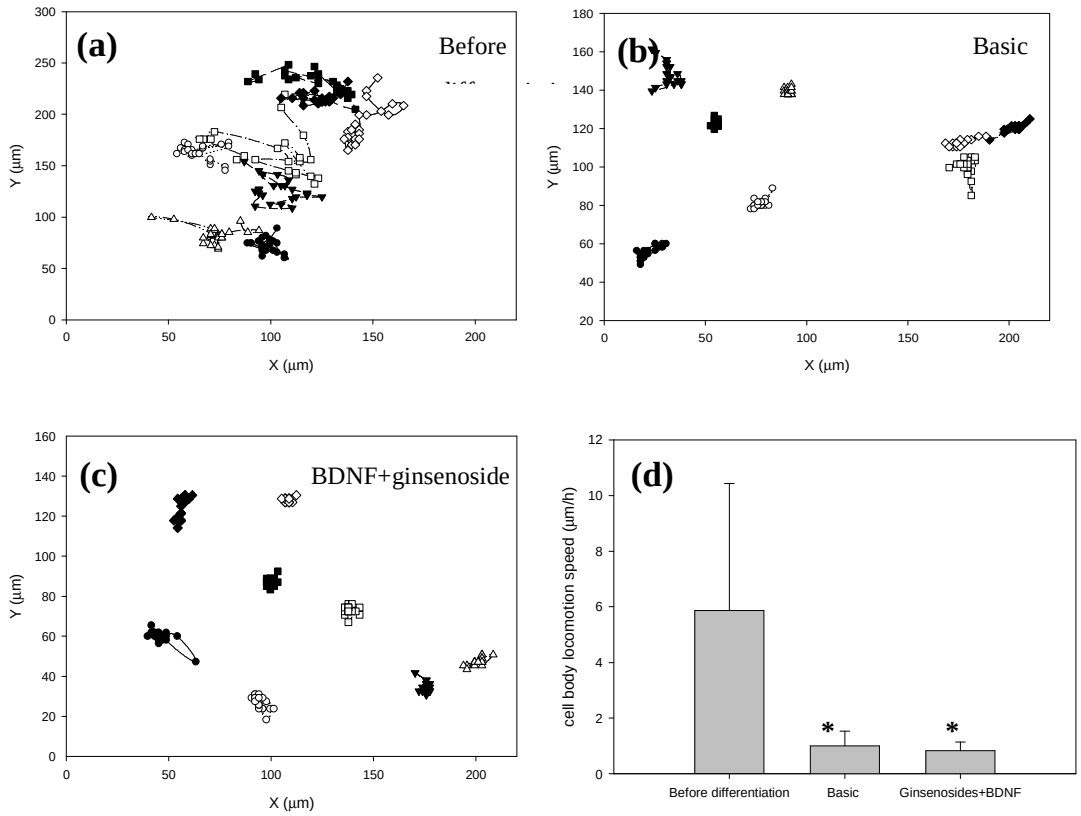

Figure 6.4. Trajectory plots for hNSCs before differentiation (a) and at week 3 in differentiation (b and c). Cells were plated and observed for 10 hours. For each group, 8 cells are presented. (a): Cells were kept in proliferation media. (b): Cells were differentiated in basic differentiation media. (c): Cells were differentiated in combinational differentiation media (BDNF (10 ng/ml) and ginsenosides Rg1 (5 μM) and Rb1 (5 μM)). (d): Cell body locomotion speed analysis. Cells before differentiation moved faster than cells in differentiation ($P < 0.05$).

During the recording, differentiated cells extended neurites to get connected and form neural network; differentiated cells also formed cellular clusters, and neurite extensions were observed outwards from cellular clusters (Figure 6.3 (b) and (c), Figure 6.4 (b) and (c)). Table 6.1 presents the quantitative analysis of neurite outgrowth for cells in basic and combinational differentiation media at week 3. There were more cells outgrowing neurites in combinational differentiation media, and these neurites were longer than those in basic differentiation media ($P < 0.05$). Neurite growth is considered a very import event in

neuronal development, synapse formation, and neural regeneration. Pharmaceutical control of neurite growth (e.g. by nerve growth factor) is of great interest in clinical application (Mitchell et al., 2007). Shetty and Turner (1999) proved that BDNF could promote neurite outgrowth of NSCs. Our results were consistent with previous studies on effects of ginsenosides Rg1 and Rb1 on neurite outgrowth in PC12 cells (Rudakewich et al., 2001). In the presence of nerve growth factor, Rg1 and Rb1 stimulate neurite outgrowth in PC12 cells at day 8 in culture. Pathways or molecular mechanisms that regulate neurite outgrowth have been explored. It has been found that balance of MAP kinase and STAT3 signal transduction pathways regulated neurite growth in PC12 cells (Ihara et al., 1997), as well as protein kinase A-dependent molecular switch in synapsins in embryonic Xenopus spinal neurons (Kao et al., 2002). Based on these observations, it may be hypothesized that combinational differentiation media could promote hNSC differentiation with respect to synaptic formation. To further confirm the neural network formation, we examined the synaptic development of hNSCs in differentiation.

Table 6.1. Summary of quantitative analysis of neurite outgrowth in neural stem cells at week 3 in differentiation in different media[1].

	Cells bearing branches (% of total cells)	Cells bearing neurites[3] (% of total cells)	Average neurite length per cell (μm)	Average length of longest neurites from each field (μm)
Basic differentiation media	49.16±10.69[2]	11.26±3.24	51.86±12.06	60.84±13.2
Combinational differentiation media	64.12±10.94 *	31.48±13.6 *	63.69±18.59 *	89.37±16.26 *

[1]4 fields were selected from each group; total cell number from basic differentiation group was 107 (25, 30, 29, 23); total cell number from combinational differentiation group was 109 (25, 21, 27, 33). [2]mean ± standard deviation. [3]neurite is defined as at least three times long of soma body. * $P < 0.05$, compared to basic differentiation group

6.4.3. The maximum expression of hNSC synaptic marker SYN occurred at week 2 in ginsenosides/BDNF combination-induced differentiation.

Figure 6.5 (a) - (d) presents the fluorescence images of cells stained for synaptophysin (SYN) at week 4 in differentiation, and staining was positive for these four differentiation conditions. At week 2, cells exhibited the strongest SYN signal under combination condition (Figure 6.5 (e)). In the combinational group, SYN signal intensities did not change significantly with time in differentiation (data not shown). Under other conditions, SYN signal intensities increased at late differentiation time (week 4) and reached the same level as that of cells under combination condition (Figure 6.5 (e)). These results indicated that combination of ginsenosides and BDNF could promote synaptic marker SYN expression at an early time in differentiation. To further confirm this expression of synaptic connection, another set of immunostaining was used in this study: staining for the co-localization of

synapsin I and MAP-2. Almost all the cells were positive for synaptic markers (MAP2, synapsin and SYN) on week 2 and week 3 in differentiation (Figure 6.6). These results were consistent with previous reports. For example, BDNF has been proven to accelerate the maturation of the synaptic vesicle protein synapsin I at developing neuromuscular junctions in cell cultures (Poo, 2001). In other studies, ginsenosides were found to enhance astrocyte differentiation from neural stem cells (Shi et al., 2005), increase neurotransmitter release (Xue et al., 2006), and increase synapse number and the density of synaptophysin, which is the hypothesized basis of Rb1- and Rg1-induced facilitation of learning and memory (Mook-Jung et al. 2001).

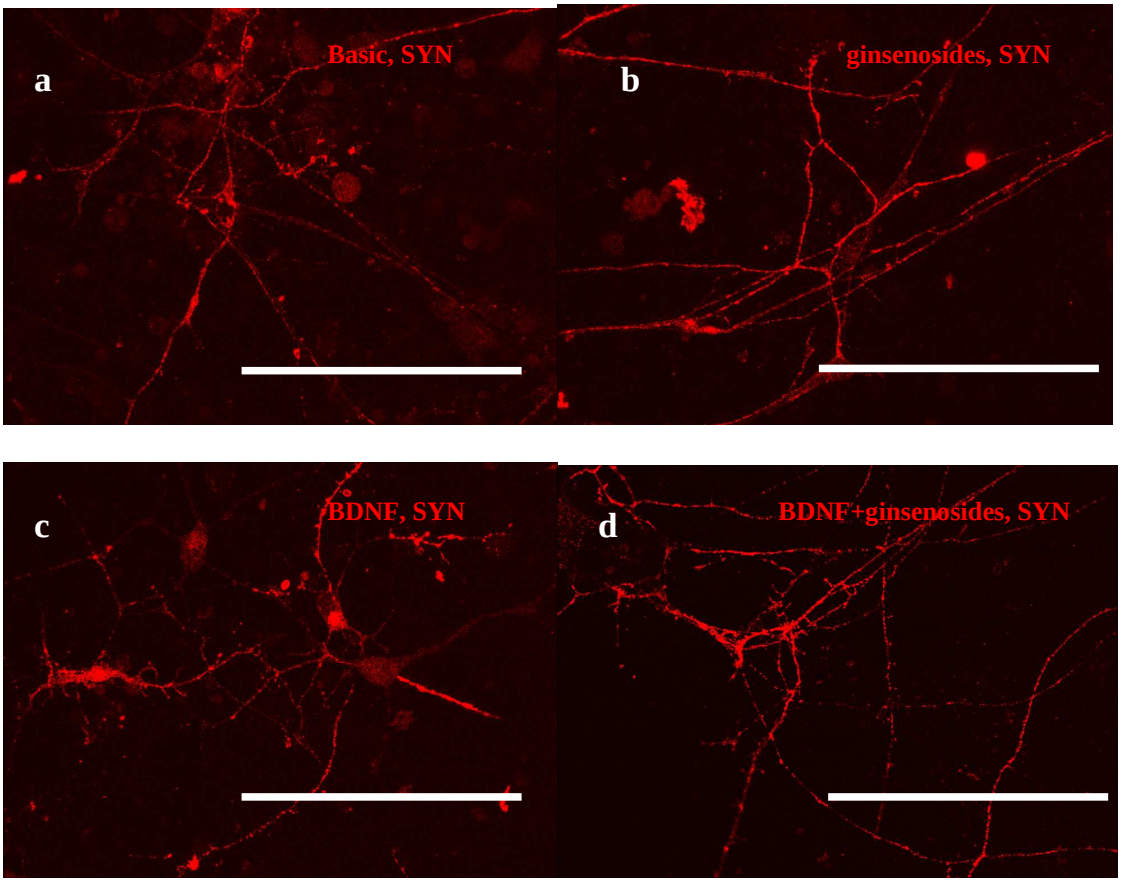
a
Basic, SYN
b
ginsenosides, SYN
c
BDNF, SYN
d
BDNF+ginsenosides, SYN

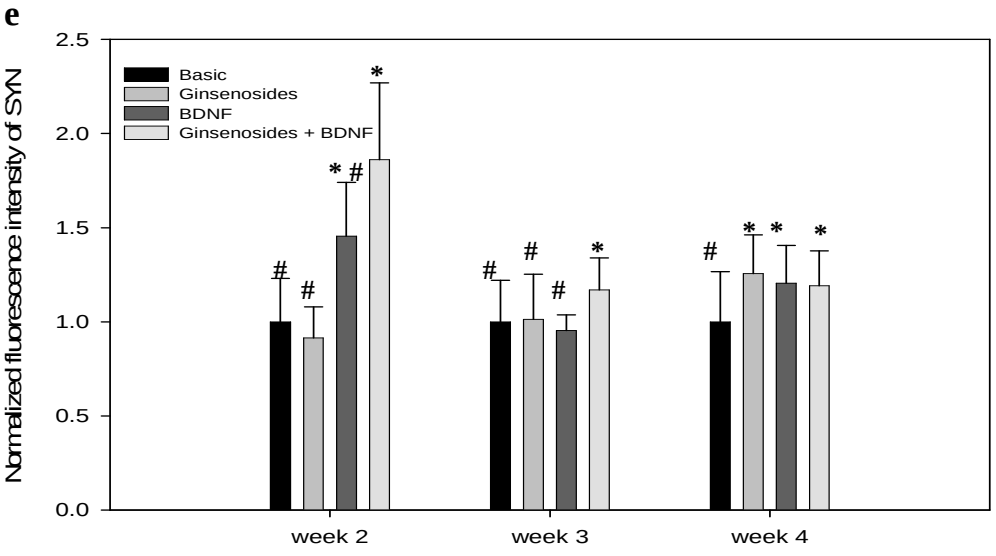
e
Normalized fluorescence intensity of SYN
2.5
2.0
1.5
1.0
0.5
0.0
Basic
Ginsenosides
BDNF
Ginsenosides + BDNF
week 2
week 3
week 4

Figure 6.5. (a-d): Confocal images of hNSCs at week 4 in differentiation. Cells were stained for SYN. Different molecules were added in basic differentiation media: a) basic differentiation media; b) ginsenosides Rg1 (5 μM) and Rb1 (5 μM); c) BDNF (10 ng/ml); d) BDNF (10 ng/ml) and ginsenosides Rg1 (5 μM) and Rb1 (5 μM). Scale bar = 100 μm. (e): Normalized fluorescence intensity of SYN staining for hNSCs in differentiation under different conditions. Basic: basic differentiation media; Ginsenosides: ginsenosides Rg1 (5 μM) and Rb1 (5 μM); BDNF: brain-derived neurotrophic factor (BDNF, 10 ng/ml); BDNF and ginsenosides: combination of BDNF (10 ng/ml) and ginsenosides Rg1 (5 μM) and Rb1 (5 μM). Values were normalized by dividing with the one under basic condition at each week in differentiation. *: $P < 0.05$, compared to the value of control group under basic condition at each week in differentiation. #: $P < 0.05$, compared to the value of the combination group at each week in differentiation.

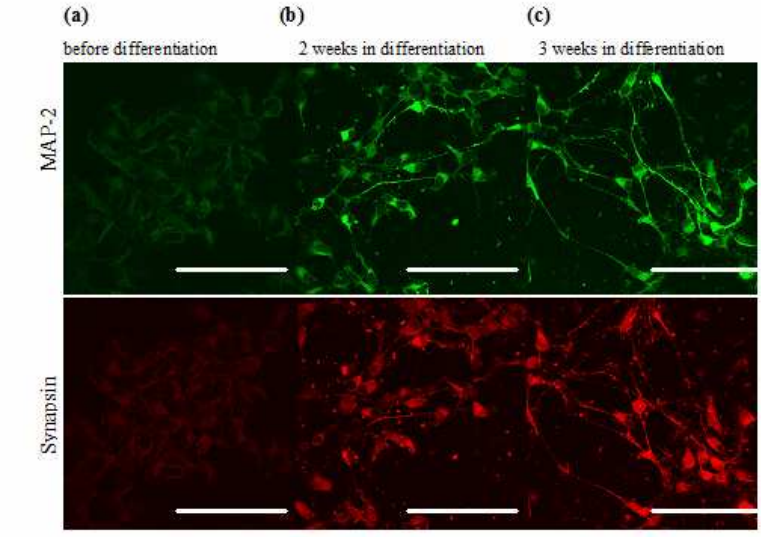

Figure 6.6. Confocal images of hNSCs stained for MAP-2 (green) and synapsin (red) before differentiation (a), at week 2 (b) and week 3 (c) in differntiation. Differentiation media contained BDNF (10 ng/ml) and ginsenosides Rg1 (5 μM) and Rb1 (5 μM). Scale bar = 100 μm.

6.4.4. Cell density is a factor in BDNF/ginsenosides-mediated synaptic marker expression.

Cells were seeded at different densities ($6x10^4$ cells/cm^2, $10x10^4$ cells/cm^2, $20x10^4$ cells/cm^2) and were differentiated for 2 weeks by combination media containing BDNF (10 ng/ml) and ginsenosides Rg1 (5 μM) and Rb1 (5 μM). Figure 6.7 (a) presents phase contrast images of hNSCs after 2 weeks in differentiation. Synaptic markers (MAP-2 and SYN) were

stained and signal intensity was measured and compared (Figure 6.7 (b) and (c)). Results showed that when cell density was too low (<$3x10^4$ cells/cm^2), few cells survived in differentiation; as cell density increased from $6x10^4$ cells/cm^2 to $20x10^4$ cells/cm^2, both MAP and SYN expression increased significantly ($P < 0.05$). Other studies have shown that cell plating density is an important factor in neural differentiation. The development of resting membrane potentials in differentiating murine neuroblastoma cells (NIE-115) was found be seeding cell density-dependent; lower cell density delayed the resting membrane potential development (Kisaalita and Bowen, 1997). Recent studies on stem cell differentiation have shown that seeding cell density is crucial in neuronal differentiation. When cell density was too low, cell viability was reduced; while dense culture resulted in increased non-neuronal differentiation (Lorincz, 2006). In order to attain high percentage of dopamine neuron population in mesencephalic precursor cultures, cultures needed to be seeded at high cell density (Ko et al., 2005). Our results are consistent with previous studies, confirming the seeding density effect on synaptic development in hNSC differentiation. Tsai and McKay (2000) reported that cell density effect on cortical stem cell fate dermination depends on cell-cell contact and membrane-bound signals. Other studies have shown that cell density-mediated neural differentiation of stem cells was related to signaling pathways such as Rho kinases and β-Catenin signaling (Otero et al., 2004; Chang et al., 2010). However, the mechanisms underlying cell density-related synaptic development are still unknown.

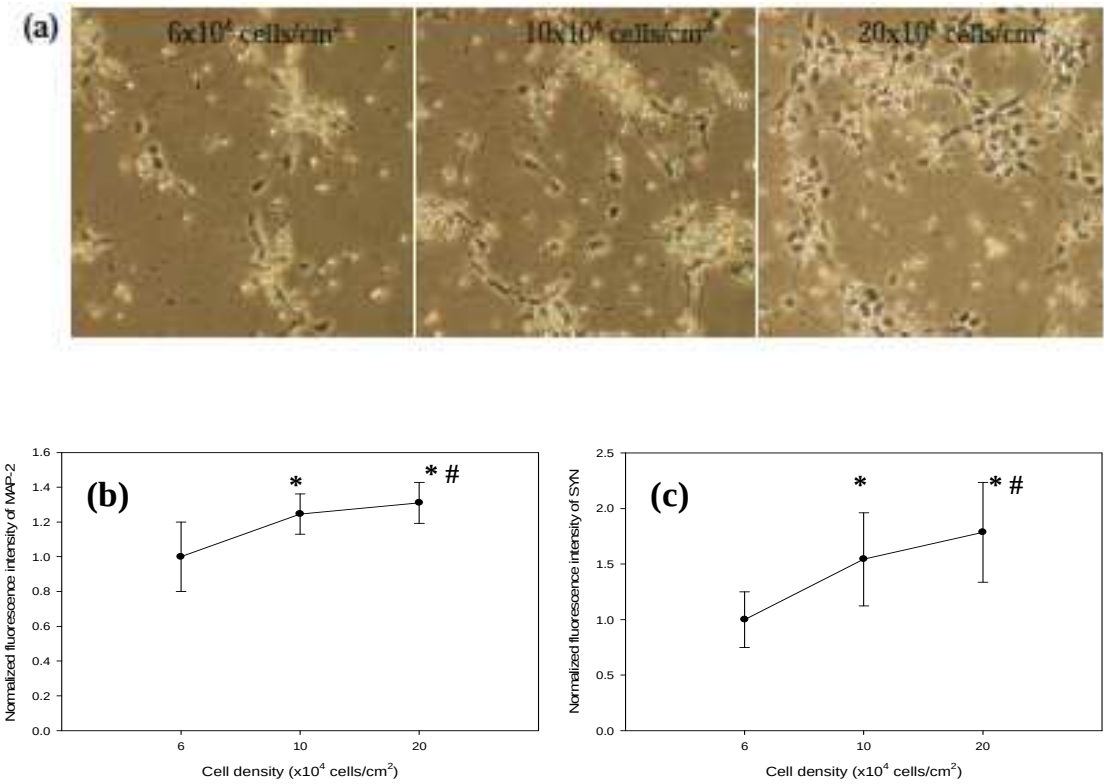

Figure 6.7. Cell density effects on hNSC differentiation with respect to synaptic markers MAP-2 and SYN expression. Cells were seeded at different cell densities (left: $6x10^4$ cells/cm^2, middle: $10x10^4$ cells/cm^2, right: $20x10^4$ cells/cm^2. Cells were differentiated for 2 weeks by combination media containing BDNF (10 ng/ml) and ginsenosides Rg1 (5 μM) and Rb1 (5 μM). (a): Phase contrast images of hNSCs. (b) and (c): Normalized fluorescence intensity of cells stained for MAP-2 (b) and SYN (c). Fluorescence intensities were measured and normalized by dividing with the value of cells seeded with the lowest cell density ($6x10^4$ cells/cm^2). *: $P < 0.05$, compared to the value at the cell density of $6x10^4$ cells/cm^2; #: $P < 0.05$, compared to the value at the cell density of $10x10^4$ cells/cm^2.

6.5. Conclusion

In this study, we examined BDNF/ginsenosides (Rg1 and Rb1)-induced hNSC differentiation with respect to cell survival, cell dynamic locomotion, neurite outgrowth and synaptic development. Results have shown that administration of BDNF/ginsenosides combination promotes cell survival, enhances neuite outgrowth, network formation and synaptic development during differentiation. Also, we examined cell density effects on hNSC

differentiation and results indicated that cell density should be kept at certain level (such as $20x10^4$ cells/cm^2) to maximize synaptic formation. Taken together, this study provided an effective protocol for hNSC differentiation with synapse formation, which is critical in neural-network based assay for drug discovery as well as in neuroregenerative medicine.

6.6 References:

Chang T-C, Chen Y-C, Yang M-H, Chen C-H, Hsing E-W, et al. Rho Kinases Regulate the renewal and neural differentiation of embryonic stem cells in a cell plating density–dependent manner. PLoS ONE 2010;5(2): e9187.

Cheng Y, Shen L, Zhang J. Anti-amnestic and anti-aging effects of ginsenoside Rg1 and Rb1 and its mechanism of action. Acta Pharmacologica Sinica 2005; 26 (2): 143-9.

Chen X, Brewer MA, Zou C, Campagnola PJ. Adhesion and migration of ovarian cancer cells on crosslinked laminin fibers nanofabricated by multiphoton excited photochemistry. Integr. Biol. 2009;1:469-76

Hamasaki T, GotoS, Nishikawa S, Ushio Y. Neuronal cell migration for the developmental formation of the mammalian striatum. Brain Research Reviews 2003;41:1-12

Heese O, Disko A, Zirkel D, Westphal M, Lamszus K. Neural stem cell migration toward gliomas in vitro. Neuro-Oncology 2005;7(4):476-84

Ihara S, Nakajima K, Fukada T, Hibi M, Nagata S, Hirano T, Fukui Y. Dual control of neurite outgrowth by STAT3 and MAP kinase in PC12 cells stimulated with interleukin-6. The EMBO Journal 1997;16(17):5345-52

Illes S, Theiss S, Hartung H-P, Siebler M, Dihné M. Niche-dependent development of functional neuronal networks from embryonic stem cell-derived neural populations. BMC Neuroscience 2009;10:93

Irion S, Nostro MC, Kattman SJ, Keller GM. Directed differentiation of pluripotent stem cells: from developmental biology to therapeutic applications. Cold Spring Harb Symp Quant Biol. 2008;73:101-10.

Johnson MA, WeickJP, PearceRA, Zhang S-C. Functional neural development from human embryonic stem cells: accelerated synaptic activity via astrocyte coculture. The Journal of Neuroscience 2007;27(12):3069-77

Kao H-T, Song H-J, Porton B, Ming G-L, Hoh J, Abraham M, Czernik AJ, Pieribone VA, Poo M-M, Greengard P. Protein kinase A-dependent molecular switch in synapsins regulates neurite outgrowth. Nat. Neurosci. 2002;5:431-7

Ko J-Y; Lee J-Y; Park C-H; Lee S-H. Effect of cell-density on in-vitro dopaminergic differentiation of mesencephalic precursor cells. Neuroreport 2005;16(5):499-503

Lim JY, Park SI, Oh JH, Kim SM, Jeong CH, Jun JA, Lee KS, Oh W, Lee JK, Jeun SS. Brain-derived neurotrophic factor stimulates the neural differentiation of human umbilical cord blood-derived mesenchymal stem cells and survival of differentiated cells through MAPK/ERK and PI3K/Akt-dependent signaling pathways. J Neurosci Res. 2008;86(10):2168-78.

Little L, Healy KE, Schaffer D. Engineering biomaterials for synthetic neural stem cell microenvironments. Chem. Rev. 2008;108:1787-96

Lorincz MT. Optimized neuronal differentiation of murine embryonic stem cells: role of cell density. Methods Mol Biol. 2006;330:55-69.

Meador-Woodruff J.H., Clinton S.M., Beneyto M., McCullumsmith R.E., 2003. Molecular abnormalities of the glutamate synapse in the thalamus in schizophrenia. Ann N Y Acad Sci. 1003:75-93.

Mitchell P.J., Hanson J.C., Quets-Nguyen A.T., Bergeron M., Smith R.C.. A quantitative method for analysis of in vitro neurite outgrowth. Journal of Neuroscience Methods 2007;164:350-62

Mook-Jung I, Hong H, Boo JH, Lee KH, Yun SH, Cheong MY, Joo I, Huh K, Jung MW. Ginsenoside Rb1 and Rg1 improve spatial learning and increase hippocampal synaptophysin level in mice. J Neurosci Res. 2001;63(6):509-15.

Kisaalita WS, Bowen JM. Development of resting membrane potentials in differentiating murine neuroblastoma cells (NIE-115) evaluated by flow cytometry. Cytotechnology 1997;24:201-12

Ogawa D, Okada Y, Nakamura M, Kanemura Y, Okano HJ, Matsuzaki Y, Shimazaki T, Ito M, Ikeda E, Tamiya T, Nagao S, Okano H. Evaluation of human fetal neural stem/progenitor cells as a source for cell replacement therapy for neurological disorders: properties and tumorigenicity after long-term in vitro maintenance. J Neurosci Res. 2009;87(2):307-17.

Otero JJ, Fu W, Kan L, Cuadra AE, Kessler JA. β-Catenin signaling is required for neural differentiation of embryonic stem cells. Development 2004;131:3545-57

Poo M-M. Neurotrophins as synaptic modulators. Nature Reviews Neuroscience 2001;2:24-32

Radad K, GilleG, Liu L, Rausch W. Use of ginseng in medicine with emphasis on neurodegenerative disorders. J Pharmacol Sci 2006; 100: 175-86.

Rudakewich M, Ba F, Benishin CG. Neurotrophic and neuroprotective actions of ginsenosides Rb1 and Rg1. Planta Med 2001;67(6):533-7

Saha K, Keung AJ, Irwin EF, Li Y, Little L, Schaffer DV, Healy KE. Substrate modulus directs neural stem cell behavior. Biophysical Journal 2008; 95: 4426-38.

Schaffer DV, Gage FH. Neurogenesis and neuroadaptation. Neuromolecular Med. 2004;5(1):1-9

Shen LH, Zhang JT. Ginsenoside Rg1 promotes proliferation of hippocampal progenitor cells. Neurol Res. 2004;26(4):422-8

Shetty AK, Turner DA. Neurite outgrowth from progeny of epidermal growth factor-responsive hippocampal stem cells is significantly less robust than from fetal hippocampal cells following grafting onto organotypic hippocampal slice cultures: effect of brain-derived neurotrophic factor. J Neurobiol. 1999;38(3):391-413

Shi Q, Hao Q, Bouissac J, Lu Y, Tian S, Luu B. Ginsenoside-Rd from Panax notoginseng enhances astrocyte differentiation from neural stem cells. Life Sciences 2005; 76: 983-95.

Shin S, Dalton S, Stice SL. Human motor neuron differentiation from human embryonic stem cells. Stem Cells and Development 2005;14:1-4.

Tsai RYL, McKay RDG. Cell contact regulates fate choice by cortical stem cells. The Journal of Neuroscience 2000;20(10):3725-35

Wang L, Mumaw J, Wu Z-Z, Xu B, Stice S, Kisaalita WS. Microwell structure-neural stem cell platform for screening compounds against connectivity-related targets. Biomaterials (under review)

Wang L and Kisaalita WS. Characterization of micropatterned nano-fibrous scaffolds for neural network activity readout for high-throughput screening. Journal of Biomedical Materials Research Part B: Applied Biomaterials 2010 (in press)

Xue J, Liu Z, Hu J, Chen H, Zhang J, Chen N. Ginsenoside Rb1 promotes neurotransmitter release by modulating phosphorylation of synapsins through a cAMP-dependent protein kinase pathway. Brain Research 2006; 1106(1): 91-98.

Yan Y, Yang D, Zarnowska ED, Du Z, Werbel B, Valliere C, Pearce RA, Thomson JA, Zhang S-C. Directed differentiation of dopaminergic neuronal subtypes from human embryonic stem cells. Stem Cells 2005;23:781-90.

Zhang S-C. Neural Subtype Specification from Embryonic Stem Cells. Brain Pathol 2006;16:132-42.

Zhuang P, Zhang Y, Pang T. Proliferation effect of neural stem cell of ginsenoside Rg1 in vitro. Zhongguo Zhong Yao Za Zhi 2009;34(4):443-6

CHAPTER 7

CONCLUSION AND PERSPECTIVE

In this dissertation, we provided a three-dimensional (3D) cell-based platform for high-throughput screening (HTS). This platform was comprised of neural stem cell (NSC)-derived neural networks in interconnected microwell structures. We are interested in apply this platform in schizophrenia drug screening.

We started with SU-8 microstructure fabrication. Through complete crosslinking and surface modification, SU-8 microstructures were tailored to be biocompatible for cell culture. SH-SY5Y human neuroblastoma cells were successfully integrated into SU-8 microwells and voltage-gated calcium channel (VGCC) function of SH-SY5Y cells on two-dimensional (2D) substrates and in microwells were evaluated. The responsiveness to high K^+ depolarization for cells on quasi-3D scaffolds was significantly lower than that on 2D substrates. This result shows that SU-8 microstructure did affect SH-SY5Y cell differentiation with respect to VGCC function and also shows that high-aspect-ratio microstructure is not merely "folded" 2D structure. This is in agreement with previous 2D/3D comparative studies carried out in polymer scaffolds, and supports the speculation that 2D cell functions may represent an exaggeration of those *in vivo*.

Compared to human neuroblastoma cells, human neural stem cells (hNSCs) provide a more attractive cell source in drug discovery due to normal cellular functionality and multipotentiality. Our second step was to integrate hNSCs with SU-8 microstructures to form controllable 3D neural network *in vitro*. hNSCs have been successfully integrated and patterned with SU-8 microwell structures and patterned neural network-like formation was observed for differentiated neural stem cells within microstructures. Microstructure architecture (e.g. presence of microchannel and microwell) can be applied to guide interaction-driven activity of neural stem cells within a 3D microenvironment. Cellular morphology, cytoskeleton organization and resting membrane potential establishment of cells within microstructures were statistically significantly different from those of cells on flat 2D surface.

Even though SU-8 has high optical transparency and excellent thermal stability, the fabrication procedures limited its integration with currently used HTS systems (e.g. 96-well plates) for neural network activity readout. As an alternative, similar microwell structures were fabricated in nanofibrous poly-L-lactic acid (PLLA) film, which was compatible with 96-well plates. Fabricated PLLA scaffolds have nano-fibrous structures that mimic collagen fibers in extracellular matrix and exhibit higher porosity, improved thermal and mechanical properties than PLLA scaffolds without nano-fibrous structures. Laser micromachined patters in the nano-fibrous PLLA films are compatible with stem cell culture and integrate easily in high-density-well plates (e.g. 96-well plates) for HTS application. Mathematical simulation confirmed that it is possible to study neural network activity induced by chemical stimulation in these micropatterned nano-fibrous scaffolds (MNFSs), and by controlling parameters in

MNFSs (such as channel), cellular responses due to cell-to-cell communication can be distinguished from those caused by chemical diffusion. PLLA scaffolds are opaque, which is unfavorable for optical detection methods. Methods have been reported to improve light transmittance at the positions with microstructures.

Based on these results, microwell structures can provide 3D microenvironments for cell integration, offering the opportunity for engineering quasi-3D neural network connectivity. The resultant microstructures can be integrated with 96-well plates for HTS purpose. Neural network formation has been observed within these interconnected microwell structures. To enhance neural network formation, we optimized hNSC differentiation condition by controlling differentiation media and cell density. We examined BDNF/ginsenosides (Rg1 and Rb1)-induced hNSC differentiation with respect to cell survival, cell dynamic locomotion, neurite outgrowth and synaptic development. Results have shown that administration of BDNF/ginsenosides combination promoted cell survival, enhanced neuite outgrowth, network formation and synaptic development during differentiation. Also, we examined cell density effects on hNSC differentiation and results indicated that cell density should be kept at certain level (such as $20x10^4$ cells/cm^2) to maximize synaptic formation. Taken together, we provided an effective protocol for hNSC differentiation with synapse formation, which is critical in neural-network based assay for drug discovery as well as in neuroregenerative medicine.

In the follow-up studies, we will first confirm neural network activity in microwell structures, reflected by both synaptic marker expression and dynamic calcium propagation within neural network. Neural network activity within 3D microwell structures will be

compared with that on 2D surface. The difference in network activity between 2D and 3D cultured neural networks is expected. Then, architecture of microwell structures will be changed to control 3D neural network activity. Microwell size, channel length and width will be adjusted, and network activity will be evaluated. Through this study, it is expected to establish protocols for engineering 3D neural network activity through controlling microstructure parameters.

With the development in schizophrenia genetic research, susceptible schizophrenia genes have been discovered. Cellular disease models for schizophrenia, induced from normal hNSCs by transfection of these target genes, can be brought in our platform to create a 3D neural network-based assay. As an alternative cell source, induced pluripotent stem cells (iPSCs), reprogrammed from human somatic cells without the need of embryos or eggs, will solve the technical and ethical problems met in derivation of human embryonic SCs (hESCs). Furthermore, iPSCs from patients can be patient-specific and disease-specific. hNSCs derived from iPSCs offer unique opportunity for neurodegenerative disease modeling and studying the neural network activities in terms of calcium transients. Even though iPSCs derived from some specific patients can not represent the whole group of people with schizophrenia, development of cell lines of iPSCs from patients grouped according to genetic characteristics or races will provide a powerful tool in drug screening assays. A 3D disease model with iPSCs-derived neural networks is expected, and neural network activity in 3D disease model is expected to be similar to that *in vivo*. Finally, drugs known to treat schizophrenia will be used to validate the assay. Z-factor will be generated to test the robustness of this assay.

APPENDIX 1

SU-8 MICROWELL STRUCTURE FABRICATION

Material(s): SU-8, SU-8 developer, MCC Primer 80/20 (20% HMDS and 80% PM Acetate). All these were purchased from Microchem (Newton, MA).

25 mm coverslips (Fisher Scientific, Pittsburgh, PA)

Equipment(s): vacuum pump (Gardner Denver Thomas Inc., Welch Vacuum Technology, Niles, IL), spin coater (Specialty Coating System Inc., Indianapolis, IN), Karl Suss MJB 3 HP Mask Aligner, designed masks manufactured by Advance Reproductions Corporation

Procedure(s):

1) Clean coverslips with 20% sulfuric acid (soaking at room temperature for at least 24 h), water, DI water, and then dried (baking at 110 ◦C for at least 3 h).
2) Before entering the cleaning room, turn on the vacuum pump, 30-40 cm Hg is O.K.
3) Turn on the baker, and set the temperature to 95°C.
4) Cover the spin coater with aluminum foil paper, clean the vacuum nozzle, chuck, baker surface, and the bench surface with acetone.
5) Turn on the spin coater via pressing the Power button, check the parameters, and adjust them if necessary (parameters as listed at the end of this protocol).

6) Take out small bottle of SU-8 from the cabinet.

7) Place one coverslip on the chuck stage, transfer around 1 mL SU-8 by glass pipette onto coverslip, and run the spin coating by pressing the Start button[1]. In some cases, HMDS was spun coated onto the coverslip before put SU-8 on to enhance the adhesion.

8) Place the coated coverslips onto the baker. Baking time can be long, but the temperature should not exceed 110 °C.

9) Before running exposure process, turn on the nitrogen (70psig).

10) Turn on the Power of UV lamp.

11) When it reads “rdy” (short form of “ready”), ignite the lamp via pressing the Start button; this may take about 3-5 minutes. A number reading regards the lamp power will appear in the panel after a successful ignition. Repeat (11) if it still reads “rdy”.

12) Turn on the Power of mask aligner.

13) Turn on the power of the microscope manipulator.

14) Load the mask by press the “Vacuum Mask” button to fix the mask.

15) Set the desired exposure time[2]. Parameters need modification according to film thickness to achieve completely crosslinked film.

16) Load the sample and contact the sample with mask.

17) Expose the sample by pressing the Start button.

[1]Parameters for spin coating

RPM1: 500

RAMP1: 0005

TIME1: 0001

RPM2: 1000

RAMP2: 0005

TIME2: 0015

RPM3: 1000

RAMP3: 0005

TIME3: 0015

RAMP4: 0015

S: 0000

N: 0000

Coating: 0000

Parameters could be varied to achieve different film thickness. For more information, refer to product information online: http://www.microchem.com/products/su_eight.htm

[2]Parameters for developing and baking

Bake ----------65 °C for 3 min, 95 °C for 9 min

Exposure ----------15 sec for 4 times, with 20 s interval

Post exposure bake ----65 °C for 3 min, then 95 °C for 9 min

Development ----------7 min in SU-8 develop, then rinsed with isopropyl alcohol (IPA) and dried with pressurized nitrgen

Bake ----------95 °C for 9 min

Exposure ----------15 sec for 4 times, with 20 s interval without mask

Post exposure bake ----95 °C for 7 min

Hard bake ----------150 °C for 20 min

Notice

1) During development, shake the beaker frequently to dissolve uncrosslinked SU-8 completely.
2) Avoid SU-8 attaching to the mask.
3) Clean the mask with acetone and dry it with nitrogen.
4) Before applying SU-8 microstructures for neural stem cell culture, treat the surface with oxygen plasma etching (15-20 min).

APPENDIX 2

MICROPATTERNED NANO-FIBROUS PLLA SCAFFOLD FABRICATION

Material(s):

tetrahydrofuran (THF), poly-L-lactic acid (PLLA) (Sigma, St. Louis, MO)

Procedures:

1) Measure 0.2 g PLLA and add it to glass conical beaker, put one stirrer bar into the flask.
2) Add 4 mL THF into the flask and seal the flask.
3) Put the flask into a beaker with water, put the beaker onto a stir plate, and keep the water temperature around 55 ℃.
4) It usually takes around half an hour for PLLA to completely dissolve in THF.
5) Quickly cast the solvent into a glass Petri dish (8 cm in diameter), cover the dish and transfer it to -80 ℃ freezer for ultra-freezing. It usually takes 2 hours or more to be gelled.
6) Immerse the gelled PLLA/THF solution into cold double distilled water (4 ℃) for 2 days to leach out the solvent (THF). Change the water three times every day and air-dry the resultant PLLA scaffolds.
7) Micropatterns within nano-fibrous PLLA scaffolds are micromachined[3] with an

excimer laser-based laser micromachining system Resonetics RapidX250 (Resonetics, USA). The excimer laser model coupled to this system is ATLEX-500-SI (ArF, 193 nm wavelength).

8) The direct write approach is used as micromachining mode. Using appropriate mask sizes, channels (10-20 μm wide) and wells (up to 100 μm in diameter) can be fabricated into the nano-fibrous structure.

[3]See APPENDIX 3 for micromachining details.

APPENDIX 3

LASER MICROMACHINING

Laser Micromachining is defined as a fabrication technique to drill, skive, strip, mill, cut plastics, ceramics, glass and thin metals with dimensions and tolerances approaching 1 micron (0.00004"). Laser micromachining is performed by two different methods: mask projection and direct-write. This technique could be applied to the following areas: 1) medical device components and assembly manufacturing; 2) semiconductor OEM components manufacturing; 3) flexible circuits manufacturing; 4) industrial components manufacturing. For more information, refer to the company website: http://www.resonetics.com/pages/

A brief operation manual

Turn on the power

Turn on the laser and wait for 10 min

Turn on the system and monitor

Open the compressed air

Load sample and insert the mask

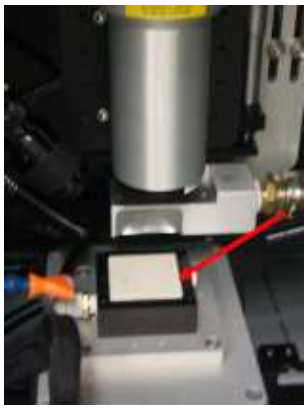

Open the software for controlling the laser and stage, upload the program

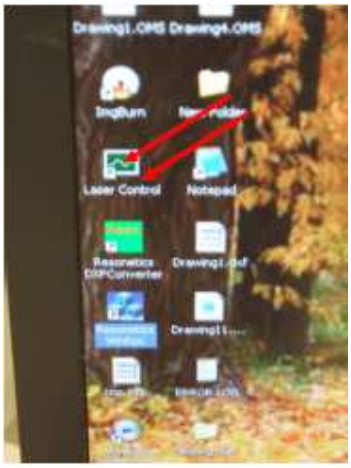

After 10 min, turn on the trigger, run experiment

When shutting down the equipment: 1) turn off the computer and monitor; 2) close the compressed air; 3) turn off the laser; 4) turn off the power.

For details, please refer to the files attached to the equipment.

A potential trouble shoot description (if you have that experience already)

A. There is a manual book with the equipment. Also the attached files help.

B. The energy level reading from the software is not the actual value working onto the sample. However, when the reading drops to around 3 mJ, it needs refilling. (since the maintenance last time, the reading is around 3 mJ even after refilling the gas.)

C. Refilling

Go to “Gashandling”

Click “Auto Gas Vacuum”

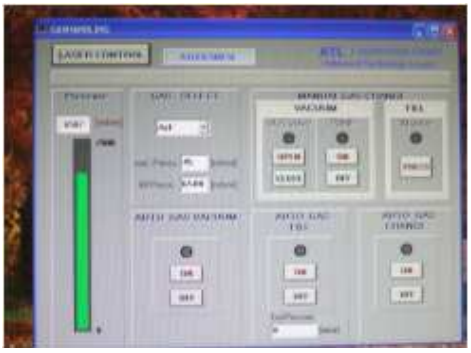

Fill the tube with gas

Click “Auto Gas Vacuum”, meanwhile open the pump. Go through this process

three times.

Close the vacuum pump and open the cylinder valve. Click the “Auto Gas

Change”. When the filling process is over, close the cylinder valve.

1) When doing the vacuuming process, make sure the cylinder is closed.

2) After refilling, close the cylinder valve.

APPENDIX 4

COATING FOR NEURAL STEM CELL CULTURE

We recommend using poly-ornithine and laminin coated plates to culture neural progenitor cells. Poly-ornithine and laminin coated plates provide the optional foundation for adhesion and growth. The preparation should be carried on in the hood to keep them sterile. The concentration of the stocking solution for poly-ornithine is 10mg/mL.

Preparation of 35mm Poly-Ornithine and Laminin Coated Plates

1) Dilute poly-ornithine to 20 µg/mL concentration in sterile distilled de-ionized (ddi) water.
2) Dispense 20 µg/mL poly-ornithine to completely cover the bottom of the dish (about 2 mL/35mm, 5 mL/100mm).
3) Incubate in a humidified 37 ℃ incubation for at least 1 hour.
4) Remove the poly-ornithine solution and rinse once with sterile ddi water.
5) Dilute the lamine to 5 µg/mL concentration in sterile ddi water.
6) Dispense 5 µg/mL laminin to completely cover the bottom of the dish (about 1mL/35mm).
7) Incubate in a humidified 37 ℃ incubator for at least 1 hour.
8) Store at 2 ℃ to 8 ℃ for up to 3 weeks.

For more information, please refer to manual form Aruna Biomedical Inc.:

http://arunabiomedical.com/Resources.htm

APPENDIX 5

MEDIA PREPARATION FOR NEURAL STEM CELL CULTURE AND DIFFERENTIATION

Prepare 50 mL growth media in a 50 mL centrifuge tube:

1) Add Penicillin/Streptomycin 0.5 mL.
2) Add L-Glutamine 0.5 mL.
3) Add B27 1.0 mL.
4) Add LIF 50 µL.
5) Add bFGF 20 µL.
6) Add neurobasal media, QS to 50 mL.
7) Filter with a 0.2 µm filter unit and store at 2 ℃ to 8 ℃ for no more that 2 weeks post preparation.

The bFGF stock solution is prepared at 50 µg/mL in Neural Basal Media supplement with 1% BSA.

Prepare 50 mL differentiation media:

1) Add Penicillin/Streptomycin 0.5 mL.
2) Add L-Glutamine 0.5 mL.
3) Add B27 1.0 mL.
4) Add LIF 50 µL.

   Add neurobasal media, QS to 50 mL. Note: other compounds for neural stem cell differentiation could also be added.

5) Filter with a 0.2 µm filter unit and store at 2 ℃ to 8 ℃ for no more that 2 weeks post preparation.
6) Differentiation media needs to be half changed every other day.

For more information, please refer to manual form Aruna Biomedical Inc.:

http://arunabiomedical.com/Resources.htm

APPENDIX 6

THAWING NEURAL STEM CELLS

1) All materials should be ready prior to thawing. Turn on water bath to 37 °C and retrieve a small bucket of crushed ice. Open and turn on hood. Locate the proper media of the needed volume for cell culture in centrifuge tubes and wrap them with foil and then place them in hood. Also place one 15 mL conical centrifuge tube, one 35 mm coated plate, one 10 mL disposable pipette and one 5 mL disposable pipette.
2) Once the water bath has come to temperature, take vial to the water bath and thaw the cells rapidly by hand rotating the vial. Note: thaw rapidly and completely for maximum cell viability. Take no more than 2 minutes and leave a small piece of ice in the vial before take it out of the water bath.
3) Spray vial with 70% ethanol (especially around the cap), and dry before placing in the hood.
4) Under hood, open the vial, remove the contents with a Pasteur pipette and place into the conical centrifuge tube.
5) Swirling slowly, drop-wise add 10 mL basal media. Note: adding media all at once may result in osmotic shock.
6) Centrifuge at room temperature at 1000 rpm for 4 minutes.

7) Carefully aspirate as much of the supernatant as possible. Note: steps 4-6 are very important in the removal of residual DMSO.
8) Add 2 mL growth media to the remaining pellet. Use the Pasteur pipette to thoroughly mix the media and pellet together.
9) Plate the cell suspension at a density of 1 vial per 35 mm poly-ornithine and laminin coated plate.
10) Incubate the cell at 37 °C in a 5% CO_2 humidified incubator.
11) After the cells have incubated for 24 hours, the growth media in the plate should be aspirated off and replaced with fresh media.
12) Check the cells every day and decide what to do with the cells.

For more information, please refer to manual form Aruna Biomedical Inc.:

http://arunabiomedical.com/Resources.htm

APPENDIX 7

MEDIA CHANGE FOR NEURAL STEM CELLS

Check the cells every morning. Usually we change the media every other day. But if you see a lot of dead cells or any change in media color, change the media right away.

1) Place the growth media of the needed volume in a centrifuge tube. Then wrap the tube with foil and put it into the hood. No need to warm the media, the room temperature is O.K.
2) Aspirate the media from the plate. Note: leave a little media in the plate to keep the cells wet).
3) Add 1.5-2 mL growth media into the plate. Note: be careful and do not dislodge the cells.
4) Put the cells back to the incubator as soon as possible.

APPENDIX 8

SUBCULTURE OF NEURAL STEM CELLS

Check the cells every morning. If the plate is 90%-100% confluent, the cells are ready to passage. We recommend passaging the cells by 1:2 or 1:3. The following steps are for passaging the cells by 1:2.

1) Place the growth media of the needed volume in a centrifuge tube. Then wrap the tube with foil and put it into the hood. No need to warm the media, the room temperature is O.K.
2) When the media reaches the room temperature, place the plates of the needed quantity into the hood. Also put the cells into the hood.
3) Label the new plates. (For example: NPH945P3 03/15/06 LN or L9/P19 03/15/06 LN).
4) Aspirate the laminin from the plates. And aspirate the media from the cell plate.
5) Add 2 mL growth media into the cell plates. Meanwhile, add 1 mL growth media to the other 2 plates.
6) Manually detach the cells from the plates. We recommend using a 200 µL manual pipetteman (160/200) to triturate the cells with pipette up and down. Cells should be triturated into an almost single cell suspension. Plates can be preserved to ensure that

all the cells have been removed. This can be achieved by frequent observation under microscope.

7) Add 1 mL cell suspension media from the cell plate to the other 2 plates.
8) Check the cells under microscope and place them into the incubator as soon as possible.

APPENDIX 9

FREEZING NEURAL STEM CELLS

Firstly prepare 10 mL 20% DMSO freezing media:

1) Add 2 mL DMSO.
2) Add 8 mL basal media.

Notes:

1) The freezing media should be wrapped with foil to avoid light and stored at low temperature. When using it, keep it in ice to keep it cold
2) When freezing the cells, use 10% DMSO

Freezing the cells:

The cells of one plate can be frozen into two vials

1) Prepare the freezing media (20%) before freezing the cells.
2) Place growth media of the needed volume in centrifuge tubes. Then wrap the tubes with foil and put them into the hood. No need to warm the media, the room temperature is O.K.
3) When the media reaches the room temperature, put the cells into the hood.
4) Aspirate the media from the cell plate.
5) Add 2 mL growth media in to the cell plates.

6) Manually detach the cells from the plates. We recommend using a 200 µL manual pipetteman (160/200) to triturate the cells with pipette up and down. Cells should be triturated into an almost single cell suspension. Plates can be observed to ensure that all the cells have been removed. This can be achieved by frequent observation under microscope.
7) Add 1 mL cell suspension media to each vial. And then gradually add another 1 mL of freezing media into each vial.
8) Put the vial into the container which contains liquid isopropyl alcohol (IPA) and put the container into the -80 °C fridge.

APPENDIX 10

IMMUNOSTAINING SOLUTION PREPARATION AND STAINING PROCEDURES FOR NEURAL STEM CELLS

Prepare 1 liter high salt buffer:

1) Add sodium chloride 14.61 g.
2) Add 1M Tris (pH 7.4) 50 mL.
3) Add distilled water to 1 L.
4) Mix by inversion until completely in solution.
5) Store at room temperature for 2 months.

Note: high salt buffer could be replaced by PBS++ (PBS containing Ca++ and Mg++, pH 7.4) to avoid cell detachment.

Prepare 10 mL blocking solution:

1) Add high salt buffer 9.4 mL.
2) Add 600 µL 6% serum from the animal that your secondary anti-body is produced in.
3) Mix by inversion.

Note: make fresh blocking solution for each use.

Prepare 50 mL wash buffer:

1) Add high salt buffer 50 mL.
2) Add Tween 20 25 µL.
3) Mix by inversion until completely in solution.

Note: make fresh buffer for each use.

Staining of Cells

1) All manipulations should be carried out with extreme care as cells may be dislodged easily. We recommend adding and removing liquids slowly with a manual pipetteman or transfer pipette. During the incubation, plates can be placed on a shaker.
2) Wash wells 2 times in PBS containing Mg++ and Ca++. Note: for all washes wells should be completely filled with solution.
3) Wash with wash buffer 3 times for 5 minutes each. In this step you are permeablizing your cells, so the time is very important. Note: if you are using an antibody that is labeling a protein that is in the membrane, use PBS ++ rather than wash buffer.
4) Add enough blocking buffer to completely cover the cells in each well. Incubate at room temperature for 45 minutes.
5) Prepare intracellular marker (first antibody) in blocking solution at the recommended dilution.
6) Aspirate off blocking solution

7) Add enough first antibody solution to completely cover the cells in each well. Cover and incubate for 1 hour at room temperature. This can be extended to over night at 4 °C if necessary.
8) Wash wells 4 times in wash buffer for 5 minutes each.
9) Prepare second antibody in blocking solution at recommended dilution before the step 8.
10) Aspirate off last wash.
11) Add enough second antibody solution to completely cover the cells in each well. Incubate for 1 hour at room temperature. During incubation, cover sample with foil to prevent fluorescence bleaching.
12) Wash cells 3 times in PBS++.
13) Prepare DAPI solution at recommended dilution. We recommend VWR Cat. # 80051-386 at a 1:10,000 dilution in distilled water. This can be done before step 12.
14) Add DAPI solution to each well. Incubate for 5 minutes at room temperature. Cover with foil during incubation.
15) Wash cells 3 times in PBS++.
16) Verify staining has taken place under UV microscope before mounting.
17) Aspirate off PBS++.
18) Gently remove sides of chamber and aspirate excess surrounding PBS++.
19) Place one drop of mounting media directly in center of each well area.
20) At an angle gently lower a cover slip onto the slide, trying to avoid air bubbles where possible.

21) Remove excess mounting media from slide and cure in dark for 24 hours.

22) Seal with nail varnish on all four sides.

23) Keep in dark storage until results are observed and documented.

For more information, please refer to manual form Aruna Biomedical Inc.:

http://arunabiomedical.com/Resources.htm